Onion Postharvest Quality Assessment Using X-Ray Computed Tomography

by

Richard Andrew Speir

(Under the direction of Mark Haidekker)

Abstract A low cost, custom-built, CT scanner was utilized to obtain cross sectional images of yellow sweet onions that were inoculated with pathogens or subjected to mechanical damage. The CT images were analyzed for features that could potentially be used to detect signs of pathogen or mechanical damage in an on-line onion packing house quality assessment apparatus.

Index words: Vidalia, onion, post harvest, computed tomography, CT, mechanical damage, bruising, Burkholderia cepacia, Botrytis allii, Pseudomonas viridiflava

Onion Postharvest Quality Assessment Using X-Ray Computed Tomography

by

Richard Andrew Speir

B.S., University of Georgia, 2006

A Thesis Submitted to the Graduate Faculty
of The University of Georgia in Partial Fulfillment
of the
Requirements for the Degree

Master of Science

Athens, Georgia

2013

Onion Postharvest Quality Assessment Using X-Ray Computed Tomography

by

Richard Andrew Speir

Approved:

Major Professor: Mark Haidekker

Committee: Changying Li
Ernest Tollner

Electronic Version Approved:

Maureen Grasso
Dean of the Graduate School
The University of Georgia
December 2013

Acknowledgments

As I write this, it occurs to me just how many people to whom I owe an incalculable debt. To start, I would like to thank Brian Bibens for being a source of encouragement and inspiration, as I would not have even thought to apply to graduate school without his assistance. I would also like to thank Drs. Roger Hilten, K.C. Das, Sudhagar Mani, James Kastner, and the other members of the UGA Biorefinery project for their letters of recommendation and helpful advice as I applied to the graduate program. Adnan Mustafic was also a source of encouragement and was always able to help me put my difficulties in perspective when they seemed insurmountable.

I would also like to thank my committee members, Drs. Changying Li, Ernest Tollner, and Mark Haidekker, without whom I would have no thesis project. I owe Dr. Haidekker a particular debt of gratitude for his willingness to take me in and allow me to work in his laboratory, and for his saintlike patience and willingness to explain (often multiple times) x-ray physics and the finer points of image analysis.

Finally, but certainly not least, I would like to thank my parents, Rick and Jeanne Speir, and my fiancee, Doreen for their constant urging, occasional nagging, but nevertheless unflinching support as I complained, whined, and vented my frustrations throughout this project. I owe them my continued sanity.

THANK YOU!

Contents

List of Figures

List of Tables

Chapter 1

Introduction

Georgia sweet onions, or Vidalia onions, as will be presented in detail in subsequent sections, are an extremely valuable economic commodity. Vidalia onions have proven to be highly desirable to consumers due to their sweet and mild flavors, and sales have steadily increased since their introduction to the market. Vidalia onions are only harvested during a brief period of time every year, and the sweet flavor and high water content that makes them desirable to consumers also confer susceptibility to disease and decay, making it difficult to store them for long periods of time after harvest. Onion growers have attempted to extend the market availability of Vidalia onions by storing them in controlled atmosphere facilities, but disease outbreaks still frequently occur in these storage facilities, leading to substantial economic losses for the onion producers. Currently, onions entering storage are screened by human visual inspection for external signs of disease or damage that can increase disease susceptibility, but many onion diseases and defects manifest inside the bulb and can pass human inspection undetected.

This paper outlines x-ray computed tomography scanning and image analysis techniques that can be used to evaluate the quality of onions before they enter or leave controlled atmosphere storage, so as to increase the overall quality of the products reaching consumers and

reduce storage losses to onion producers. Internal lesions caused by infectious pathogens, bruise damage, and bulb malformations are some features that can be detected by the methods proposed. Such an evaluation system could be used to ensure that only high quality, healthy onions that have a high probability of storing for long periods enter controlled atmosphere storage. Additional quality factors such as bulb shape, consistency, and internal structure can be evaluated, leading to a premium onion grade that would command higher market prices, further increasing the value proposition of such a system to onion producers.

1.1 Economic Importance

Worldwide, the onion (*Allium cepa*) is one of the most widely cultivated vegetable crops, second only to the tomato. According to the United Nations Food and Agriculture Organization, worldwide production of onions was 78.5 million metric tons in 2010, the most recent year for which statistics are available. That same year, total harvested land area devoted to onion cultivation exceeded four million square hectares [15]. In the United States, 2010 onion production was an estimated 3.72 million metric tons, with an aggregate farm gate value of approximately $1.15 billion [48].

In the state of Georgia, the onion is one of the most economically important agricultural commodities. With a 2010 farm gate value of $139 million, the onion is currently Georgia's most valuable vegetable crop [50]. The sweet yellow Granex varieties of onion grown in Georgia are collectively called Vidalia sweet onions, so recognized under a 1986 state legislative action that defined the southeastern region of the state in which such onions are grown, and by a 1989 Federal Market Order that provided national protection to the brand [4]. Between 1989 and 2001, production of Vidalia sweet onions increased threefold [5], and the farm gate value of Vidalia onions nearly doubled from $70.5 million in 2002 [49] to its 2010 figure of $139 million.

1.2 Vidalia Onion Characteristics

Granex onions are characterized by their high water content, high sugar content, and low quantities of pungent sulfur-containing compounds relative to other onion varieties. The light, sandy soils of the Vidalia region of Georgia tend to be low in sulfur-bearing compounds necessary for the formation of pungent flavor precursors, and onions grown in these soils are prized for their superior sweet and mild flavors [5].

Onions are biennial plants, growing vegetatively during the first year of life to maximize sugar production for storage in the bulb. As the plant matures, the leaves die and the plant enters a dormant stage until the next growing season when the plant produces flower stalks and seeds. These growth stages are regulated by the day-night cycle, and Granex varieties belong to a class of onion cultivars known as short-day (SD) onions due to the relatively short photoperiod (11-12) hours required to induce bulb formation in the plant [9]. In the southern latitudes of the US, greenhouse-grown plantlets are typically transplanted to production fields in the late fall, where they grow vegetatively during the short winter days. As day length increases, plant growth shifts from leaf formation to bulb formation, and the onion bulbs are harvested from late April to early May when the bulbs reach a marketable size [5].

1.3 Cultivation and Storage Practices

As harvest time approaches, the onion plant's leaves begin to break down, signaling that vegetative growth has stopped and that the plant is entering dormancy. It is at this point, when the onion leaves fall, that the bulbs can be harvested [4]. A mechanical blade is run underneath the onion bulbs to sever the roots, and the bulbs are lifted out of the ground by the leaves and are left to cure for several days. Excessively hot or cold temperatures as well as heavy rains during the harvest and field curing of the onions can lead to increased incidence of bacterial and fungal rots that adversely affect their storability, leading to substantial losses

for the growers [19]. After field curing, the dead leaves are cut off, and bulbs are collected and transported to a sorting facility. There, human inspectors check for signs of disease or damage to the bulbs, and the bulbs are sorted by size [4]. While human visual inspection can be useful in culling bulbs with obvious external defects, many bulbs may have internal damage or latent infections that are not detectable by eye [46].

Because Vidalia onions have such a short harvest season and do not store for long periods of time at room temperature, they were traditionally only available to consumers for a few weeks shortly after the harvest period. Since the early 1990s, however, growers have begun setting aside as much as half their harvest for storage in controlled atmosphere facilities. Controlled atmosphere storage facilities utilize refrigeration and atmospheres with decreased oxygen (3%) and elevated carbon dioxide (5%) and nitrogen (92%) to retard the growth of bacteria and fungi and to prevent dormancy breaking and seed stem formation. Controlled atmosphere storage can extend the market availability of Vidalia onions for several months [19].

While Vidalia onions remain popular with consumers because of their sweetness and lack of pungency, there are associated drawbacks. Laboratory tests of extracted onion flavor compounds have been shown to inhibit the growth of pathogenic fungi and bacteria [8]. Vidalia onions are thought to be particularly susceptible to fungal and bacterial diseases because of their lack of these protective compounds. This increased susceptibility to disease has been a particular problem with regard to controlled atmosphere storage of onions for later sale. During particularly severe disease outbreaks, growers can lose more than 50% of their stored onions to postharvest diseases [38].

Several factors can affect the storability of sweet onions. Maw et al. [32] conducted a study examining the effects of several factors on the shelf life of onions. They determined that early harvested onions had the greatest storage potential, but that at this early stage of development, the bulbs had not reached their optimal size. Another factor affecting storabil-

ity is mechanical damage. Purvis and Hakim [39] determined that bulb mass loss and decay in storage can be directly correlated with severity of bruise damage inflicted upon the bulbs. With as many as 30% of onion bulbs experiencing minor or major damage in harvest [33], one can see how onion growers can realize severe losses, and end consumers can be left with substandard produce.

1.4 Onion Pathogens, Damage, and Quality Factors

There are numerous pathogens and damage modes that can lead to diminished quality or complete loss of harvested onions, particularly as they are stored for increasing durations in controlled atmosphere facilities. A study of every postharvest onion pathogen would be infeasible owing to the sheer number of diseases. Therefore, this project will focus on the detection of three of the most common post-harvest diseases affecting sweet onions: Botrytis fungal neck rot, *Burkholderia cepacia* bacterial rot, and *Pseudomonas viridiflava* bacterial rot.

Additionally, this project will examine the detection of mechanical damage such as puncture wounds, crushing, and bruising of onion bulbs that can lead to reduced storage life. Though puncture wounds and severe crushing may be immediately obvious to human inspectors, internal bruise damage may pass unnoticed, and these disease-susceptible onion bulbs can lead to the spread of disease in controlled atmosphere storage.

Finally, this project will explore the detection of onion bulb features that can contribute to perceived diminution of quality (and reduction in value) in the eyes of the end consumer. The ability to quickly and reliably detect internal sprouting, uniformity and number of internal scales, double-center bulbs, and overall bulb shape can allow onion producers to diversify their market offerings by providing premium quality inspected onions.

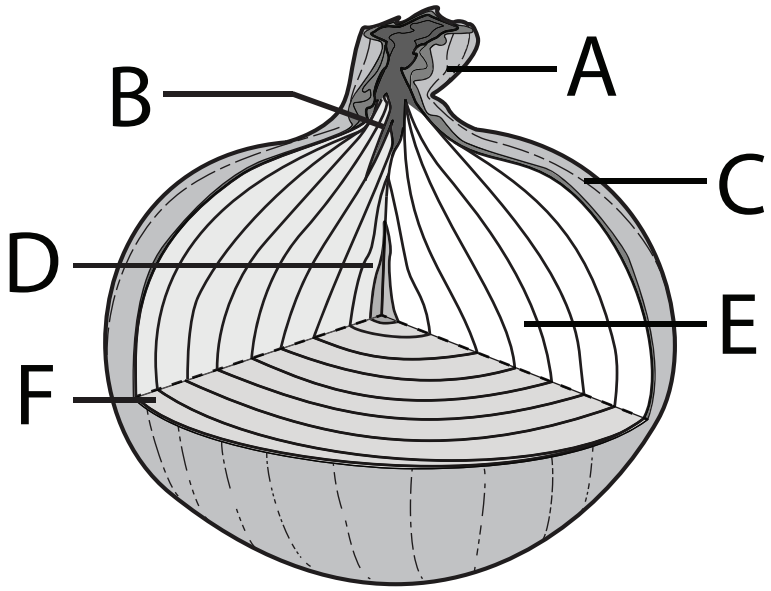

Figure 1.1: *Sketch of a dissected onion bulb.* ***A****: Dry leaves and outer scales comprising the neck.* ***B****: Fleshy onion scales in the neck region of the bulb.* ***C****: Dry outer scale (skin).* ***D****: Emerging green shoot.* ***E****: Fleshy inner scales.* ***F****: First fleshy scale. The outer scales tend to be nonuniform in thickness.*

1.4.1 Botrytis Rots

Bulb rot caused by various species of fungus of the Botrytis genus is recognized as one of the most common and devastating onion storage diseases [38]. There are seven named species of Botrytis that are associated with onion disease, and of these, five are recognized as causal agents of neck rot in onion bulbs. *B. aclada*, *B. allii*, and *B. byssoidea* are the three species most commonly associated with fungal neck rots of onions in storage [54]. Botrytis infections typically begin as a watery decay at the top of the bulb where the leaves have been removed (part B in Figure 1.1). This decay progresses to the interior of the onion, causing the bulb to eventually rot from the inside out [11]. Human visual inspection, the method most onion packing houses employ to discard damaged or diseased onions, is notably incapable of detecting internal Botrytis infections [46].

Figure 1.2: *A Botrytis-inoculated onion bulb exhibiting advanced stage internal rot. The extensive damage to this particular onion could likely be detected externally, but in many cases, damage is restricted to the internal scales of the bulb.*

There are several ways Botrytis fungi can infect onion bulbs. The fungi have been known to survive inside onion seed, causing neck rots once the plant is mature [14], they form sclerotia on decaying onion bulbs and foliage in the field that can opportunistically infect injured bulbs [40], and they form conidia that can be carried in the wind or lay dormant in the field before infecting the foliage of the plant and spreading to the bulb [3].

Environmental factors play an important role in determining disease incidence. Prolonged wet periods prior to harvest lead to increased incidence of neck rot, as does over-application of nitrogen fertilizer and overcrowding of plants in the field [40]. Additionally, conidia formed under particularly cold conditions (-2° C), have been found to lead to faster growing infections in onion tissues than those formed at higher temperatures [3]. Because unpredictable climate patterns lead to increased or decreased incidence of Botrytis outbreaks from year to year, onion growers can face great difficulty in managing and predicting their crop yields.

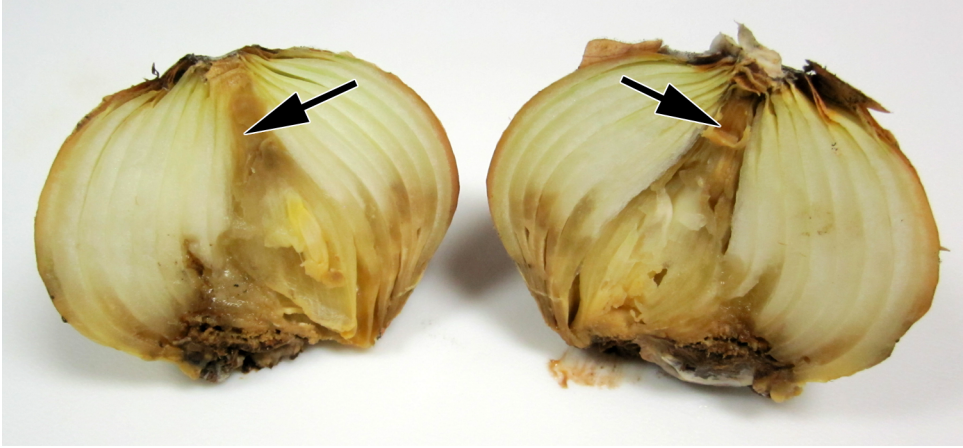

Figure 1.3: *Sour skin-inoculated onion bulb. The infection originated at the neck of the bulb (indicated by the arrows) and spread downwards toward the root end. A secondary fungal infection has begun to spread from the root end of the bulb inwards.*

1.4.2 *Burkholderia cepacia*

Onion sour skin, caused by the bacterium *Burkholderia cepacia*, is another common and highly destructive onion disease, causing as much as 50% harvest losses during particularly severe outbreaks [40]. Though *B. cepacia* infections frequently present as a soft, slimy decay of the outer layers of the onion bulb (part F in Figure 1.1) that is readily identifiable to human inspectors at the onion packing house, internal infection is also common, and infected onions can pass inspection and be placed in storage where they spread the infection to surrounding bulbs [29]. Infection typically occurs when bacteria enter a wound, either on the surface of the onion bulb, or through the neck of the onion when the leaves deteriorate at plant maturity, or through vulnerable new shoots as they emerge from the bulb [29]. Figure 1.3 shows a laboratory-inoculated bulb exhibiting advanced stage sour skin rot.

Burkholderia cepacia is not a single species, but rather a complex of seventeen closely related species of bacteria that occupy several ecological niches and are also known to cause infections in people with cystic fibrosis or compromised immune systems [26]. *B. cepacia*

species have been found as mutualistic symbionts in grasses and cereal grains [28]. Because of the ubiquity of *B. cepacia* bacteria in nature, onion growers have experienced great difficulty in preventing infection of onion bulbs, and no known chemical controls exist [53].

Like Botrytis infections, *B. cepacia* infections are more prevalent when onion fields are particularly wet prior to harvest. Additionally, application of nitrogen-rich fertilizer late in the growing season was found to coincide with higher incidence of Burkholderia infection [53]. *B. cepacia* thrives at high temperatures, 30-35 degrees Celsius, and disease outbreaks are more common under hot, moist conditions at harvest time [29]. Though onion growers can take some steps to mitigate the outbreak of sour skin such as carefully timing and dosing fertilizer applications, uncontrollable weather patterns have a greater effect on the prevalence of sour skin in a particular harvest, and better methods to detect latent infections are necessary to prevent the spread of the infection.

1.4.3 *Pseudomonas viridiflava*

Pseudomonas viridiflava typically infects onion plants through their foliage, forming dark, wet oval-shaped lesions that appear along the leaves [40]. Though most affected plants rot while still in the field, during excessively rainy or humid field conditions, the bacterium can spread to the interior of the onion bulb, leading to postharvest infections in storage [53]. Onion bulb scales affected by *P. viridiflava* are characterized by reddish discolored lesions that, while softer than healthy tissue, are more firm than those damaged by *B. cepacia*. The infection does not appear to spread readily throughout the onion bulb, but remains confined to individual scales, leading to a ring-shaped region of infection when the bulb is sliced into transverse cross sections [18].

Bulbs containing internal *P. viridiflava* infections may present a hazard to surrounding bulbs in storage, particularly if they are improperly or incompletely cured. The damaged tissues also tend to host secondary opportunistic pathogens that can spread to surrounding

onions as the bulb decays [29]. While *P. viridiflava* is not known to survive for long periods in soil or water, it does appear to survive as an epiphytic organism in association with several common species of weeds native to the Vidalia region of Georgia, making control of the bacterium difficult [17].

1.4.4 Mechanical Damage

One of the most common forms of damage to onion bulbs is bruising due either to rough handling during harvest or packing or being crushed under the weight of other onions. According to Maw et al. [31], bruise damage can result in internal separation of the layers of an onion bulb that may be difficult to detect externally. This bruising can disrupt cell walls, leading to the leakage of cellular contents between the onion scales, and providing a water and nutrient rich environment for pathogens [39].

Herold et al. [24] conducted an extensive study on the effects of mechanical impacts on the storability of onion bulbs, developing linear regression models to help predict storage losses based on drop height, static load conditions, and number of impacts on hard concrete and conveyor belts. They then utilized an instrumented sphere to measure the impact forces that an onion bulb would experience through a harvesting system and sorting line, determining that onion bulbs were subjected both to high drop height impacts and repeated low-impact drop forces, both negatively affecting the storability of the bulbs.

1.4.5 Multi-center Bulbs and Seed Stems

Multi-center bulbs, or "doubles", as they are often called, result when a single onion plant produces more than one bulb, resulting in multiple growing centers sharing a common root base. Such multi-center bulbs can arise from a number of causes including plant density in the field and the age of seedlings at transplant [6] as well as high nitrogen fertilization levels

[44] and water stress during early growth stages [36]. Such multi-center bulbs are undesirable to commercial buyers, especially onion ring producers, who typically require that their bulk purchases consist of more than 70% single-center bulbs [36]. The scales between the two growing regions inside a multi-center bulb also appear to provide favorable environments for the growth of sour skin infections [10], making them potential vectors for the spread of the bacterium to other onions in storage.

Seed stems and internal sprouts are also unfavorable onion characteristics, leading to hard, bitter-tasting leaves at the center of the bulb. Several factors affect the formation of seed stems in storage, including temperature, variation between different cultivars, and low nitrogen levels in the field [12]. Properly curing the outer scales of the onion bulbs can help reduce the rate at which seed stems form [30], as premature formation of these seed stems often times occurs in response to stress caused by damage to the outer layers of the bulb. Such damaged bulbs are more likely to harbor pathogens, thus the detection and removal of these damaged onions from storage can help prevent the spread of disease.

1.5 Sweet Onion Quality Control

Diseased and damaged onions take up valuable space in controlled atmosphere storage that could be dedicated to healthy onions. Furthermore, bruised, crushed, or otherwise damaged onions that enter controlled atmosphere storage tend to be more susceptible to post-harvest disease, and the addition of such onions to storehouses can lead to the spread of infections and substantial financial losses for onion producers. Improved quality assurance technologies could lead to a grading system that would rate individual onion bulbs in terms of their storability, allowing onion producers to discard bulbs with latent infections and divert lightly damaged but still salable bulbs to immediate sale at fresh markets or for processed foods, while ensuring that only the most sound bulbs enter controlled atmosphere storage.

Current research in the area of nondestructive onion postharvest disease detection can be divided into three broad classes: chemical detection, via gas chromatography or electronic nose technologies, of volatile metabolites associated with pathogen infection in onion bulbs; imaging technologies that detect damage or signs of infection on the surfaces or first inner scales of onion bulbs; and x-ray imaging modalities that detect internal damage and defects in onion bulbs.

1.5.1 Chemical Detection of Pathogens

Several researchers have explored detection of volatile metabolites associated with onion pathogens. Vikram et al. [51], using gas chromatography mass spectroscopy, were able to detect 12 distinct volatile compounds associated with several pathogen species, including *Botrytis allii*, that they injected into onion bulbs. Of these 12 compounds, 6 were only detected in pathogen-inoculated bulbs, and not in water-inoculated controls. Such results show promise in the development of a metabolic chemical fingerprint that could potentially be utilized in the detection of pathogen growth in storage facilities. Prithiviraj et al. [37] also found disease discriminatory compounds in laboratory-inoculated onions, using GC-MS. They determined that acetic acid-hydrazine propylcarbamate, 1-bromo-1-propene, acetone, 1-ethenyl-4-ethyl-benzene, thiirane, and 1-(methylthio)-E-1-propene were all specific to bulbs that had been inoculated with *B. allii*. Though these results differ from those found by Vikram et al. [51], different onion species being studied as well as differing time periods between inoculation and measurement as well as the quantity of headspace gases allowed to accumulate could account for these differences.

Li et al. [27] utilized a gas sensor array (electronic nose) and principal component analysis to generate metabolic fingerprints of onions inoculated with *B. allii* and *B. cepacia*. They determined that volatile compound profiles changed substantially as an active infection progressed, and were able to discriminate diseased bulbs from healthy control samples with over

97% accuracy. Though the volatile profiles associated with *B. allii* and *B. cepacia* were more similar to each other than to the healthy control group, Li et al. [27] were able to develop a model that could discriminate between the two diseases. Such findings could be useful not only in locating diseased onions in storage, but also in determining appropriate treatment strategies to control specific pathogens once they have been detected.

1.5.2 Surface Imaging

Hyperspectral imaging has been widely used in the agricultural field, owing to its ability to nondestructively detect differences in chemical compositions within a commodity. Wang et al. [52] developed such a system to discriminate healthy onion bulbs from those that had been inoculated with *B. cepacia*. In this study, it was found that near-infrared images of 1070 nm and 1400 nm combined with a support vector machine model could be utilized to successfully detect detect the presence of this bacterium with a classification accuracy greater than 87%, and data could be obtained from as deep as the third inner scale of the bulb. Such techniques could be useful in detecting and screening out onion bulbs that show the presence of *B. cepacia* but do not yet exhibit human-detectable signs of damage.

Meglinski et al. [34] proposed an optical coherence tomography-based screening method to detect disease and bruise damage in intact onion bulbs. In this study, the researchers were able to detect histological changes in the outer layers of onion bulbs that occurred in response to disease and bruise damage as well as changes that occurred as the bulbs were stored for progressively long periods in controlled atmosphere storage. One notable drawback of these technologies is that they are only capable of imaging the outer layers of onion bulbs, limiting them to the detection only of surface defects.

1.5.3 Planar X-ray Imaging

Planar x-ray line scanning has been explored in recent years as a means to detect internal infections of onion bulbs. X-ray scanners have been touted for their ability to detect morphological features such as double onion bulbs that are less desirable to consumers, as well as the presence of foreign inclusions and seed stems [46]. Shahin et al. [41] developed Bayesian and neural network-based classification systems that could automatically detect image features that could be indicative of disease. These systems were found to be 84% and 90% effective, respectively. In field trials, a commercial x-ray line scanner system was found to reliably detect signs of gross damage, but still had accuracy scores under 90% and a false-positive rate exceeding 10% in detecting diseased or damaged onions [46]. These accuracy and false positive rates, while good, were not deemed good enough for use in actual onion packinghouse quality control.

Mosqueda et al. [35] studied the economics associated with x-ray line scan technologies in onion packinghouses and determined that x-ray line scanners could be economically feasible, based on a simulation model that included multiple machines operating with conveyor belt speeds of 0.25 meters per second. This economic feasibility is greatly diminished, however, during years with high disease incidence as a larger portion of the harvest is discarded as unsalable. Mosqueda et al. [35] argue that the creation of a premium x-ray inspected grade of onion would likely be necessary for such technologies to be utilized in large scale onion packing facilities. These findings align with those of Tollner et al. [47] and Tollner [45], who conclude that the addition of inspection technology to onion packinghouses may increase quality from the end consumer's standpoint, but may negatively impact profit margins of the growers unless the market system governing the sale of onions shifts to reward quality of produce above quantity.

1.5.4 Volumetric Imaging with CT and MRI

The use of CT imaging in quality control of agricultural commodities has been explored in only a very limited capacity. The only known specific instance of CT imaging of onion bulbs in the literature is Maw et al. [31], who briefly addressed the possibility of using CT to detect internal layer separation of bruise-damaged bulbs. Though the researchers provided some example images, there is no in-depth analysis of these images.

As for other agricultural commodities, Fromm et al. [16] used high resolution CT imaging to determine water content and distribution in oak and spruce trees. By first imaging freshly harvested trunk and limb sections, then drying and re-imaging these same sections, the researchers were able to determine the specific localization and concentration of water inside the vascular tissues of the trees. Such research could prove useful in developing monitoring protocols for forestry applications and determining optimal growing conditions for harvestable timber.

Donis-Gonzalez et al. [13] utilized response surface methodology plots to develop an automated image quality optimization system for quality assessment of chestnuts. The researchers modified such parameters as tube voltage and current as well as the thickness of CT slices in a commercial scanner and plotted the values of these parameters against image quality factors such as signal to noise ratio, volume accuracy, high contrast spatial resolution, and low contrast object detectability. By correlating high image quality scores with individual scan parameters, the researchers were able to mathematically determine the optimal scan parameters. Individual scans were then visually inspected and rated by image analysis experts, and these ratings were compared to scores predicted by the statistical model. The statistical scores all fell within a 95% confidence interval of the human perceived quality scores.

Some research groups have utilized magnetic resonamce imaging in concert with x-ray CT to study the effects of pathogens on fruits. Lammertyn et al. [25] utilized both modalities in an exploration of core breakdown in Conference pears. According to this research, MRI

and CT both proved to be effective methods for detecting core breakdown, though both modalities under-reported the actual size of the affected volume. MRI was found to be slightly more reliable than CT in terms of volumetric estimation of browned tissues, as such tissues exhibited relatively uniform densities compared to healthy tissues. Different proton densities and mobility in these browned tissues were more easily detected by MRI. Sonego et al. [43] examined the effects of fungal woolly breakdown on nectarine tissues. By comparing NMR and CT images of decaying nectarines, they were able to determine that woolly breakdown does not lead to pectin depolymerization, but rather leads to water redistribution and micro-scale gas pockets in the tissues of affected fruits. CT proved to be a more reliable diagnostic tool in this instance, owing to the reduction in tissue density caused by gas pockets.

Other research has focused on the use of CT in measuring physical changes in fruits over time. Brecht et al. [7] explored the use of CT imaging to determine maturity levels of tomatoes. By examining x-ray attenuation values within seed-forming cavities in tomatoes, the researchers were able to assign green tomatoes to one of four separate maturity classes. Though average overall x-ray absorption values did not correlate well to specific maturity classes, the researchers found significant correlations between these maturity classes and the number of pixels in cross sectional images exhibiting absorption values above a specific threshold.

Barcelon and colleagues have also utilized CT imaging to study physical changes in fruit maturity, specifically peaches [1] and mangoes [2]. The researchers were able to correlate moisture loss and increased pH with diminished x-ray absorption as peaches and mangoes ripened in storage after harvest. They then generated linear regression models that could be used to determine the age and quality of peach and mango tissue based on x-ray absorption as measured by a CT scanner.

1.5.5 Summary

Each of the onion disease detection modalities addressed above has its associated strengths and weaknesses. Chemical based methods that detect volatile metabolites can reliably detect the presence of specific pathogens, but may not be useful in quickly and accurately locating a single spoiled onion in a larger population. Light-based imaging methods have demonstrated capability in detecting surface damage and the presence of certain pathogens on the outer layers of onion bulbs, but are unable to provide any information about the interior of the bulbs. Planar x-ray scanning has shown some promise in detecting internal rots, seed stems, and physical damage, but has difficulty detecting early-stage infections. Ultimately, a robust onion postharvest quality monitoring system would utilize several modalities: initial light-based imaging could be used to screen out bulbs with pathogens on their surface, planar x-ray or CT imaging would be used to screen out bulbs with internal damage, and a chemical detection system could be utilized inside a controlled atmosphere facility for long-term monitoring of the stored bulbs.

The specific focus of this study is on the development of X-ray computed tomography-based methods for the detection of onion quality factors and under the hypothesis that CT imaging will provide reliable detection of internal damage to onion bulbs due to bacterial and fungal rots and mechanical damage while also providing for the overall assessment of onion bulb quality and market value. Because CT images provide cross-sectional reconstructions of the subject under study, CT scans of onion bulbs could be used not only to detect damage from disease, but also cuts and bruises that increase an onion bulb's susceptibility to disease, as well as the presence of shoots or seed stems and overall shape of the bulbs. Future studies could utilize such data to train machine learning algorithms that could score an onion bulb based on its potential storability and market value, thereby allowing onion growers to store only the best onions and command premium prices for high quality specimens.

1.6 X-rays and Computed Tomography: An Overview

1.6.1 X-ray Emission and Absorption

In most therapeutic and industrial x-ray equipment, x-rays are generated by accelerating electrons in an electric field which are directed to a metallic target. As these kinetic electrons impact the target, they decelerate and release energy in the form of high-energy photons. Equation 1.1 gives the maximum photon energy emitted in relation to electron velocity, v, the mass of an electron, m_e, the fundamental charge of an electron, e, and the potential difference of the electric field used to accelerate the electrons, V:

$$E_{max} = \frac{1}{2} m_e v^2 = eV \tag{1.1}$$

Because the colliding electrons can interact with the metal target in a variety of ways and dissipate varying levels of energy, the x-rays emitted are not all at E_{max}, but exhibit a continuous spectrum of energies (see Figure 1.4 for an example diagram). Lower energy, or soft x-rays, are more easily absorbed by objects, whereas higher energy, or hard x-rays are more readily transmitted through objects [23].

The transmission of a monochromatic x-ray beam through a solid object of homogeneous composition and density can be expressed mathematically by Lambert-Beer's law:

$$N(x) = N_0 e^{-\mu x} \tag{1.2}$$

Where N_0 is the number of incident photons impinging upon the object, x is a linear distance through the object in centimeters, $N(x)$ is the number of photons that have been transmitted through the object at depth x, and μ is the x-ray attenuation constant of the object in inverse

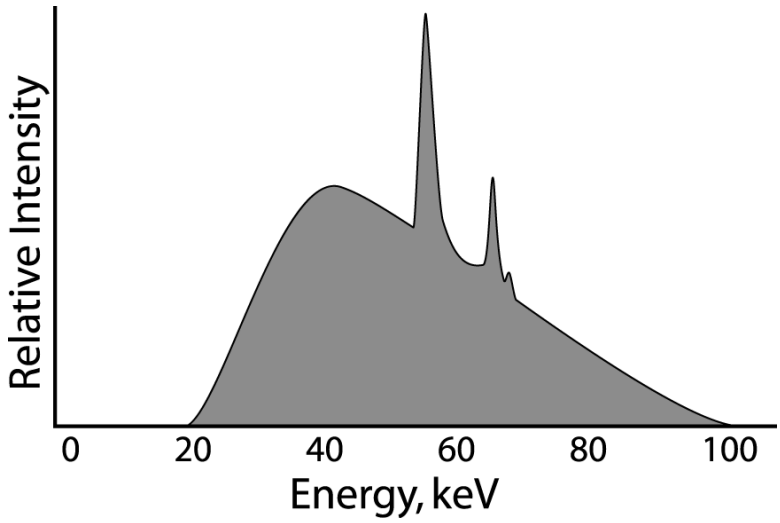

Figure 1.4: *Diagrammatic representation of the spectral output of a tungsten x-ray source operating at 100 keV peak energy. The spikes are due to k-shell emission, in which inner layer electrons in the tungsten target are knocked out of orbit by kinetic electrons. Outer layer, higher energy electrons then fill the vacated spaces, emitting x-ray energy in the process.*

centimeters. It is important to note that μ is a function of both the density of the material of which the object is composed as well as the energy level of the incident x-rays.

The intensity of a polychromatic x-ray beam transmitted through an attenuating object can be calculated from equation 1.3 below:

$$N = N_0 \cdot \int_0^{E_{max}} S(E) \cdot \exp\left(-\int \mu(E,x)dx\right) dE \tag{1.3}$$

Where $S(E)$ is a function describing the spectral intensity of the x-ray beam at energy E as well as the detector's sensitivity to the x-rays at energy E, and $\mu(E,x)$ is the object's x-ray absorption coefficient at energy E and depth x through the object.

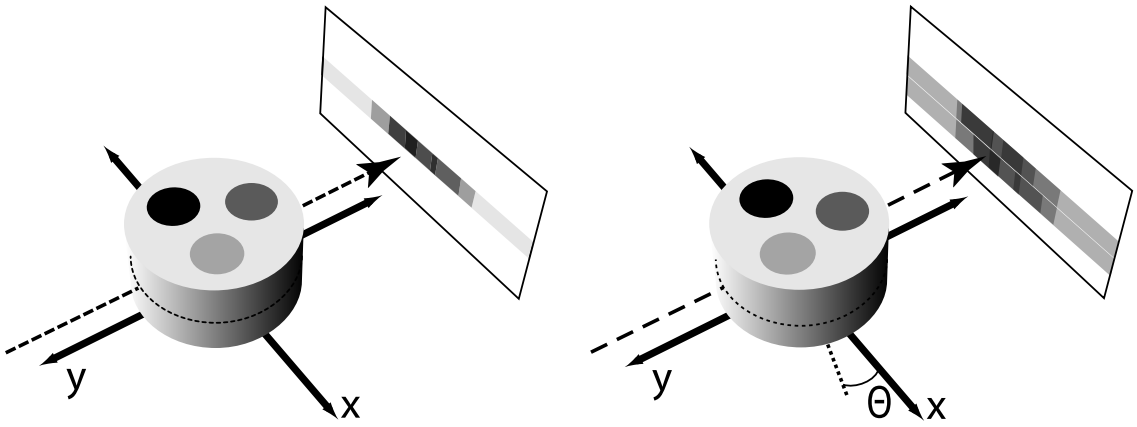

Figure 1.5: ***Left:*** *A single linear projection scan of a phantom. The dashed arrow line shows the path of an example x-ray beam, and the dashed line on the phantom object shows the path the x-ray beam follows.* ***Right:*** *The phantom object is rotated by angle* Θ *and a second linear projection is obtained.*

1.6.2 Tomographic Reconstruction

In computed tomography, a spatially resolved map of the x-ray absorption coefficients throughout a two dimensional slice of an object is constructed. Multiple slices can be obtained to build a three dimensional image of the x-ray absorption in the object. This spatially resolved x-ray absorption map is realized by obtaining multiple parallel beam linear x-ray projections through the same object from different angles and employing computer algorithms to reconstruct the data. See Figure 1.5 for a diagrammatic representation of the acquisition of two such projections. Typical CT scans obtain 180 to 360 of these projections with one degree rotation or less between projections so as to cover 180° or 360° through the object. The resulting collection of projection data is known as a sinogram, as local highly absorptive regions in the object being scanned result in sinusoidal dark regions running the length of the sinogram. Figure 1.6 shows a representative example.

There are a number of reconstruction techniques that can be utilized to obtain a spa-

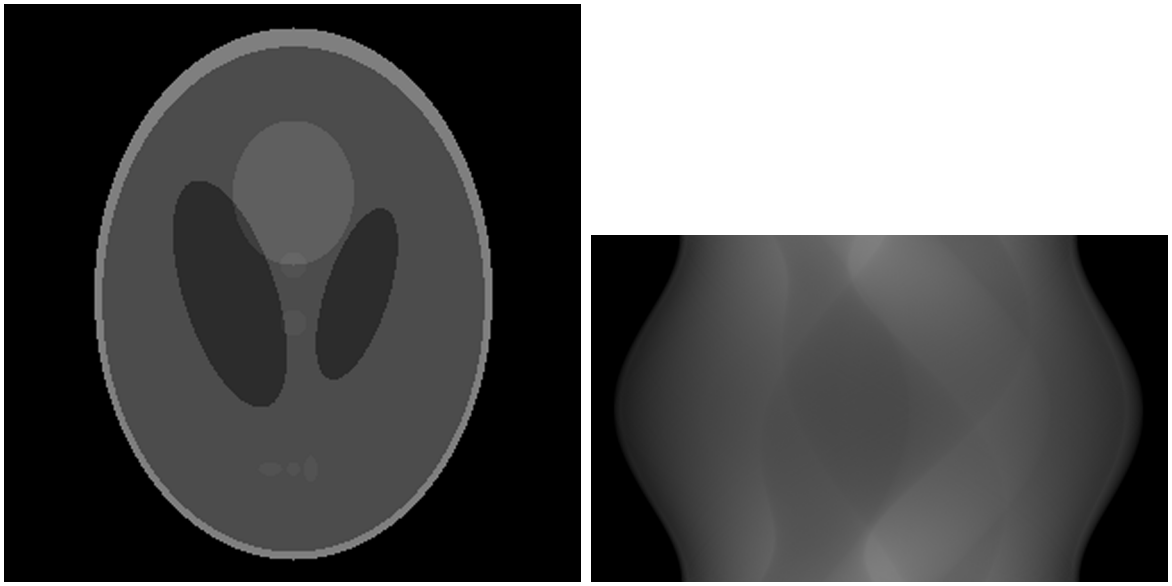

Figure 1.6: ***Left:*** *A computer-generated CT cross section known as the Shepp-Logan head phantom.* ***Right:*** *A sinogram of the Shepp-Logan head phantom consisting of 180 linear projections.*

tially resolved x-ray absorptivity map from a sinogram. Such techniques include arithmetic reconstruction techniques that treat the data as a series of linearly dependent equations. Arithmetic reconstruction requires extensive processing power, and most algorithms will not converge to a stable final solution without some interpolation of missing data. Even with modern hardware acceleration techniques to increase the solution of arithmetic reconstructions to realtime speeds, the final image results are frequently no better than those obtained with less processor-intensive methods. Another technique is to solve the reconstruction in the frequency domain. According to the Fourier Slice Theorem, a Fourier transform of a line from a sinogram obtained at rotation angle θ is the same as the Fourier transform of a slice through the object being scanned running through the origin and slicing through the object at angle θ. These Fourier-transformed projections can then be radially arranged at the center of a placeholder image, and an inverse Fourier transform of this place holder will reveal the

cross section of the object being scanned. The main drawback of this technique is that the place holder image will contain large quantities low-frequency data toward the center of the image where the scan coverage is greater, but high frequency data at the far edges of the image are sparse unless many more time-consuming projections are obtained. The dearth of high frequency data leads to loss of image sharpness, particularly of the edges of features and fine textures. Fourier reconstruction of sinograms frequently relies on data interpolation to artificially recover these high frequency image components [22].

Most medical and industrial CT scanners rely on a technique known as filtered back projection to reconstruct sinograms. In filtered back projection, the lines from the sinogram are rotated by the angle at which they were obtained and "smeared" along the x-ray beam path into a new place holder image. These back projections sum to form a blurred reconstruction of the original image. This blurring is a side effect of the $1/r$ point spread that emerges due to the overlapping back projections. The projections can be filtered in the frequency domain prior to back projection to correct this blur, and several specialized filters have been developed that not only remove blur, but also remove image noise or enhance certain features [22]. All reconstructions in this project will utilize the filter kernel developed by Shepp and Logan [42] (Figure 1.7). The Shepp-Logan filter kernel attenuates the low frequency spectral components of an image to compensate for the $1/r$ point spread, while also slightly attenuating the highest frequency spectral components that are typically caused by noise. The Shepp-Logan filter, therefore, provides a compromise between image sharpness and noise attenuation. Figure 1.8 shows an example of an image reconstructed by back projection without any filtering and an image that has been reconstructed via Shepp-Logan filtered back projection.

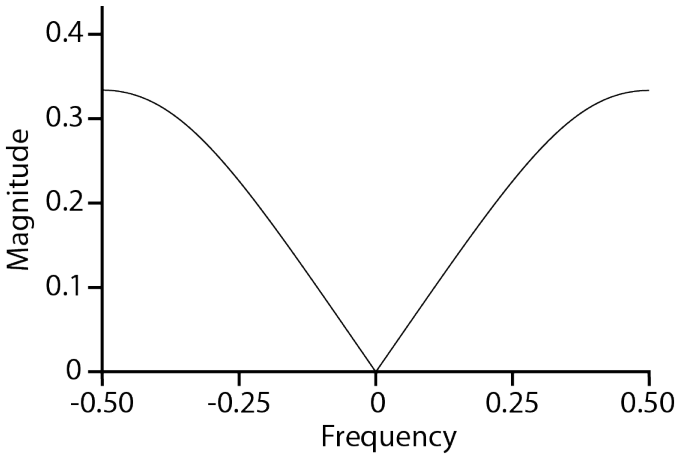

Figure 1.7: *Plot of the frequency response of the Shepp-Logan filter. Low frequencies from the characteristic* $1/r$ *point spread associated with back projection that contribute to blur are suppressed, as are high frequencies that are typically caused by noise.*

Though reconstruction techniques convert sinogram images into planar mappings of x-ray absorption coefficients, they must be normalized if they are to be compared to other reconstructed images. Several factors affect the intensity of emitted and detected x-rays, and these high levels of variability can make comparisons between two images, even those obtained within the same CT scanner, difficult to compare reliably. Ambient temperature, power fluctuations, and age of the x-ray tube are just a few factors that can affect x-ray absorption values in images. To control for this variability, the absorption value of water in a particular CT scanner is obtained by scanning a phantom, the absorption values in the image are normalized according to this value, and this normalized value is multiplied by 1000:

$$I_{Hounsfield} = \frac{\mu_{pixel} - \mu_{water}}{\mu_{water}} \cdot 1000 \tag{1.4}$$

Pixels in the image corresponding to water, therefore, have a value of 0, whereas low

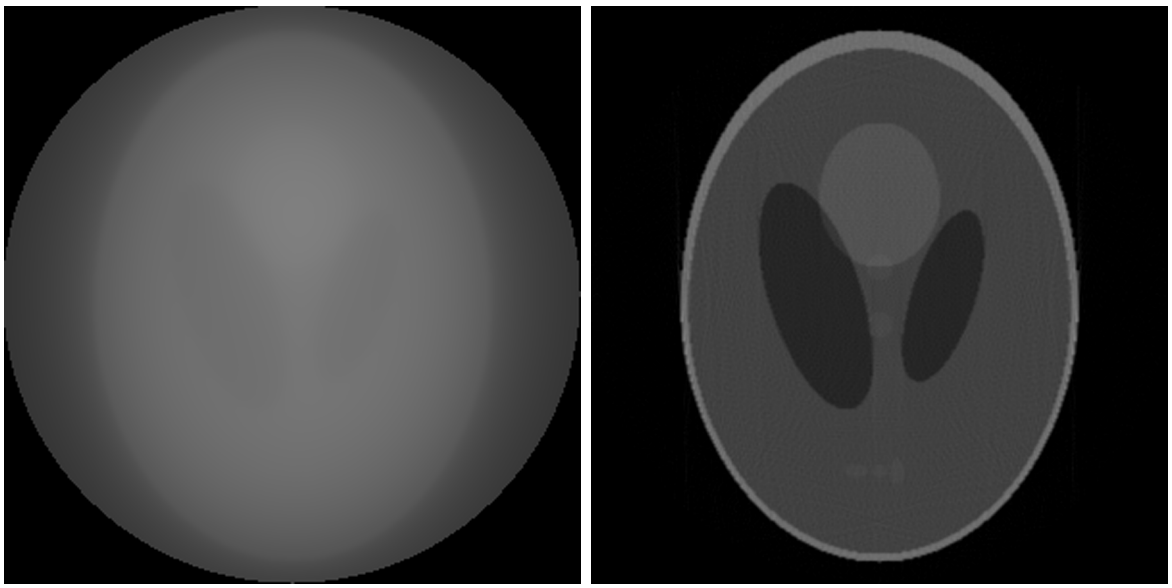

Figure 1.8: ***Left:*** *A Shepp-Logan head phantom image that has been reconstructed without any filtering.* ***Right:*** *The same image reconstructed with a Shepp-Logan reconstruction filter.*

density materials have negative values (air has a Hounsfield value of -1000), and materials of higher density than water have Hounsfield values greater than 0.

1.7 Image Analysis

1.7.1 Cluster Analysis

In reconstructed CT images, regions of an object with low x-ray absorptivity (i.e. low density) appear as dark pixels, whereas denser, more x-ray absorptive regions appear as brighter pixels. Using these properties, one can segment regions of an image into low density and high density components based on the pixel intensity values of the regions. One of the simplest methods of image segmentation is a bimodal operation in which a threshold value is selected, and pixels in the image with intensity values below this threshold are determined

to be background and are separated from pixels whose intensity values are equal to or above this threshold value.

Groups of adjoining pixels that have been segmented from the image's background are known as clusters or features. There can be several distinct clusters within a single image. Since the size and shape of these clusters or features are determined by actual physical properties of the object being analyzed, analysis of these traits can yield valuable information about the physical structures of the object under study. The size of a feature can be determined by counting the number of pixels within its borders. If the resolution of the image is calibrated to real world units, this pixel surface area can be correlated with the physical size of the associated structure in the object under study.

The aspect ratio of a cluster is a quantitative measure that describes the shape of the cluster in terms of its width and height. The centroid of the cluster is determined, and the maximum distance between the centroid and the boundary of the cluster, as well as the maximum distance between the centroid and boundary are calculated. The aspect ratio is the ratio of these two distances. Thus, a circle has an aspect ratio of 1, whereas elongated or elliptical shapes have aspect ratios greater than 1 [21].

The compactness of a cluster is the squared length of its perimeter divided by its surface area. As the most compact shape possible is a circle (lowest ratio of perimeter to surface area), clusters exhibiting high compactness values may exhibit highly irregular outlines or may be greatly elongated [21]. The discrete nature of image pixels can be a problem when computing these metrics, as the physical object being imaged may have regions that are so small that their boundaries can not be accurately represented at the resolution that the scanner is capable of obtaining.

Irregularity is an additional measure that can indicate how irregular the outline of a cluster is. The irregularity is the ratio of the standard deviation to the mean value of the distance from the cluster's centroid to its outer perimeter. Clusters with irregular outlines

have higher computed irregularity values, whereas elliptical shapes with smoother outlines have lower irregularity values. Therefore, this measure is a better indication of the characteristics of the outline of a cluster, whereas compactness simply indicates how acircular a cluster is [21].

1.7.2 Fourier Shape Descriptors

As noted in the previous subsection, a cluster can be described in terms of the distance between its centroid and the points that make up its outer perimeter. This perimeter can effectively be "unrolled," and described as a function of distance from centroid versus angle. As the outer perimeter of a cluster is a closed shape, this function is periodic, and can be analyzed using the Fourier transform. A perfect circle has a constant distance between its centroid and outer perimeter; therefore its spectral decomposition will yield only a single frequency component in Fourier space. An ellipse will yield two frequency components correlating with its major and minor radii, and irregular shapes will have several frequency components [21]. Equation 1.5 shows how the discrete Fourier coefficients C_n are computed, where K is the period of the function and r_k is the cluster's radius at angle k.

$$C_n = \frac{1}{K} \sum_{k=0}^{K-1} r_k \cdot \exp\left(-\frac{2\pi jnk}{K}\right) \tag{1.5}$$

As C_0 is the mean radius of the cluster being studied, a size invariant form of the Fourier descriptors, ζ_n is used, which normalizes all coefficients by this mean radius: $\zeta_n = \frac{C_n}{C_0}$. The value of Fourier shape descriptors is their ability to quantify abrupt changes in the outer perimeter of a cluster. A round shape with a sharp divot in its surface, for example, will exhibit high values for high order coefficients.

Chapter 2

Materials and Methods

This project utilizes a custom-built x-ray computer tomography scanner system that was constructed at the University of Georgia's College of Engineering by Dr. Mark Haidekker.

The goals of this study were to assess the capabilities of this low-cost x-ray CT imaging system in determining the overall quality of onion bulbs, and to characterize cross sectional images of the scanned onions to determine the presence of pathogen infections, mechanical damage, or morphological features that could lead to losses in storage. Four separate CT-based onion quality assessment experiments were undertaken:

1. Initial exploratory scans of pathogen-inoculated onion bulbs and phantom objects to assess the feasibility of the project and to characterize the CT scanner and determine optimal scan parameters

2. Transverse and longitudinal cross sectional scans of onion bulbs that were hypodermically inoculated with pathogenic bacteria

3. Three dimensional scans of bulbs whose neck regions were inoculated with pathogenic bacteria or fungi

4. Transverse and longitudinal scans of onions that were subjected to impact damage

2.1 Overview of the Apparatus

Onion bulbs were scanned in a custom-designed computed tomography (CT) scanner apparatus. The components of this apparatus include a dual energy pencil beam x-ray emitter salvaged from a dual energy x-ray absorptiometry (DEXA) machine which produces x-rays at 140kV and 70kV peak energies (Figure 2.1, part a). The x-ray detector is a photomultiplier tube (PMT) (Figure 2.1, part b) with an anode voltage that can be adjusted by the user to a maximum of 1kV. The PMT and its associated driver circuitry convert incident x-ray intensity to a proportional voltage. The overall sensitivity of this conversion is adjusted through the anode voltage, and through gain-adjustable amplifiers that adjust the overall signal levels before they are digitized and sent to a computer system for analysis. This amplifier system has an added capability of separate gain levels for the low energy 70 kVp x-rays and higher energy 140 kVp x-rays, allowing the user to increase the gain for the weaker 70 kVp signals and decrease the gain associated with the 140 kVp x-rays, preventing signal clipping.

Specimens are rotated and translated in the x and y dimensions between the x-ray emitter and detector by a mechanical positioning system (Figure 2.1, part c) and rotational stage (Figure 2.1, part d). The x-ray beam is collimated with two sets of apertures. A rotating wheel with 13 user selectable positions is placed directly in front of the x-ray emitter (Figure 2.1, part e). This wheel contains 0.6 mm, 2.25 mm, and 3.1 mm diameter round apertures as well as several slit apertures and a mirror for reflecting a laser beam along the approximate path of the x-ray beam so users can position the specimen being scanned more accurately. A second set of apertures is located on a brass plate that is placed between the photomultiplier tube and the x-ray source (Figure 2.1, part f). This plate contains 0.6 mm, 1.0 mm, and 2.5 mm diameter round apertures for detector side collimation, and the user can position this plate so the appropriate aperture is directly in the path of the x-ray beam.

The apparatus is controlled from a personal computer by custom-designed computer

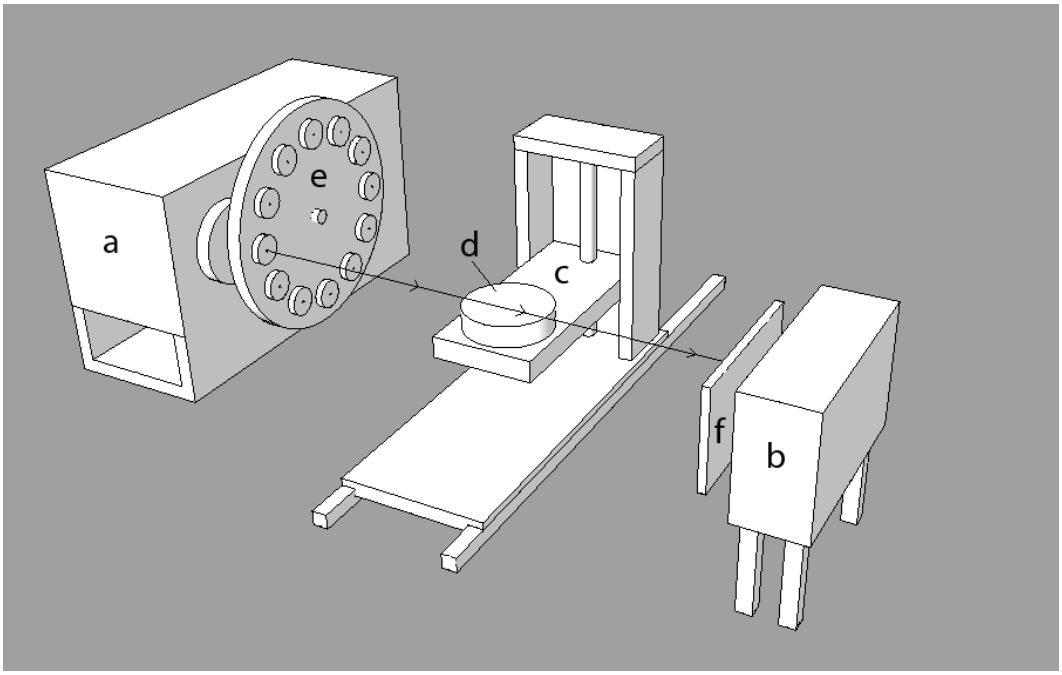

Figure 2.1: *Diagram of the CT scanner. The line with arrowheads shows the path of the x-ray beam. The x-ray tube (**a**) emits x-rays that travel through a user-selected collimator on a Geneva wheel (**e**). The x-ray beam travels through the specimen under study, which is placed on a rotating stage (**d**), which, in turn, rides on a vertical positioning stage (**c**). After passing through the specimen under study, the x-ray beam travels through a detector-side collimator (**f**) and impinges upon a photomultiplier detector (**b**).*

software with a graphical user interface. This software allows the user to specify the image acquisition mode, collimator settings, number of projections to obtain, angle between projections, and photomultiplier anode voltage. Acquisition modes include a 1-dimensional profile scan which moves the object under study laterally through the x-ray beam and produces a plot of the detected x-ray intensity versus lateral position. Such scans are useful to quickly verify that proper scan width and photomultiplier settings have been set. The scout scan mode combines multiple profile scans at varying y-positions to generate a two dimensional projection of the object, and is essentially a planar x-ray projection scan obtained line by line. Figure 2.2 shows a scout scan of an apple. The cross sectional scan mode works by scanning the object laterally, rotating it by a set amount, and repeating this lateral scan to produce a sinogram. By repeating this 2d scan at varying y-positions of the object and generating multiple sinograms, a 3-dimensional voxel reconstruction of the object can be generated. In all scan modes, the high x-ray energy (140kVp) and low x-ray energy (70kVp) images are simultaneously acquired. The in-plane resolution of reconstructed cross sectional images is 0.5mm square, and in three dimensional mode with 0.5mm slice thickness, isometric voxels are possible. As the diameter of the x-ray beam is effectively 0.6mm with collimation, voxel dimensions less than 0.5 mm are impractical, though still technically possible.

Tomographic reconstruction was accomplished with the software package Crystal Image v.0.9.4, .0.9.5, and .0.9.6 beta [20]. Raw sinograms are loaded into Crystal Image and the intensity of pixels associated with the (non-attenuated) x-ray beam through air is determined as a baseline value. The intensities of the pixels in the image are then scaled by this baseline value, and the logarithm of this ratio is the line integral of the absorption of the x-ray beam through the object. Finally, the Shepp-Logan backprojection reconstruction method is applied to this logarithmatized sinogram, yielding a two dimensional cross sectional image of the scanned object's x-ray absorption values. The reconstructed image is saved as a 32-bit floating point grayscale image in the TIFF image format for further analysis.

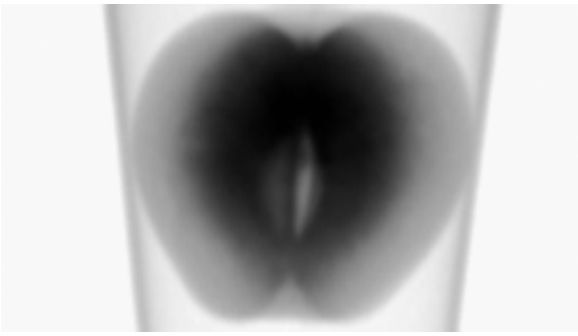

Figure 2.2: *Scout scan of an apple secured to the specimen stage in a plastic drinking cup. Darker shades indicate higher x-ray absorption.*

2.2 Experiment 1: Initial Exploration and Image Optimization

Numerous initial tests were conducted to ascertain the optimal operating parameters of the CT scanner. Such parameters include photomultiplier tube anode voltage settings, x-ray aperture sizes, and the number of projections necessary to build a sinogram that will yield sufficient image quality upon reconstruction to detect damage to the onion bulbs. Additionally, several methods of securing the onion bulbs in the path of the x-ray beam were tested, and the lateral movement stage inside the CT apparatus was modified to increase stability and dampen mechanical vibration.

Vidalia onion bulbs were provided by Dr. Changying Li's research group in Tifton, Georgia. Several of these bulbs had already been inoculated with B. *allii*, B. *cepacia* or P. *viridiflava* as an early initial test to determine whether damage caused by these pathogens was detectable with the CT apparatus. Overall sixteen total bulbs were scanned, four samples inoculated with each pathogen, and four untreated bulbs.

The first operational parameter to determine was minimum number of sinogram lines

necessary to obtain images of usable quality. While more sinogram projections provide more information about the object being scanned, making for sharper and cleaner reconstructions, each scan obtained adds to the total time of image acquisition. A balance must be struck between scan time and image quality. Images were obtained with 360 sinogram projections (the object was rotated a full 360 degrees in one degree increments), 180 projections (180 degrees of rotation with 1 degree increments), and 90 projections (180 degrees of rotation with 2 degree angular increments). These sinograms were reconstructed, and the reconstructed cross sections were subjectively evaluated to determine which parameters provided the best balance of scan time and image quality.

The dynamic range of the image reconstructions is also an important image quality factor to consider. An experiment was conducted to determine optimal photomultplier anode voltage and x-ray aperture configurations. Photomultplier anode voltage determines the sensitivity of the detector to the x-rays impinging upon it, and the x-ray apertures determine the overall density of the x-ray flux interacting with the detector. Setting a too low photomultplier anode voltage or too narrow aperture decreases the overall sensitivity of the system and results in images with a narrow range of pixel intensity values, making it difficult to differentiate between distinct regions inside the object being scanned. Setting the photomultplier anode voltage too high, or allowing too many x-rays the reach the detector by choosing a too large aperture results in clipping, that is, the actual x-ray intensity value is beyond the system's maximum detectable range, thus these high intensity values are clipped to this maximum value and data are lost. To determine optimal detector anode voltages and apertures, a water phantom was scanned with the detector anode set to 600, 700, 800, 900, and 1000 volts, with beam aperture sizes of 0.6 mm and 2.25 mm, and a 2.5 mm detector side collimator. The phantom object was constructed out of a water-filled plastic drinking cup that could be bolted to the rotational stage in the CT scanner. Because onion bulbs are composed primarily of water, this phantom object was thought to be provide a good

approximation of an onion bulb. The reconstructed images were evaluated subjectively to determine the best combination of settings.

Finally, a two-channel switchable amplifier was added to the photomultiplier detector's output. This amplifier allows the user to specify separate gain levels for the detected signals resulting from 140kVp and 70kVp x-ray energies. Weak signals resulting from the 70kVp x-ray beam can be greatly amplified at the expense of decreased signal to noise ratio, whereas the higher signal levels from the 140kVp x-rays can be amplified less so as to avoid oversaturation and clipping.

2.3 Experiment 2: Hypodermic Inoculation

This next experiment was conducted to determine the best two-dimensional projection images for determining damage caused by pathogens, and to chart the progress of a pathogenic infection in the onion bulb. Agar plates with B. *cepacia* and P. *viridiflava* inoculum and Vidalia onions were supplied by Dr. Changying Li's research group. Bacterial pathogens such as B. *cepacia* and P. *viridiflava* typically require a wound to enter onion bulb tissues, thus it was decided to utilize hypodermic needles to introduce the bacterial pathogen cultures to the sample onion bulbs[1].

2.3.1 Inoculation Procedure and Imaging Protocol

The onions were stripped of their dry outer skins and submerged in a 2% sodium hypochlorite solution for one minute to sterilize the surface of the bulb. Prior to inoculation, the onions were pre-screened for signs of infection or damage via visual inspection, and imaged by CT in transverse and longitudinal projections to obtain baseline pre-infection images and to confirm that there were no internal defects.

[1]Personal communication with Dr. Ronald Gitaitis, May 23, 2012

Bacterial colonies were swabbed from culture plates and suspended in 5 mL sterilized water. Approximately 0.3 to 0.5 mL of the bacterial suspension was injected approximately 1-2 cm deep into the side of the bulb with a 19 gauge hypodermic needle, and the injection site was marked with a permanent marker. The inoculated onions were placed individually into plastic bags to prevent cross-contamination and to provide a high humidity environment for the pathogen to grow. Onions inoculated with B. *cepacia* were placed in an incubator set to 30 ° C, while onions inoculated with P. *viridiflava* were placed in a dark drawer at room temperature.

The precise location of the cross sectional scans was chosen so the scan plane coincided with the injection site of the hypodermically inoculated onion bulbs. The reasoning behind this was that damage to the onion tissues caused by the bacteria would first be evident in the immediate vicinity of the injection site. The pathogen-inoculated onion bulbs were imaged at 3-7 day intervals over the course of a 28 day long incubation period in transverse and longitudinal cross sections until clear signs of damage were evident.

2.3.2 Image Analysis

The 140kVp x-ray energy level sinograms were reconstructed with Crystal Image v.0.9.5 and saved as 32-bit signed floating point TIFF files. After reconstruction, negative-valued pixel intensities existed throughout the image; such physically impossible values are a side effect of the filtered backprojection reconstruction technique used to reconstruct the images, and Crystal Image's soft thresholding algorithm was applied to the image to clip any negative values to zero.

The images were then converted to a 16-bit integer format that is more widely recognized by other image processing software packages via a custom program written in the C programming language. Images were imported into Adobe Photoshop CS4 (version 11.0), and an image gallery of each specimen was constructed so as to show the progression (or lack

thereof) of the pathogen infections in the bulbs. To prevent the plastic specimen holders and foam cushioning from interfering with these additional image analysis procedures, they were manually painted out of the images with Photoshop.

For analysis of internal features, the un-modified transverse cross section images were opened in Crystal Image, a 3x3 Gaussian blur was applied, and the bi-level binary threshold algorithm was applied such that internal voids and lesions in the images showed up as black features inside the white bulb silhouette. The black-white image values were then inverted so the image background appeared white in color, the bulb tissues appeared as black, and the voids and lesions inside the bulb appeared as white. The now white image background was flood filled with black, resulting in a final image consisting only of the isolated voids and lesions on a black background. Crystal Image's "Cluster Labeling" command was then applied to the image. This command computed the size, aspect ratio, compactness, and irregularity of each isolated onion damage feature, and these feature characteristics were saved in tabular format in a text file for further analysis.

For analysis of the outer edges of the onion bulbs, transverse cross section images were opened in Crystal Image, a 3x3 Gaussian blur was applied to reduce image noise, and a bilevel thresholding algorithm was applied to produce a binary segmented image such that onion bulb tissues were white and the background completely black. The threshold level was set to 30% of the maximum pixel intensity value in the image. In many cases, internal voids in the onion bulb also showed up as black, and Crystal Image's "Fill Holes" command was utilized so that a monolithic silhouette of the onion bulb was the only remaining image feature. Crystal Image's shape descriptors command was then run on this image, calculating the onion bulb silhouette's centroid, compactness, aspect ratio, irregularity, and Fourier shape descriptors.

The Fourier shape descriptors ($C_0 ... C_9$) for each onion specimen were imported into a Microsoft Excel spreadsheet, and each set of Fourier descriptors was normalized according to

the mean radius (C_0) of each onion's silhouette. These normalized descriptors, $\zeta_1 ... \zeta_9$, have the advantage of being scale invariant, thus individual onion bulbs can be compared to one another. The mean value for the descriptors ζ_1 through ζ_9 was computed for all day 0 bulb cross section images. This day 0 population average was used as a baseline against which to compare Fourier coefficients associated with scans of damaged bulbs.

2.4 Experiment 3: Onion Neck Inoculation

As the neck region of the onion bulb is a particularly vulnerable area and potential point of entry for several pathogens, additional inoculation techniques were explored in hopes that inoculation of the neck regions of the specimen bulbs would provide a pattern of tissue damage more consistent with those of naturally occurring infections. Botrytis neck rot, in particular, is noted for its growth pattern, originating at the neck region of the onion bulbs, and traveling downward inside the bulb.

2.4.1 Inoculation and Imaging Protocols (2D)

An initial study was conducted to observe the spread of Botrytis neck rot through onion bulbs. Georgia-grown Vidalia onions and *B. allii* culture plates were obtained from Dr. Changying Li's research group in Tifton, Georgia. Onion bulbs were pre-screened for signs of preexisting damage or infection, and those displaying such signs were discarded. Each bulb was scanned prior to inoculation for a baseline set of images in longitudinal and transverse cross section at the widest point of the bulb. The bulbs were then immersed in a 2% sodium hypochlorite solution to sterilize their surfaces. The dried tops of the bulbs were then removed with a sterilized razor blade until the fresh ends of the onion scales were revealed, and *B. allii* fungal colonies and spores were swabbed onto the wound from the culture plate. The inoculated onions were stored in a plastic container at room temperature in the dark

with moistened paper towels to increase the ambient humidity. Each bulb was re-imaged in transverse and longitudinal section after 7, 14, and 28 days, or until the bulbs had decayed to the point that they could no longer be handled for imaging.

2.4.2 Inoculation and Imaging Protocols (3D)

A similar experiment was conducted later in the year, when Vidalia onions were unavailable, with imported Peruvian-grown sweet onions, and three dimensional images were obtained. Nine specimen bulbs were chosen at random and pre-screened for signs of existing damage or infection and surface sterilized with sodium hypochlorite solution. Prior to inoculation, baseline scans of the bulbs were conducted. Transverse cross sections were obtained at 5 mm increments along the root-shoot axis of the bulb. Three bulbs were then inoculated with *B. allii* via the neck inoculation procedure described above. Another three bulbs were inoculated with *B. cepacia*, and the remaining three were inoculated with *P. viridiflava* via a similar method in which bacterial colonies were swabbed from culture plates and smeared directly onto the exposed onion scales.

After the baseline scan and inoculation, the *B. allii* and *P. viridiflava* bulbs were stored in separate plastic containers at room temperature with moist paper towels, and the *B. cepacia* bulbs were stored in another container in a 30° C incubator with moist paper towels. Three dimensional transverse scans were repeated at seven day intervals unless clear external signs of damage appeared before the next seven day period had elapsed. In some cases, in the interest of saving time, exploratory transverse scans were conducted to ascertain whether the pathogen-induced damage had progressed sufficiently to yield useful transverse images. If no signs of damage were present in the transverse images, the 3d scan was not conducted. The inoculated onion bulbs were incubated for a seven week time period and discarded upon the conclusion of this period, whether pathogen damage was evident or not, after obtaining a final set of scans.

2.4.3 Image Analysis

Transverse and longitudinal images of the Botrytis-inoculated Vidalia onions were reconstructed and the specimen holders were removed using the same techniques outlined in Experiment 2. The transverse images were segmented, and interior lesions and voids were also segmented and analyzed using the same techniques outlined in Experiment 2 (page 33).

Transverse slices of the Peruvian onions obtained at 140 kVp were reconstructed in Crystal Image and saved as 32 bit TIFF files. These TIFF files were imported into ImageJ v.1.46r, and ImageJ's 3D projection tool was used to create composite images displaying all slices of a bulb at an angle so as to facilitate side by side comparison of the slices of initial baseline scans of a bulb and later, post-inoculation scans of the same bulb (See Figures 3.41 – 3.49).

Textural analysis was conducted on the baseline scans of the bulbs for the identification of multiple bulb centers. Image slices were loaded into ImageJ, converted to a 16 bit grayscale format, and ImageJ's variance filter was executed with a 3x3 pixel kernel size on each slice. The slices were then combined via a Z-projection of the mean pixel values along the Z-length of the stack to diminish the effects of small textural inhomogeneities between slices while retaining the bright regions associated with abrupt changes in pixel intensity that persisted between slices that were more likely to be associated with air gaps caused by multiple centers in the bulbs.

2.5 Experiment 4: Onion Bruising

This experiment seeks to build on the work of Maw et al. [31], who demonstrated that internal onion layer separation due to bruising can be seen in CT images, and the work of Herold et al. [24], who demonstrated that onion storage losses could be correlated with the severity of mechanical bruise damage inflicted on the bulbs. An automated, detectable method of

determining the level of mechanical stresses individual onion bulbs have experienced could help determine their storability and susceptibility to postharvest diseases.

Onion bulbs subjected to impact damage from falls or rough handling frequently do not display any outward signs of damage, and even bulbs that have substantial internal bruising may appear externally healthy. According to Purvis and Brock [38], bruised onions tend to be more susceptible to the spread of Botrytis neck rots in storage, thus a scanning system that can detect and discard these non-obviously damaged onions could help prevent storage losses in controlled atmosphere systems. These bruised onions could still be sold for use in processed foods or at reduced price at fresh markets, allowing onion producers to devote storage space to onions that are more likely to survive for long periods in storage.

2.5.1 Treatment and Imaging Protocols

Following the procedure outlined in Herold et al. [24], medium sized onion bulbs were chosen at random, dropped onto a hard concrete floor one or more times from varying heights, and imaged in transverse and longitudinal cross section at the site of impact to determine detectable damage thresholds in the CT images. The procedure is as follows:

Healthy, untreated onions were imaged in transverse and longitudinal cross section to obtain baseline image data, and any bulbs exhibiting signs of damage were discarded and replaced until healthy ones are located. As the mass of the bulb plays an important role in the impact forces experienced due to a fall, the onions were weighed prior to any experiments. The onions were dropped from heights of 17.5 cm, 35 cm, 70 cm, or 105 cm onto a hard concrete floor. As a single fall from 17.5 cm is unlikely to cause substantial damage, the effects of repeat impacts were examined. The onion dropped from 17.5 cm was dropped a total of six times; the 35 cm bulb was also dropped six times; the 70 cm bulb was dropped twice, and the 105 cm bulb was dropped once. The point on the onion bulb at which the initial impact is made was marked with a permanent marker, and subsequent drops were

conducted such that each additional impact occurred at or near this initial site, causing repeated damage to the same general area on the bulb.

Every onion was re-imaged in longitudinal and transverse cross section at the site of impact immediately after the initial drop. The dropped onion bulbs were stored for three days at room temperature in the dark, and then re-imaged in longitudinal and transverse cross sections.

2.5.2 Image Analysis

Images were reconstructed from 140 kVp sinograms using Crystal Image v.0.9.5, negative pixel intensity values that remained as artifacts of filtered back projection reconstruction were clipped to zero, and images were saved as 32-bit signed floating point grayscale TIFF image files. These 32 bit images were then batch converted to 16 bit images via a custom-designed program written in the C programming language.

Transverse cross section images were opened in the Mac OS X version of NIH ImageJ v.1.46r, and ImageJ's Threshold operator was used to segment the images by pixel intensity value. Threshold values were chosen manually and subjectively, and these thresholds varied from image to image. After segmentation, onion tissues and the specimen holder appeared as white features on a black background, with some black low density features inside the white onion shape. Specimen holder features were manually selected by enclosing them with a polygon selection tool, and these selections were filled with black, thereby leaving only the onion and its low density features in the image. This segmented image was then saved as a grayscale PNG file.

The centroid of the overall onion shape was obtained by filling all the black low density features inside the onion's silhouette with white, and using ImageJ's 'Analyze Particles' command. The pixel area of the shape as well as the x and y coordinated for its centroid were recorded. The segmented PNG files were then reopened, and the dark low density regions

inside the onion were isolated by inverting the pixel values so onion tissues were black on a white background. This white background was then flood filled with black, leaving only the low density internal onion features as white shapes on a black background. The pixel values were the inverted again, and ImageJ's 'Analyze Particles' command was executed, reporting the x and y centroid values, pixel area, aspect ratio, circularity, and solidity of each contiguous block of white pixels. These values were exported to a Microsoft Excel file for further analysis.

A weighting system was devised that would give preference to low density features farther from the center of the onion, as these features were deemed to be most likely caused by bruise damage, whereas low density features near the center of the onion were more likely to be due to emergent shoots or damage caused by infections. Feature data were loaded into Microsoft Excel:Mac 2011, and each low density pixel cluster's distance from the centroid of the overall onion shape was calculated. Each cluster's distance from the centroid was normalized by the maximum feature distance detected in the image, and this normalization was squared. Therefore, the maximum normalized squared distance weighting factor in the image is 1, which corresponds to the most distant feature, and features near the center of the onion bulb have weighting factor values less than 1. Each weighting factor was then multiplied by the pixel area of the corresponding feature, yielding a weighted damaged area metric. Equation 2.1 describes the weighted damage area metric, where a is the area of the individual cluster, d is its distance from the onion centroid, and d_{max} is the distance between the onion centroid and the most distant cluster. If the weighted damaged area of a given cluster exceeds a pre-determined threshold value it is considered part of a bruise; features whose weighted damaged area values are beneath the threshold are not considered bruise damage.

$$WeightedDamageArea = a \cdot \left(\frac{d}{d_{max}}\right)^2 \tag{2.1}$$

Finally, an additional metric was developed to determine the localization of bruise damage in an onion bulb and to prevent spurious, naturally occurring, low density regions in the onion bulb from being considered in damage estimation of a bulb. Bruise damage features appear to cluster around the center of impact, so closely clustered damage features are more likely to be caused by bruising than features that are spread throughout the bulb. A weighted center of mass function was devised to accomplish these goals. Each damage feature is assigned a weighting factor consisting of its normalized distance from the onion centroid multiplied by the pixel area of the feature. Each feature's weighting factor is then multiplied by its x and y coordinates. The weighted x and y coordinates are summed, and these sums are divided by the sum of the weighting factors to obtain the weighted center of mass for the damage features. Equation 2.2 shows how the x-coordinate for the weighted center of mass is calculated for an image exhibiting m low density clusters, where x_n is the x-coordinate of cluster n's centroid, a_n is cluster n's pixel area, d_n is the distance of cluster n from the onion's centroid, and d_{max} is the maximum distance between a cluster and the onion's centroid. This process is repeated for the y-coordinates, and the resultant x,y coordinate is the estimated center of damage in the onion bulb. Standard deviations for the weighted x and y coordinates are calculated, and damage features whose centers fall outside one or two standard deviations from the weighted center of mass can be excluded from consideration. Specimens exhibiting widely distributed, large sized low density features would have high standard deviations, and such specimens would likely have extensive damage, rendering them unsalable.

$$x_{weighted} = \frac{\sum_{n=1}^{m} \left(x_n \cdot a_n \cdot \frac{d_n}{d_{max}} \right)}{\sum_{n=1}^{m} \left(a_n \cdot \frac{d_n}{d_{max}} \right)} \tag{2.2}$$

Chapter 3

Results and Discussion

3.1 Experiment 1: Initial Exploration and Image Optimization

3.1.1 CT Scanner Mechanical Modification

Initial tests of the CT scanner revealed image blurring that was thought to be due to mechanical vibration of the mechanical stages in the apparatus. As the x-dimension resolution of the scanner is 0.5 mm per pixel, even slight vibrations proved to result in unacceptable images (Figure 3.1). In the device's original conception, the x-direction translational stage was constructed of a sheet of $\frac{1}{4}$ inch thick aluminum. A shallow channel was milled into this stage to accommodate a portion of the y-stage translational gantry that did not sit flush with the surface of the stage. This setup was found to be unacceptably flimsy, and the aluminum sheet was replaced with a repurposed $\frac{3}{4}$ inch thick aluminum optical breadboard.

Subsequent images obtained with this new setup were deemed acceptable based on qualitative visual assessment, and the images presented in the results section for subsequent experiments were all obtained with this new, sturdier stage.

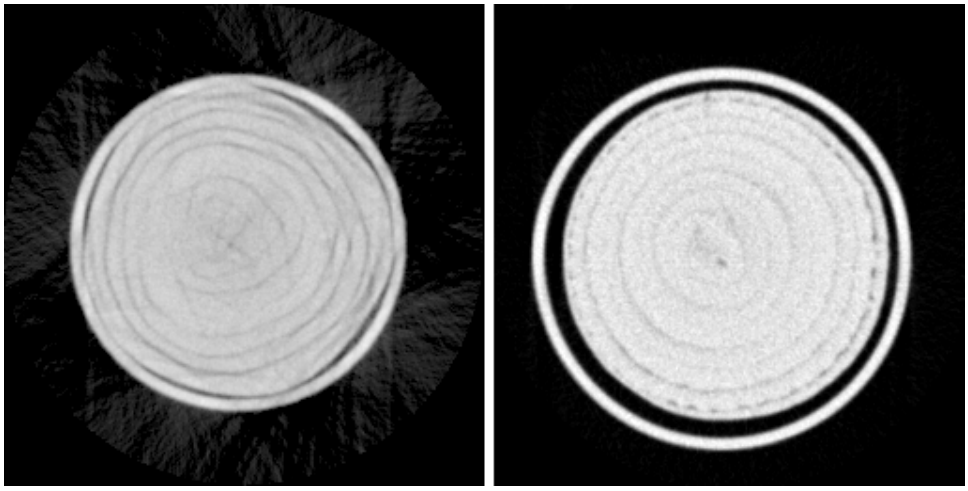

Figure 3.1: ***Left:*** *Movement of the specimen during scanning leads to poor image reconstructions and exhibits typical motion artifacts.* ***Right:*** *Specimen mounted on a stable mechanical stage in a stable holder. Internal structures are sharp and clearly defined.*

3.1.2 Securing the Samples

In early tests of the device, onion bulbs were secured to the rotational stage of the CT scanner by sticky modeling clay. This was found to be unreliable, as the acceleration of the mechanical stages led either to tearing of the dry onion skin to which the clay was adhered, or the warm temperatures inside the scanner led to sagging of the clay. It is of utmost importance to hold the onions securely and prevent them from moving during the scan, and alternative methods were therefore required.

In later experiments, a plastic drinking cup was utilized to secure the onions (Figure 3.2). A hole was drilled in the bottom of this cup, and it was attached to the CT scanner's rotational stage with a machine bolt. The onion to be scanned was wedged in the opening of the cup, and the friction between the onion skin and cup's walls proved sufficient to hold the onion stationary during the scan. This proved to be a more reliable and secure method of holding onion specimens, and several dozen images were obtained using this system.

Figure 3.2: *First onion holder built out of a plastic drinking cup.*

The plastic cup specimen holder did have associated drawbacks. Particularly large onion bulbs would not fit in the holder securely, and small onion bulbs fell to the bottom of the cup and were not held in place by the wall of the cup. Irregularly shaped onion bulbs also proved difficult to secure reliably, as they would only come in close contact with the cup walls at a few points, rather than the entire perimeter as was the case with more round shaped bulbs. A new holder was constructed to solve these problems. This holder was constructed of two sheets of $\frac{1}{4}$ inch thick clear acrylic plastic that had been shaped to approximate the profile of the drinking cup holder, but with a smaller small radius and larger large radius than that provided by the cup-based holder, providing four points of contact with the onion bulb under study (Figure 3.3). The edges of this holder that were to contact the onion bulb were covered in foam insulation for cushioning. The base of this holder was composed of $\frac{1}{2}$ inch thick clear acrylic sheet, and the entire apparatus was secured to the CT scanner rotational stage with a machine bolt.

In practice, this specimen holder was deemed unsuitable for two reasons. First, the overall width of this holder proved to be much larger than the plastic cup-based holder, and lateral scan dimensions had to be greatly increased to accommodate this increased width, particularly when large onions were scanned. This ultimately led to unacceptably long scan times per sample. Additionally, because of the geometry of the holder, in certain orientations, the x-ray beam had to pass through a substantial length of the acrylic plastic before reaching the onion being scanned. This led to severe beam hardening artifacts in the reconstructed onion cross sections as the x-ray beam was attenuated by the plastic (Figure 3.4).

Finally, an adjustable onion holder was constructed out of polyacetal plastic (Figure 3.5). One L-shaped piece bolts to the CT scanner's rotational stage, and another L-shaped piece is allowed to slide to accommodate larger or smaller onions. This movable section is secured to the other by way of machine screws and wing nuts. Large diameter holes have been drilled into the sides of the two L-shaped sections to allow onion roots or necks to protrude, making

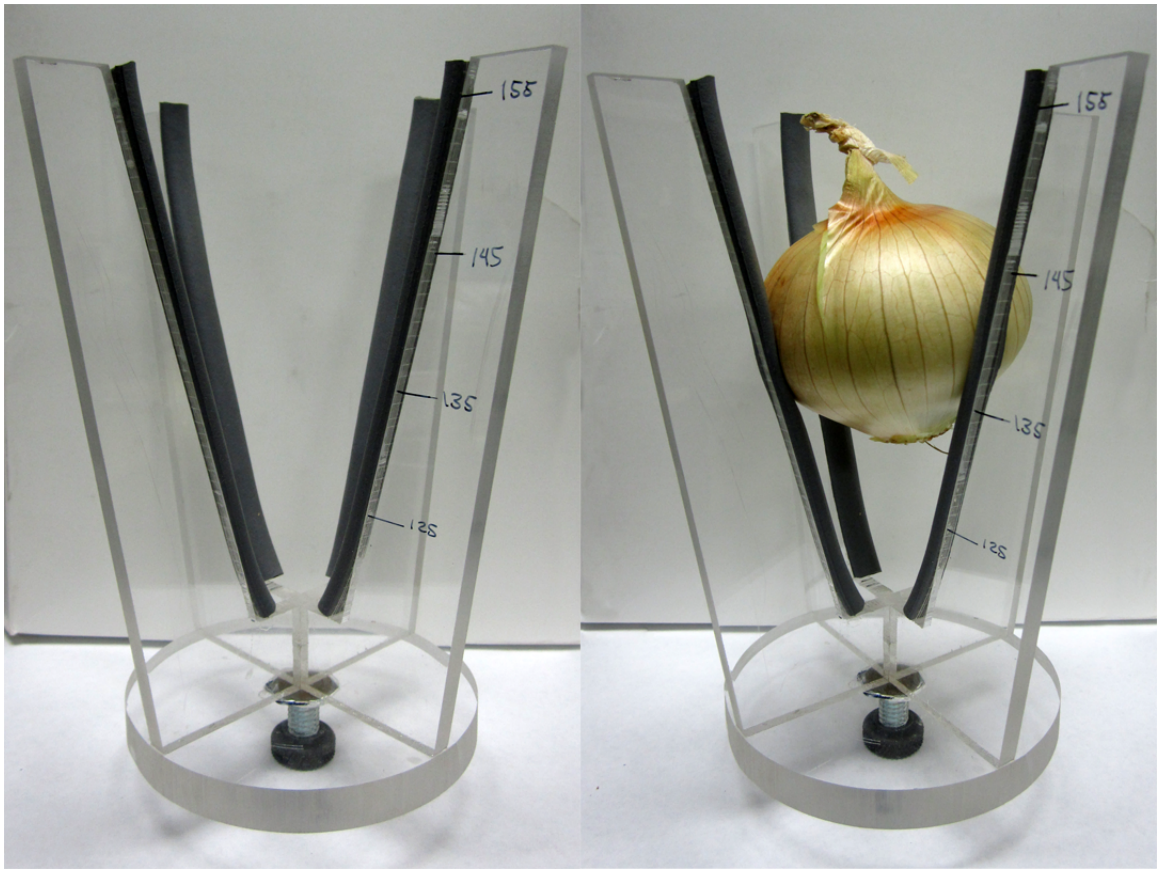

Figure 3.3: *Second-generation onion holder built out of acrylic sheet.*

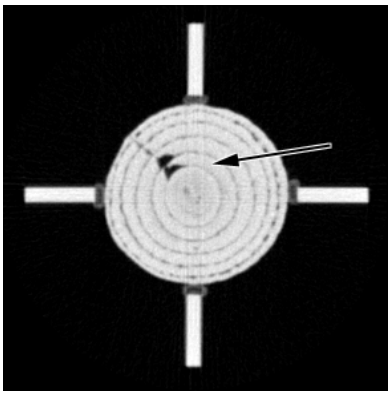

Figure 3.4: *Vertical and horizontal beam hardening artifacts appear in this onion's cross section as dark streaks in line with the edges of the holder. These artifacts appear because of x-ray attenuation caused by the long path the x-ray beam must follow through the acrylic holder.*

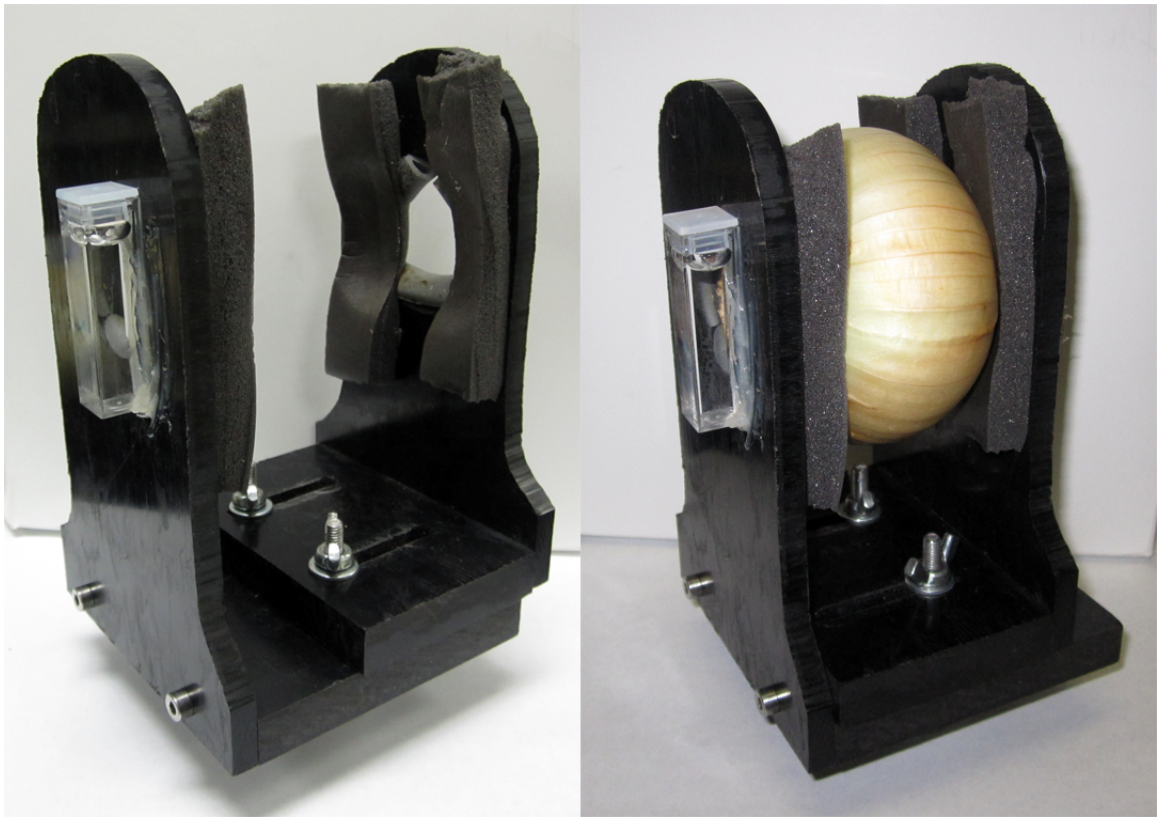

Figure 3.5: *Adjustable polyacetal onion holder with water phantom.*

the holder ideal for securing onion bulbs for transverse cross section scans. This same holder was found to be useful for securing onions for transverse section scans as well, and was used exclusively for subsequent onion scans. Foam padding was added to the sides of the holder that contact the onion, as well as the edges of the bore holes to prevent damage to the onion bulbs. A plastic cuvette filled with water was secured to the outer edge of one of the sample holder sections, providing a water x-ray absorption reference.

3.1.3 Collimators and Photomultiplier Parameters

Collimator pairings were also found to be important factors affecting image quality. Larger collimator apertures in front of the x-ray beam led to loss of fine detail in the reconstructed images, whereas small apertures in front of the PMT were found to attenuate the overall signal to the point that light-dark contrast was compromised. In every case, images obtained with the 1 mm collimator aperture in front of the PMT were found to have unacceptably low dynamic ranges and high noise content. Ultimately, it was determined that the 0.6 mm emitter aperture and 2.5 mm detector collimator provided the optimal compromise between fine detail resolution and image contrast.

The photomultplier tube's anode voltage affects the image and its signal to noise ratio. Ideally, a line from a CT sinogram should exhibit a wide range of pixel intensities, with the highest intensities being associated with the unattenuated x-ray beam through air, and the lowest values associated with the attenuated x-ray beam through an absorptive object. High PMT anode voltages lead to increased sensitivity, but at the cost of dynamic range (Figure 3.6). There is also the potential that the highest recorded output values from the PMT are outside the operating range of the instrument's amplifiers, resulting in these values being clipped to the maximum possible output value of the circuitry. Low PMT anode voltages can lead to unacceptably low sensitivity, again reducing the dynamic range of the images, and decreasing the signal-to-noise ratio (Figure 3.7).

Further complicating this matter are the two differing peak x-ray energy levels of the x-ray source. In the CT scanner's initial conception, a profile scan of an object may have been acceptable at the 140kVp energy level, but produce an unacceptably shallow attenuation profile for the 70kVp level. Qualitatively, the best quality images of onions were found to be with 800-900 volts at the PMT anode for 140kVp x-rays. The 70kVp images had relatively low dynamic ranges and more noise.

A phantom was constructed out of a plastic drinking cup and filled with water. This water

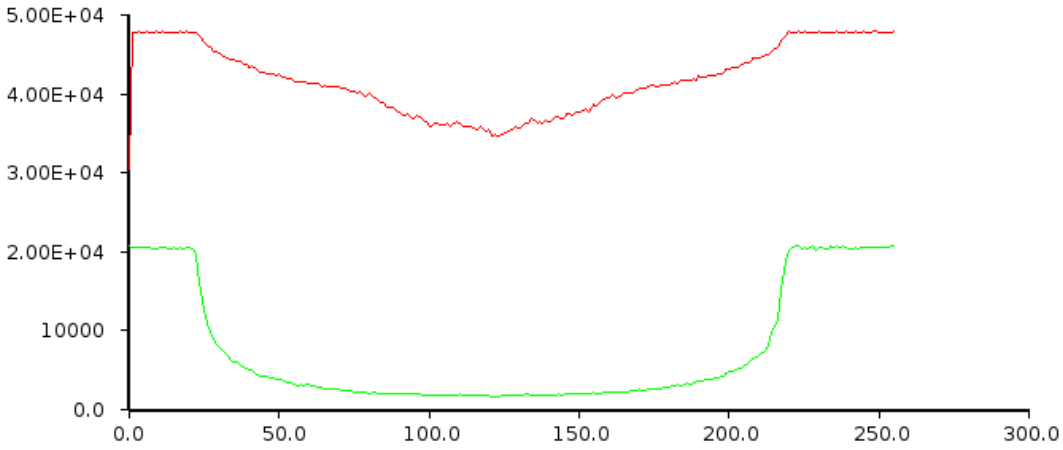

Figure 3.6: *PMT anode voltage set too high. The red line (140 kVp energy) shows a low range of values, likely due to clipping of the highest values. Y-axis values are the output from the PMT in mV that have been amplified and digitized.*

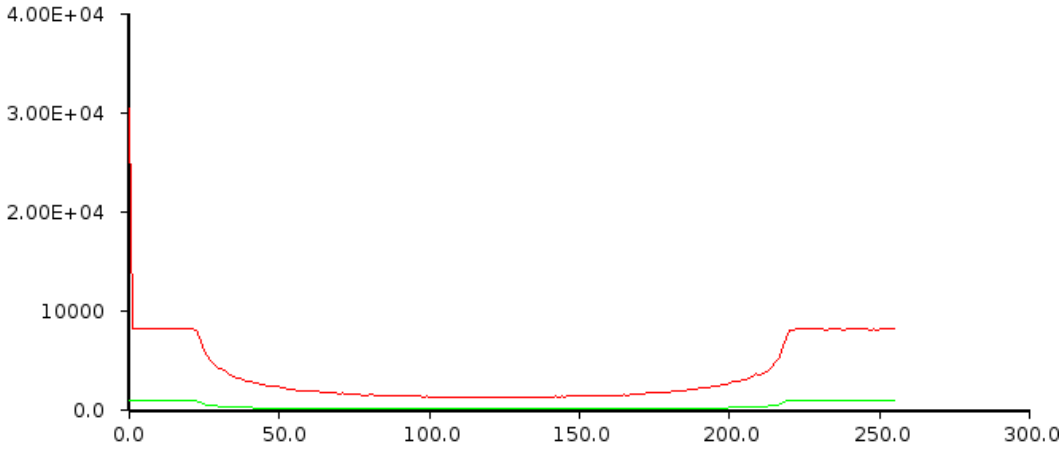

Figure 3.7: *PMT anode voltage set too low. Both the 140 kVp and 70 kVp plots show a low range of values. Reconstructions of such scans result in images with unacceptably high noise levels as well as poor contrast.*

phantom was scanned under several combinations of PMT anode voltages and apertures. Figure 3.8 shows the results of these scans. With the 2.25 mm x-ray beam aperture, the effects of clipping become apparent at PMT anode voltages of 800 and above. Subsequent scans of onion bulbs were obtained at a PMT anode voltage of 800V, with a beam aperture size of 0.6 mm and a PMT collimator size of 2.5 mm. Table 3.1 shows the minimum, maximum, mode, and mean x-ray absorptivity values for images obtained at these settings, as well as the signal to noise ratio of the images. Random sampling of nine points in images obtained of the empty drinking glass at 70kVp and 140kVp yielded mean absorption values of 0.266 cm^{-1} and 0.208 cm^{-1} respectively, meaning the absorption values of the plastic drinking cup are very close to those of water.

Table 3.1: Characteristics of 800V PMT Images (All μ values in cm^{-1})

Energy	Mean μ	STDEV μ	Mode μ	Min μ	Max μ	SNR (dB)
70 kVp	0.265	0.012	0.262	0.216	0.316	26.88
140 kVp	0.202	0.004	0.203	0.185	0.217	34.07

3.1.4 Number of Projections

In all cases, it was determined that angle between projections taken when producing a 2d scan should be as small as possible. This is logical, as more projections are taken to fill an entire 180 or 360 degree rotation, and there is therefore more information for the reconstruction algorithm. The effects of noise also tend to average out with a large number of projections. Images with larger rotational angles and fewer projections have lower resolution and apparent radial blurring of fine features due to aliasing.

One final factor potentially affecting image quality is the alignment of the rotational stage with respect to the x-ray beam. When conducting a full 360 degree scan of an object, it is imperative that the rotational stage's axis of rotation be perpendicular to the x-direction translation stage's plane of travel. Non-perpendicular alignments lead to artifacts in recon-

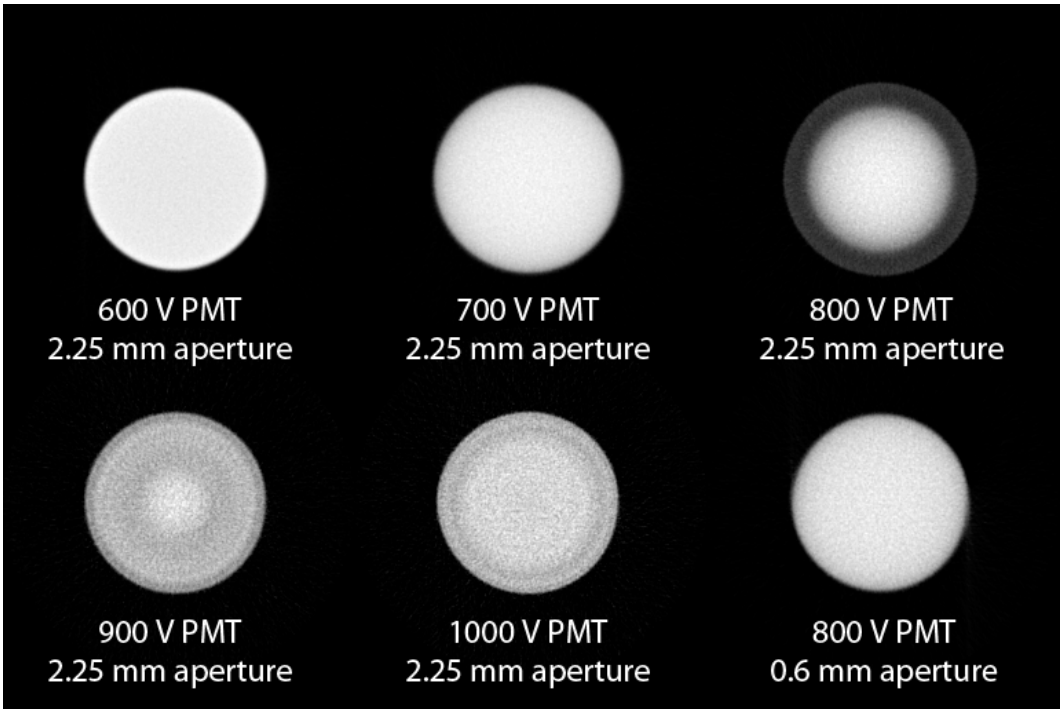

Figure 3.8: *Water phantoms scanned under varying PMT anode voltages and beam aperture sizes with a constant detector collimator size of 2.5 mm. Images obtained with high PMT anode voltages and large apertures display the effects of detector clipping. The bottom right panel shows a scan of the phantom conducted under optimal settings: a 0.6 mm beam aperture, 2.5 mm detector collimator, and PMT anode voltage set to 800V.*

struction, as projections of the same location taken from diametric opposites of the object are not aligned. Such images are, however, recoverable, though the sinograms must be split into two 180 degree scans and reconstructed separately. This misalignment of the rotational stage with respect to the x-ray beam was improved slightly, but such precise alignment so as to eliminate reconstruction artifacts proved impossible in practice. The CT reconstructions from 180 degree sinograms were, however, deemed to be of acceptable quality to locate damage in onion bulbs due to pathogen infection.

3.2 Experiment 2: Hypodermic Inoculation

B. cepacia proved to be the fastest-growing and most consistently damaging pathogen studied. Every one of the five bulbs inoculated over the course of this experiment exhibited clear signs of internal (and in some cases, external) damage. *P. viridiflava*, in contrast, did not grow nearly as readily when injected into onion bulbs and incubated in the laboratory. Incubation times were longer than those observed for *B. cepacia*, and tissue damage tended to be more localized and subtle. In some samples, there was no detectable evidence of internal tissue damage caused by the bacterium after four weeks of incubation. A gallery showing the progression of the bacterial rots in the inoculated onions and a discussion of each sample is provided in the following sections.

3.2.1 *B. cepacia Images*

The first bulb injected with *B. cepacia* showed signs of damage after 14 days of incubation (Figure 3.9). Tissue damage was not localized to the internal regions of the onion bulb, but appeared to spread along the path the hypodermic needle took through the bulb. Dark regions can be seen in the day 5 transverse image, but whether these are due to bacterial

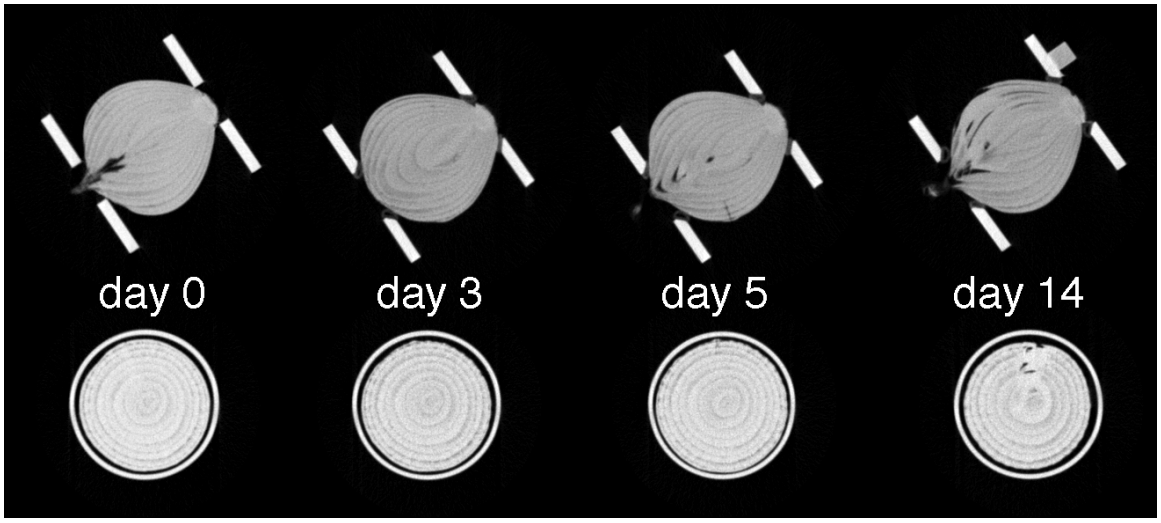

Figure 3.9: *The first bulb inoculated with* B. cepacia*. The outer ring in the transverse images is due to the drinking cup holder used to secure the specimen to the scanner stage. Bacterial damage is not evident until day 14 and is not localized, but spread throughout the region near the injection site.*

decay or voids that arise as the onion tissues shift with changes in water content of the formation of leaf shoots is ambiguous.

The second bulb inoculated with *B. cepacia* showed minor signs of damage after two weeks, and moderate damage after three weeks of incubation (Figure 3.10). Gaps between the onion scales are evident in both transverse and longitudinal scans after 21 days.

One difficulty encountered in the study of *B. cepacia* infections is its growth pattern. The bacterium appeared to exhibit a latent period of several days before suddenly causing rapid and extensive damage to the inoculated bulb. This can be seen in the third onion bulb inoculated (Figure 3.11). The bulb appears to be sound seven days after inoculation, but shows extensive damage only three days later. Like the first *B. cepacia*-inoculated bulb, bacterial damage seems to have spread rapidly to the outer portions of the bulb, rather than growing in the interior. In the transverse scans of this particular bulb, a dark region can be

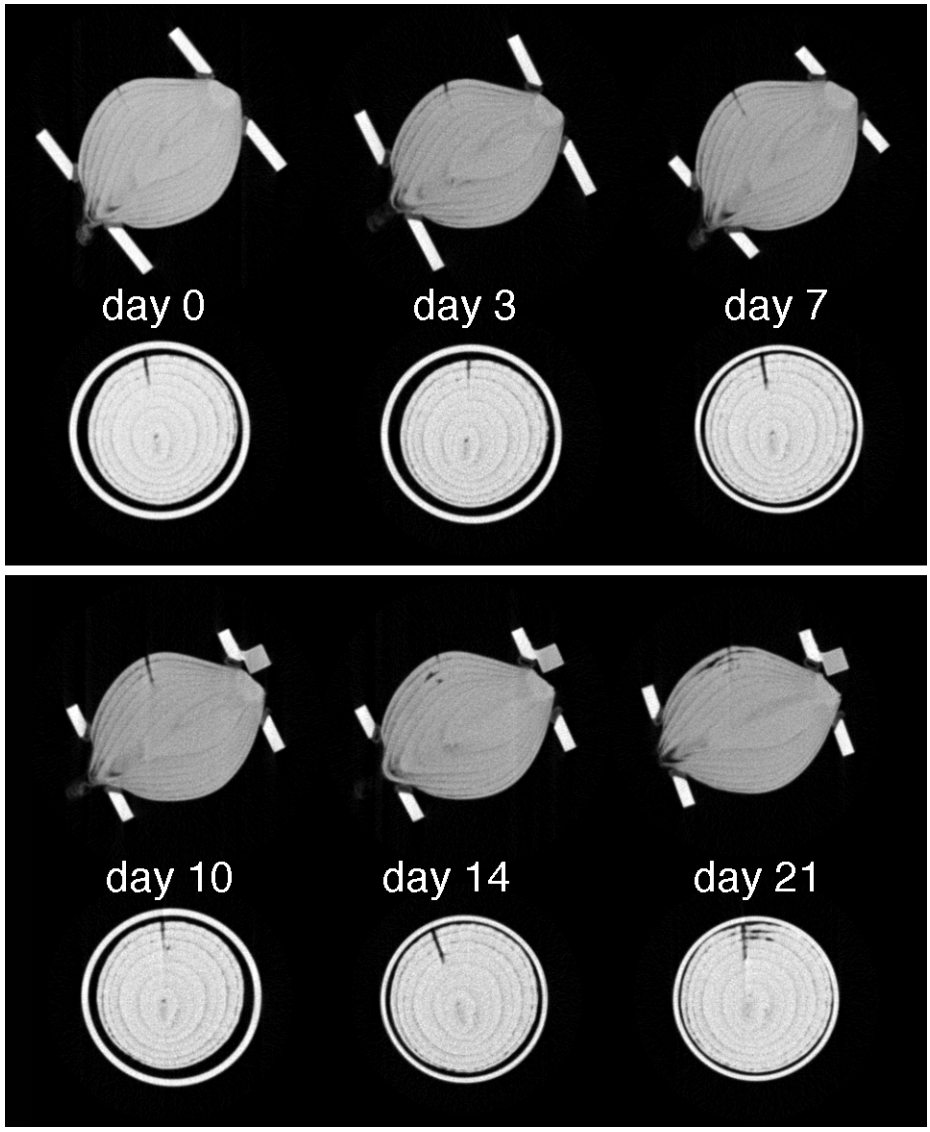

Figure 3.10: *Second bulb inoculated with* B. cepacia. *The path of the hypodermic needle can be seen in transverse cross sectional images. Some small lesions can be seen in longitudinal images by day 10, and by day 21, large lesions can be seen in both projections near the injection site.*

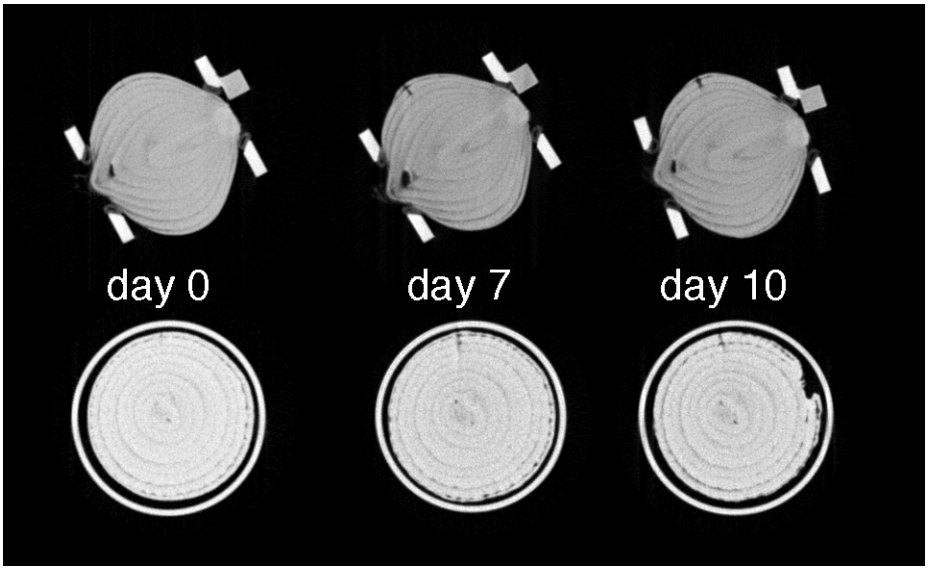

Figure 3.11: *Third bulb inoculated with* B. cepacia*. Bacterial damage erupted seemingly overnight with this particular specimen.*

seen near the neck end of the bulb that is likely due to natural variations in the lengths of the bulb's scales rather than pathogen damage, introducing more ambiguity to the analysis of these images.

The fourth bulb inoculated with *B. cepacia* showed signs of internal damage after only seven days, though the progression of this damage appears to have stalled until after two weeks of incubation, when additional lesions can be seen on the opposite side of the bulb from the inoculation site (Figure 3.12).

The fifth and final *B. cepacia*-inoculated bulb showed the same early-stage damage as the fourth bulb (Figure 3.13). An additional difficulty associated with image classification of onion CT images is illustrated in the longitudinal cross sections. A dark, crescent-shaped void can be seen developing near the neck of this bulb. However, by day 21, it can be seen that the bulb has grown leaf shoots, demonstrating that formation of such voids could also

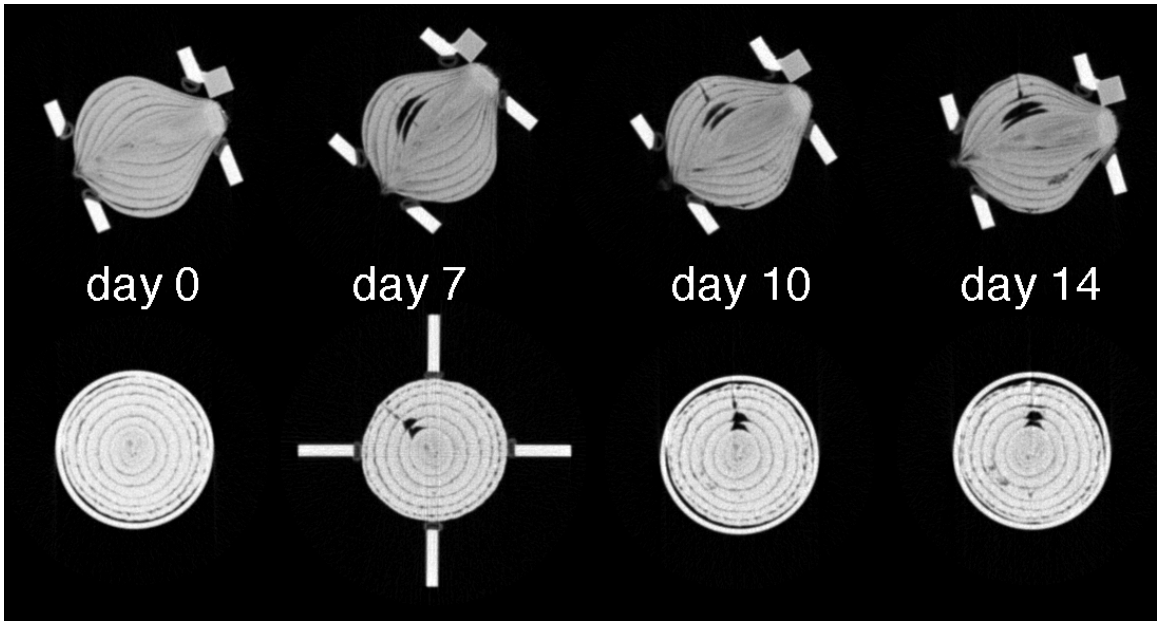

Figure 3.12: *Fourth* B. cepacia*-inoculated bulb. The day 7 transverse image was obtained with a different, experimental specimen holder. Crescent-shaped damage features appear in both transverse and longitudinal cross sections as early as seven days after inoculation, though growth does not appear to progress in these areas in subsequent scans. By day 14, signs of decay are evident on the side of the bulb opposite the injection site.*

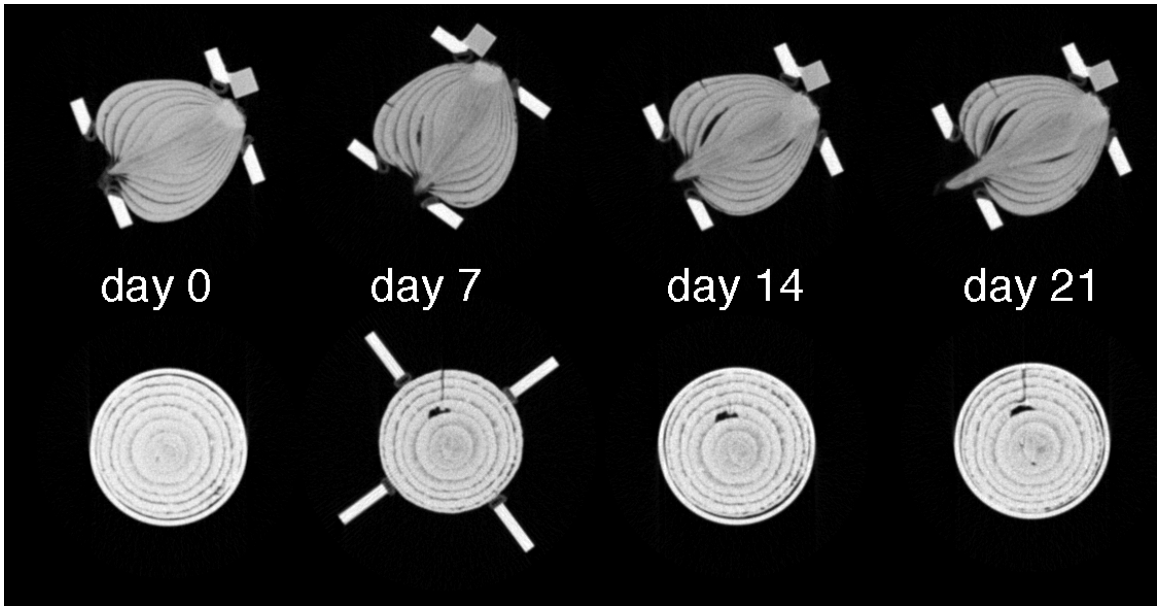

Figure 3.13: *The fifth onion bulb inoculated with* B. cepacia. *This bulb began to sprout during incubation.*

be due to deformation of the bulb's tissues as the shoots formed, rather than due to bacterial decay.

Figures 3.14-3.18 show the results of binary segmentation on the transverse cross section images. The first three specimens reveal relatively small dark spots near the outer edges of the bulb. A concentration of small dark spots localized to a specific portion of the bulb could be indicative of an active pathogen spreading from a single point of infection, whereas scattered, diffuse small lesions could emerge due to spaces between onion layers. On the fourth specimen, a feature resembling two crescent shapes on top of each other is evident near the center of the bulb. The fifth specimen has a single crescent shaped dark region near the center of the bulb. These features appear to indicate an infection spreading throughout one or two layers of onion tissue that is constrained within the already infected layers.

Table 3.2 shows the size, compactness, aspect ratio, and irregularity values of the isolated

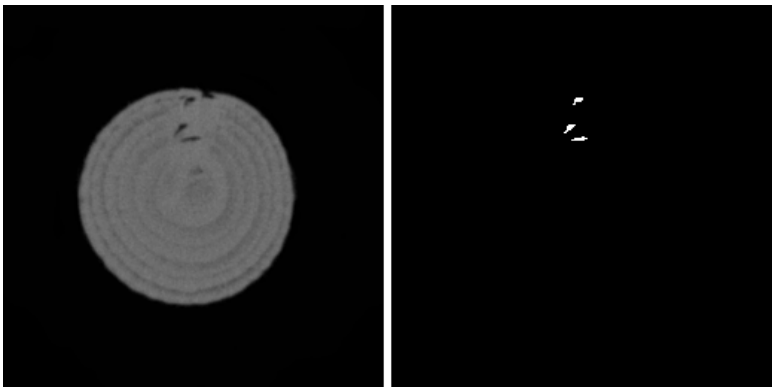

Figure 3.14: *Segmented features in the first* B. cepacia*-inoculated bulb. A few small dark spots were isolated near the injection site in this specimen, indicating the spread of the infection from this injection site.*

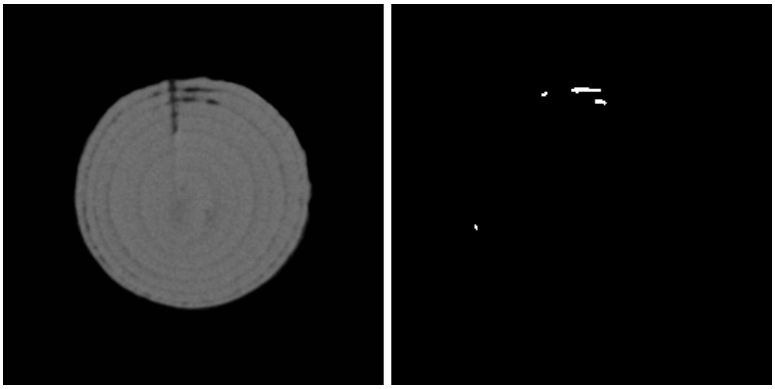

Figure 3.15: *Segmented features in the second* B. cepacia*-inoculated bulb. Again, the majority of the dark features segmented from the image appear near the pathogen's point of entry.*

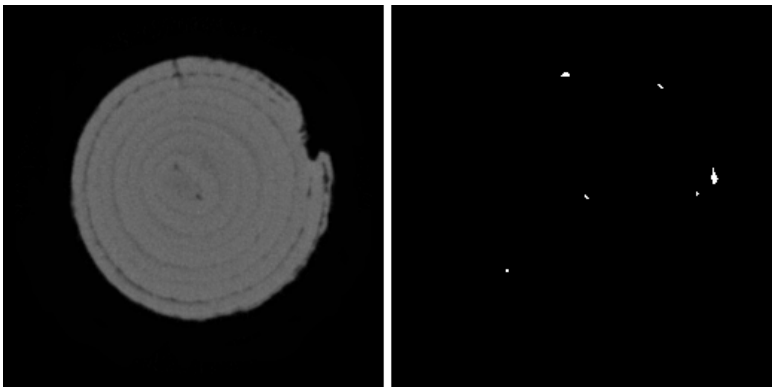

Figure 3.16: *Segmented features in the third* B. cepacia*-inoculated bulb. Small dark spots are scattered throughout the bulb, making discrimination between damage and natural variation difficult. Additional methods will be utilized to recognize the gash missing from the right side of the bulb.*

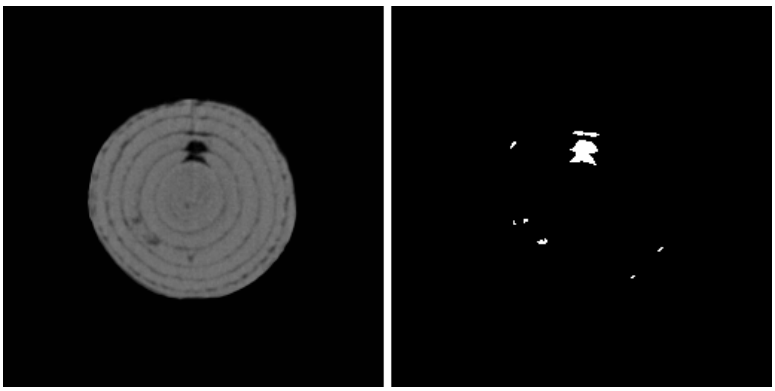

Figure 3.17: *Segmented features in the fourth* B. cepacia*-inoculated bulb.*

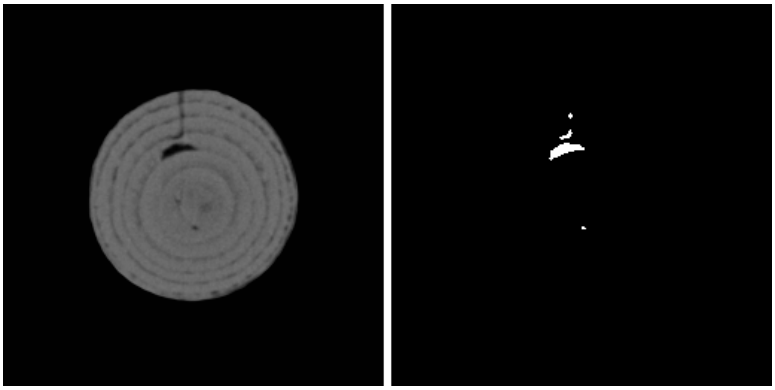

Figure 3.18: *Segmented features in the fifth* B. cepacia*-inoculated bulb.*

features in the fourth bulb inoculated with *B. cepacia*. The high compactness values of the largest features indicate a large perimeter relative to the surface area of the feature. Such characteristics are highly unlikely to occur in healthy onion tissues and can be useful indicators of damage or morphological anomalies in onion tissues. In this particular specimen it appears that bacterial growth has progressed through two adjacent layers, traveling along their boundaries. The narrowing associated with the layer boundary in the largest damage feature has resulted in a much lower irregularity value for the feature, compared to the other segmented features.

Table 3.2: *B. cepacia* Onion #4 Feature Characteristics

Feature	Size (Pixels^2)	Size (mm^2)	Compactness	Aspect Ratio	Irregularity
1	200	50.00	17.91	3.32	0.23
2	39	9.75	25.6	9.06	0.55
3	16	4.00	11.53	3.16	0.41
4	9	2.25	8.1	3.16	0.52
5	6	1.50	7	2.24	0.57
6	5	1.25	6	2.24	0.62
7	3	0.75	4	1.41	0.7
8	3	0.75	4	1.41	0.7

A large region of bacterial decay has been constrained to the interior of an onion layer near the center of the bulb. This large feature, whose characteristics are tabulated along with the other smaller features in Table 3.3, exhibits a relatively high compactness value. Unlike the large lesion seen in the fourth *B. cepacia*-inoculated bulb, the irregularity value of this feature is relatively high, owing the the smooth boundaries caused by the neighboring uninfected layers of the onion bulb.

Table 3.3: *B. cepacia* Onion #5 Feature Characteristics

Feature	Size (Pixels^2)	Size (mm^2)	Compactness	Aspect Ratio	Irregularity
1	127	31.75	20.32	6.48	0.43
2	23	5.75	15.04	4.47	0.38
3	7	1.75	4.5	2	0.3
4	4	1.00	5	2.24	0.72

3.2.2 *P. viridiflava* Images

The first bulb inoculated with *P. viridiflava* exhibits signs of later separation in transverse cross section near the injection site, while transverse cross sections reveal small, round lesions (Figure 3.19). Damage signs appear to be localized to the region surrounding the injection site, and the damage appears to progress at a slow and steady pace.

The second *P. viridiflava*-inoculated bulb showed little evidence of damage, even after 28 days of incubation (Figure 3.20). Some small dark regions can be seen in the vicinity of the injection site from day 7. However, several other small dark spots caused by natural variations in onion tissue density and vasculature are also evident in the images. The onion bulb began so sprout before any signs of extensive tissue damage were detected.

The third bulb inoculated with *P. viridiflava* (Figure 3.21) also shows little, if any, evidence of bacterial damage. The most prominent dark regions in the cross sectional images of this bulb were due to variations in tissue structure and water content, not due to bacterial lesions.

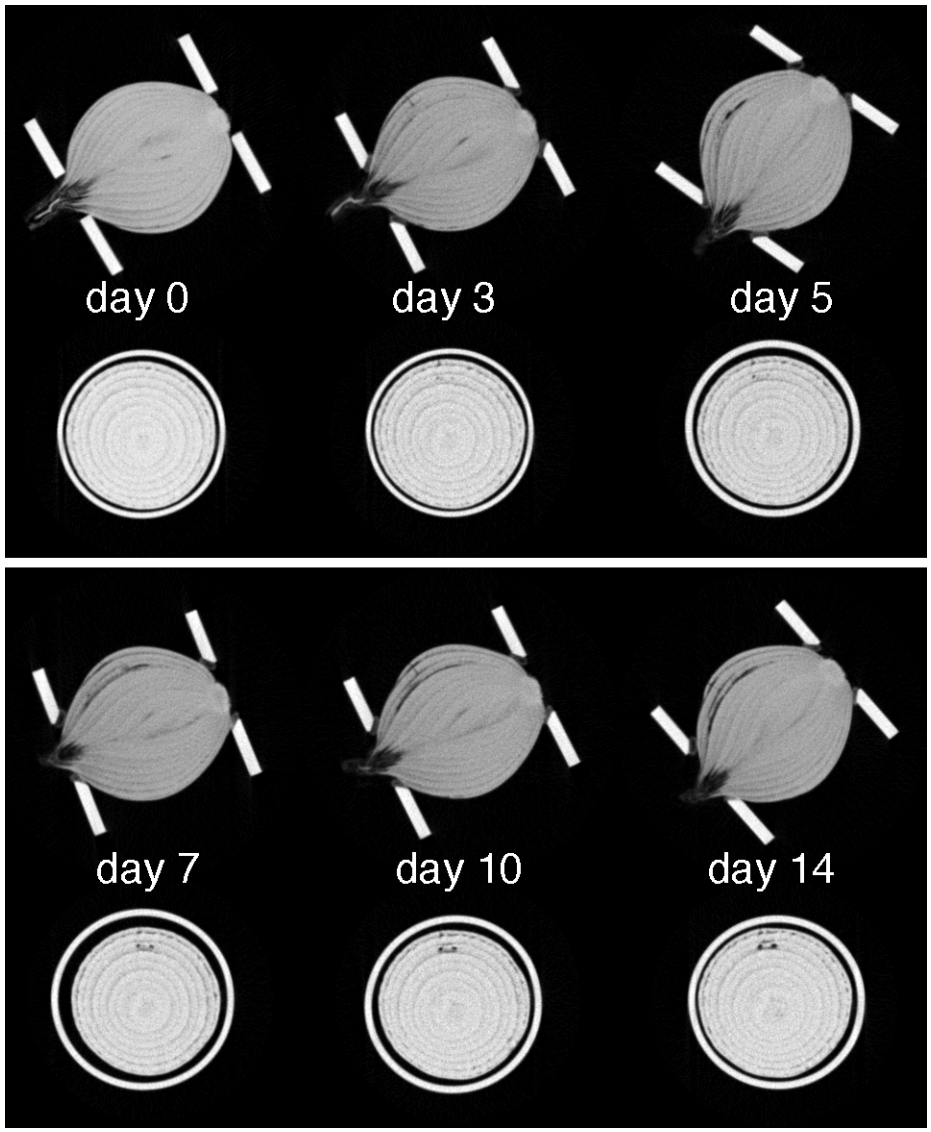

Figure 3.19: *The first bulb inoculated with* P. viridiflava*. Damage is evident after five days, and this damage slowly progresses over the course of subsequent scans.*

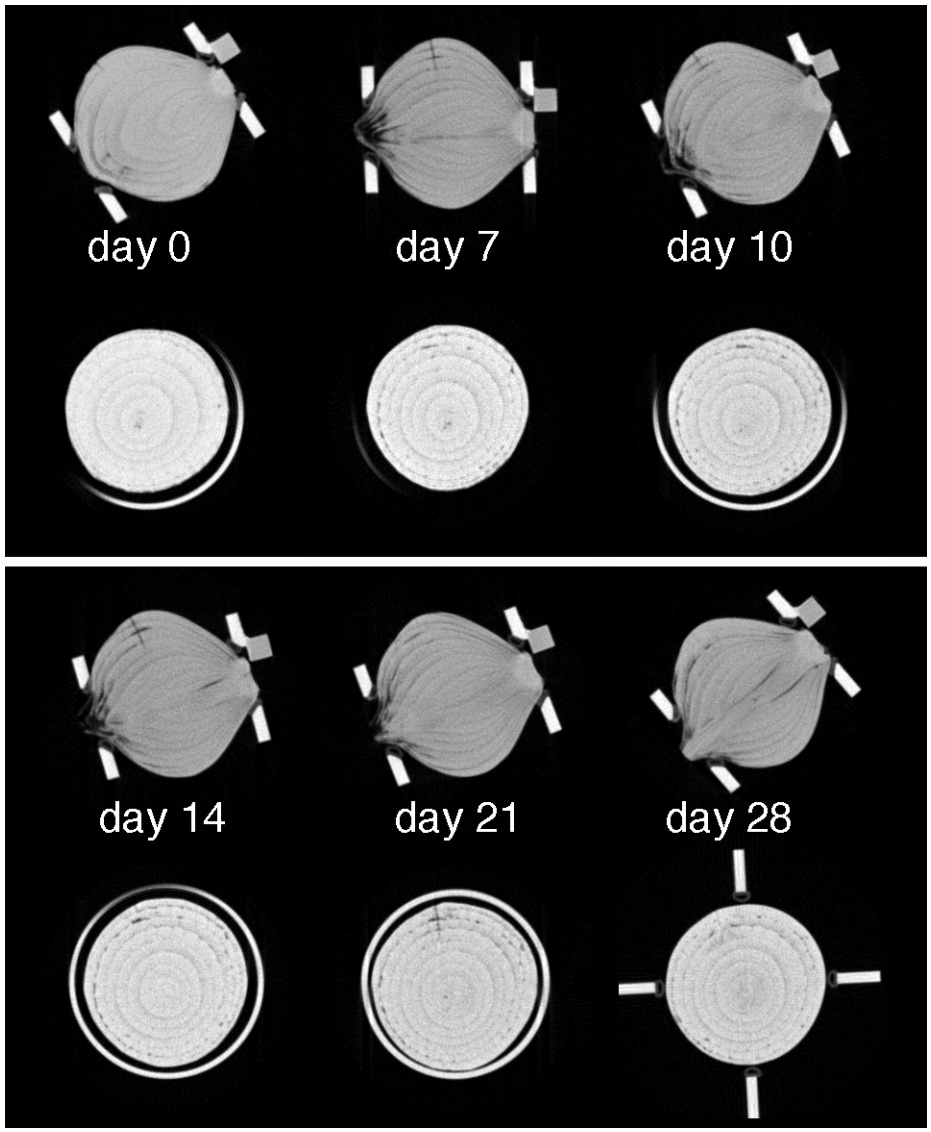

Figure 3.20: *Second bulb inoculated with* P. viridiflava*. There is essentially no detectable damage to the bulb, even 28 days after inoculation.*

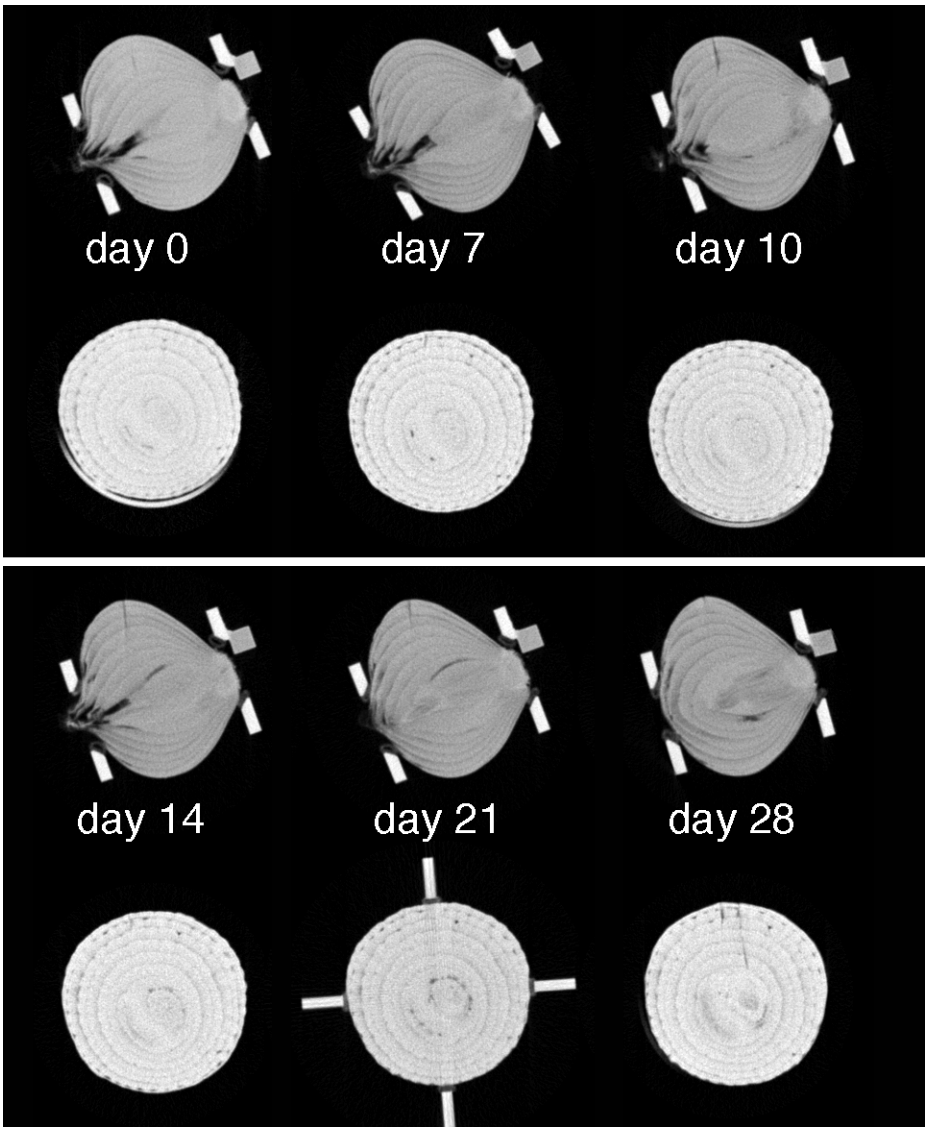

Figure 3.21: *The third bulb inoculated with* P. viridiflava.

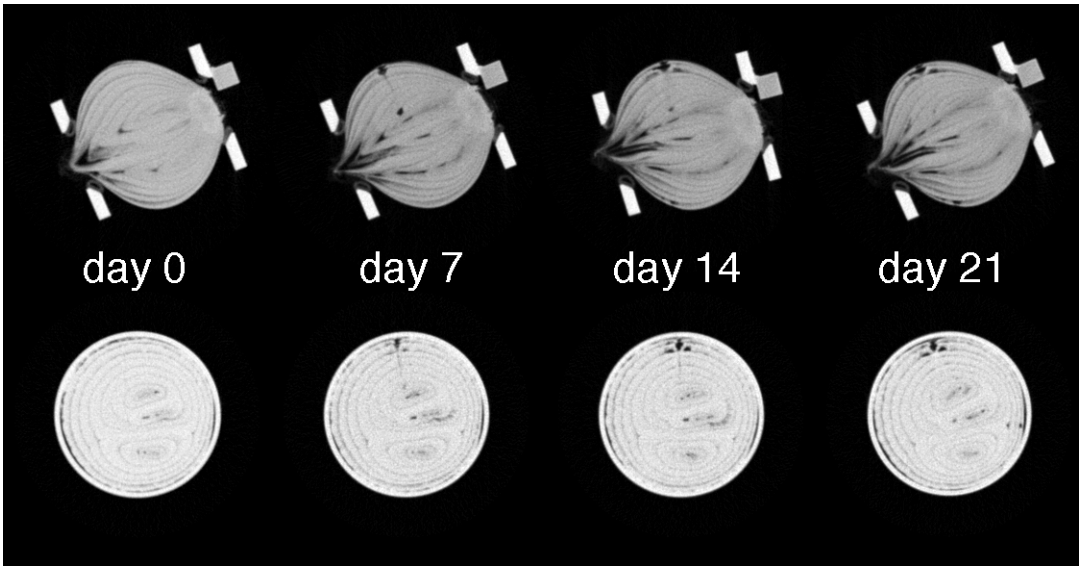

Figure 3.22: *The fourth bulb inoculated with P. viridiflava.*

The fourth *P. viridiflava*-inoculated bulb (Figure 3.22) shows signs of damage as early as day 7. Though this initial damage could have been caused by the inoculation of the bulb, rather than bacterial rot, the day 14 and day 21 transverse images show evidence of layer separation. This particular bulb also provides a demonstration of how capable CT imaging is of detecting multi-center onion bulbs. The transverse cross sections clearly show three sets of concentric rings, and the transverse cross sections show the emergence of three separate sets of shoots. Another interesting feature of this specimen is the relative abundance of internal voids, compared to the single center bulbs that had heretofore been scanned. Such voids could provide an ideal environment for fungal or bacterial intrusion and growth, perhaps explaining the increased disease susceptibility associated with multi-center bulbs.

Only the first and fourth specimens inoculated with P. viridiflava showed any segmentable dark regions in transverse cross section images (Figures 3.23-3.24). In both cases, two small, round dark spots were isolated near the outer edges of the inoculated bulbs.

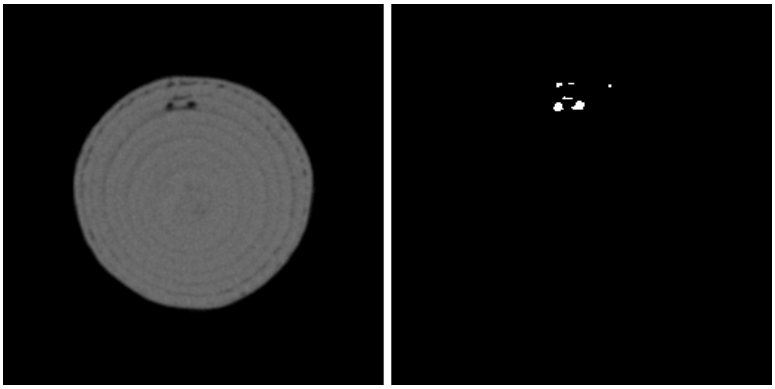

Figure 3.23: *Segmented features in the first P. viridiflava-inoculated bulb.*

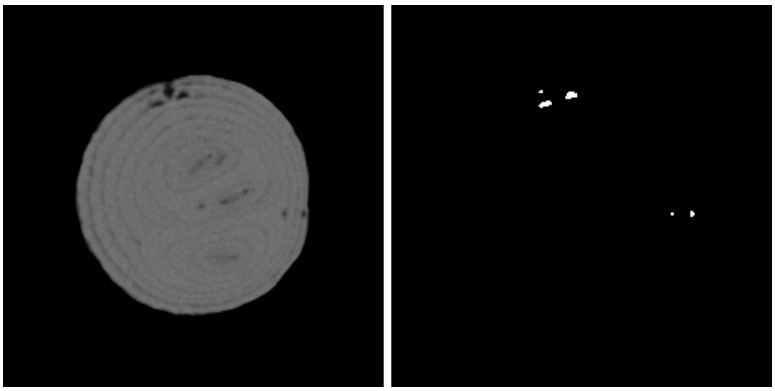

Figure 3.24: *Segmented features in the fourth P. viridiflava-inoculated bulb.*

3.2.3 Fourier Shape Analysis

As expected, bulbs that exhibited signs of surface damage tended to have higher than average values for descriptors ζ_6, through ζ_9 of their outlines, owing to the complex harmonics that are introduced to a Fourier transform of a parameterized curve when an abrupt change in radius is encountered. Oblong, ovoid shaped bulb cross sections exhibited higher than average values of ζ_2 and ζ_3, due to the contributions of the minor radii to the Fourier transform of the parameterized shape outline.

Figures 3.25 through 3.29 show plots of the day 0 mean ζ values for the population (14 specimens, total) alongside the individual's day 0 and final day ζ values. In all cases, elevations in some of the values of ζ_5 through ζ_9 can be observed, relative to both the initial population mean as well as each individual's day 0 values. The parameterized shape of each onion is displayed in an inset in each of these graphs to illustrate the effects of specific types of damage on Fourier ζ coefficients. Though some undamaged bulbs may have larger day 0 values for some Fourier coefficients when compared to the population mean, in all cases, signs of damage led to increases in these same coefficients beyond the initial day 0 values. Thus, the larger ζ values relative to the mean for final day images can be attributed to malformation of the onion bulb's outer surface, and not to natural variation of healthy specimens.

Figure 3.30 demonstrates the possibility of using Fourier analysis of onion outer edges as a quality control measure. This particular specimen exhibits a particularly ovoid shape, and its ζ_2 value is particularly elevated. Such large elevations in ζ_2 are indicative of elliptical shapes, and could be useful in screening out doubled bulbs. Though the sample size in this particular study was too small for rigorous statistical analysis, future studies could be conducted to develop statistical models and threshold values useful for screening onions exhibiting surface malformations from more valuable and potentially more storable onions.

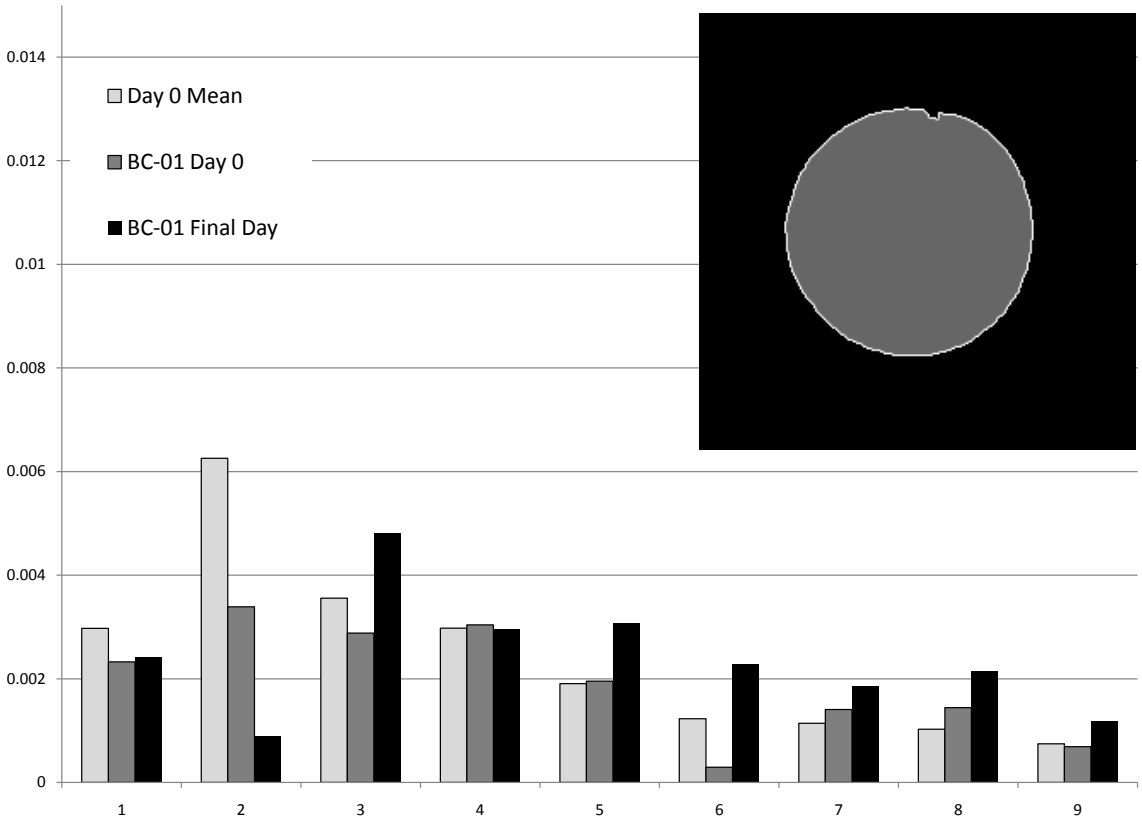

Figure 3.25: *First bulb inoculated with B. cepacia. A small nick in the onion's surface can be seen at the top of the inset image. The values of ζ_5 through ζ_9 show slight elevation compared the mean value for this population. Note that ζ_0 is equal to 1, due to normalization, for all specimens, and is omitted in the charts.*

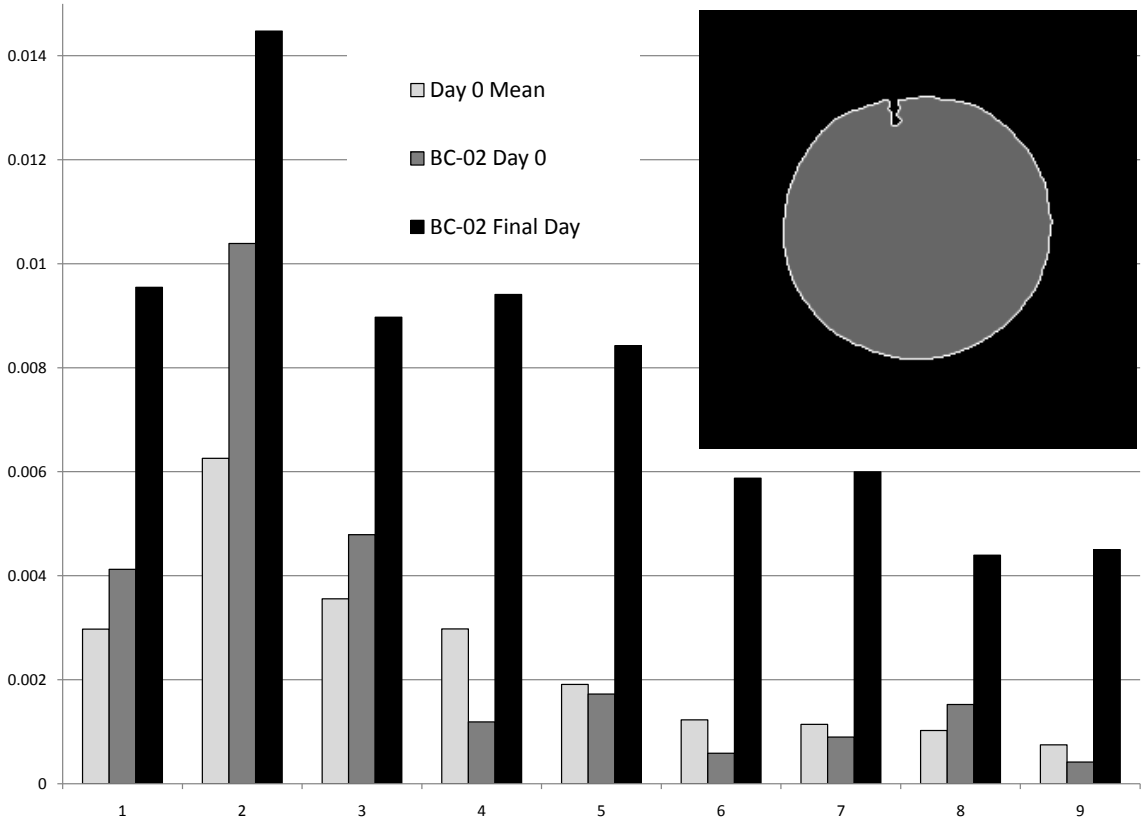

Figure 3.26: *Second bulb inoculated with B. cepacia. The particularly deep and narrow decayed channel in this specimen has led to large increases in all ζ values.*

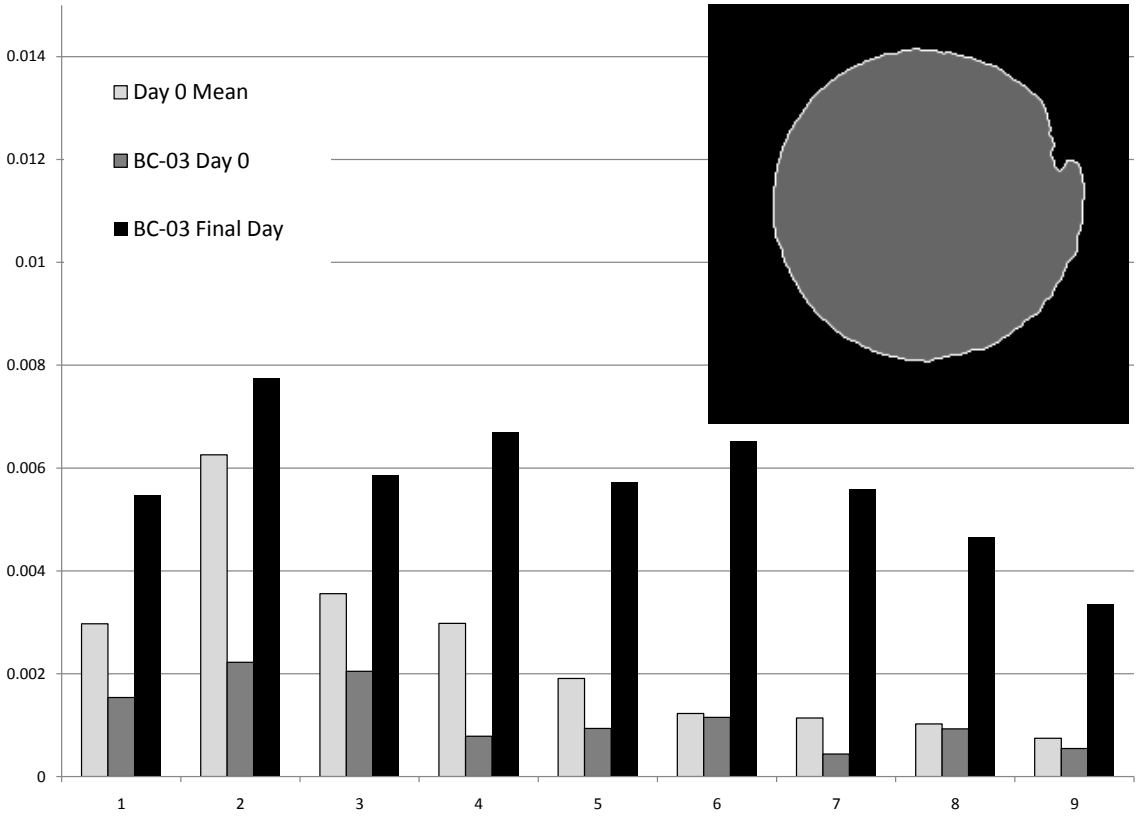

Figure 3.27: *Third bulb inoculated with B. cepacia. Again, extensive and deep surface damage lead to large increases in all ζ values.*

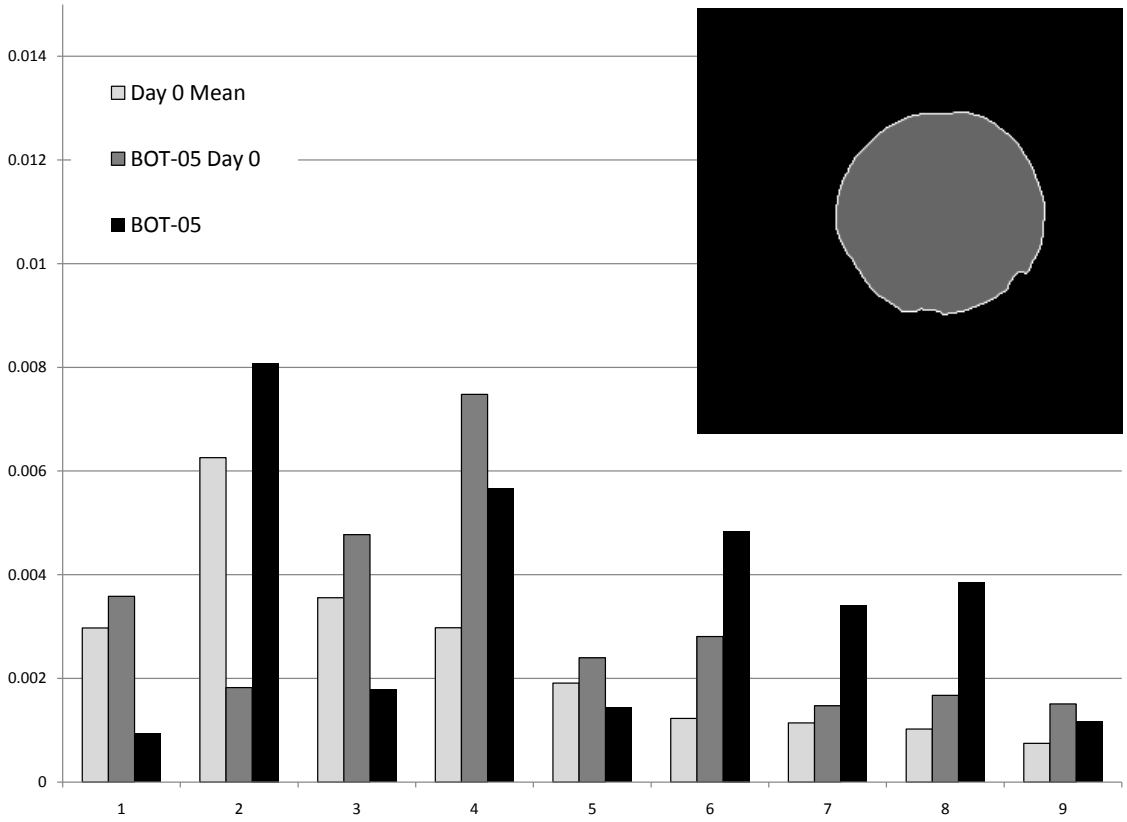

Figure 3.28: *Fifth bulb inoculated with B. allii. The damage to this specimen is more subtle than the others, but the two small dents at the bottom of the bulb have led to increases in value for* ζ_6, ζ_7, *and* ζ_8.

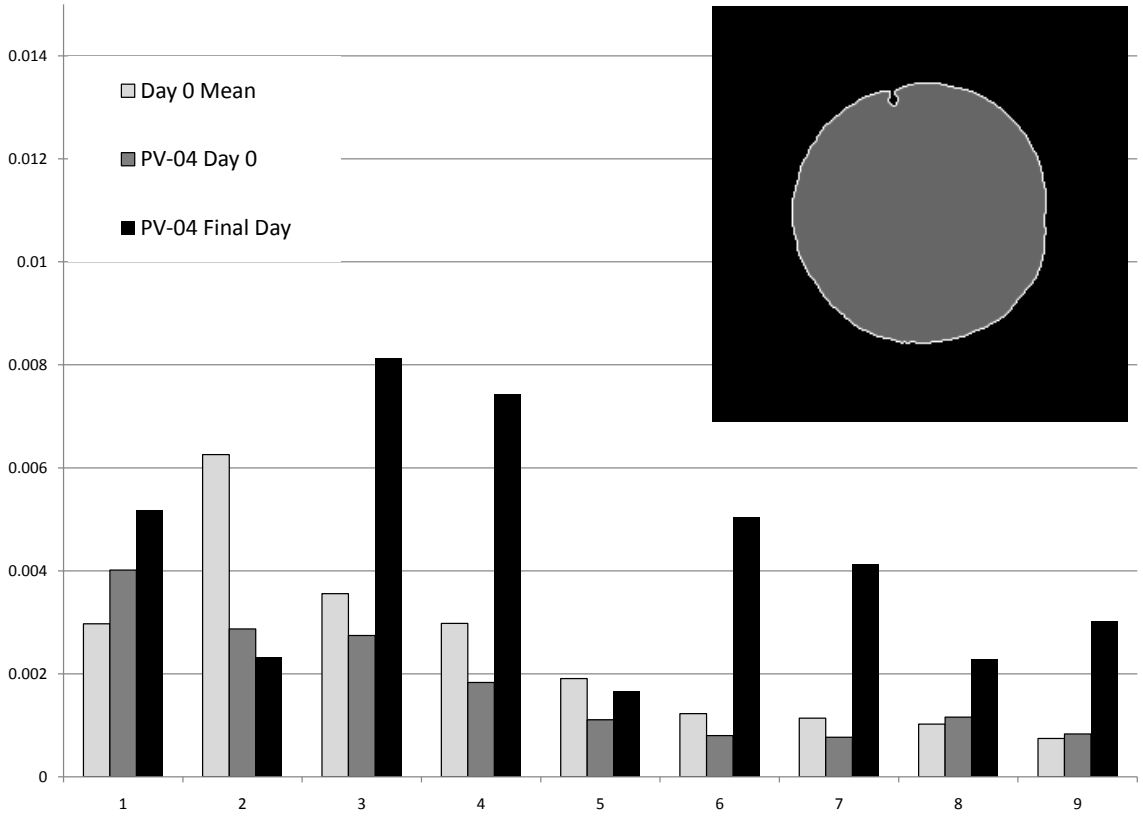

Figure 3.29: *Fourth bulb inoculated with P. viridiflava. Again, small, abrupt changes in the radius of the outer edge of the specimen relative to its centroid lead to large values for* ζ_6 *through* ζ_9.

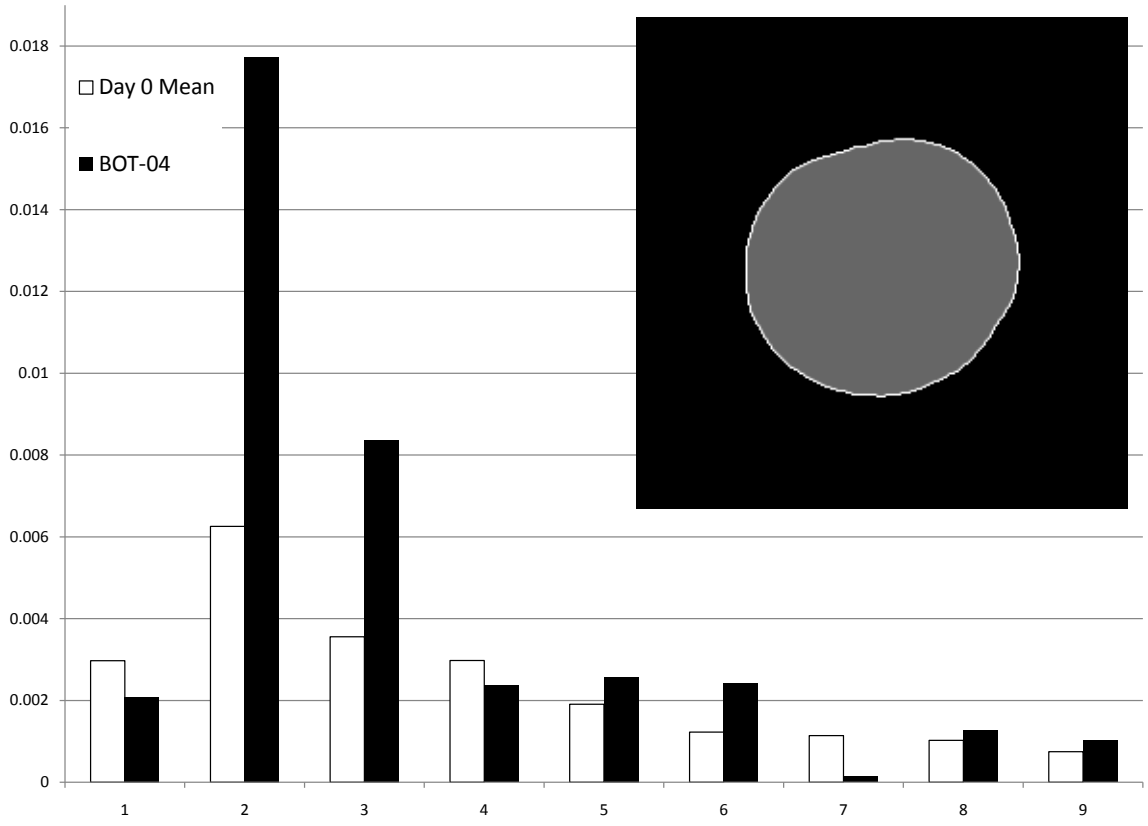

Figure 3.30: *Fourth bulb inoculated with B. allii. Though no signs of disease are present, the comparatively large values of ζ_2 and ζ_3 associated with this specimen demonstrate the ability of this analysis method in detecting misshapen ovoid bulbs.*

3.3 Experiment 3: Onion Neck Inoculation

Vidalia onions proved to be particularly susceptible to Botrytis neck rot directly introduced to exposed onion neck tissues. All five of the sample onions inoculated exhibited signs of decay within a four week period. The Peruvian-grown onions utilized in later experiments, by contrast, exhibited less sensitivity to neck-based inoculation of the pathogens.

3.3.1 Botrytis-Inoculated Vidalia Onions

In general, the longitudinal cross section images appeared to provide more useful information regarding the spread of Botrytis neck rot, though this was largely due to the location of the scan sites relative to the actual location of the infection. It was initially believed that as the infection spread downward from the onion's neck towards its root end, it would eventually intersect the transverse cross sectional plane and reveal characteristic damage patterns. While this appears to have occurred in a few of the images, detection of rot-induced damage is complicated by the formation of leaf shoots which can cause internal voids and localized low-density regions near the center of the bulb.

The transverse images of the first Botrytis-inoculated bulb (Figure 3.31) revealed signs of decay in one of the internal layers after fourteen days of incubation, and this decayed region increased in size in the subsequent transverse scan two weeks later. Longitudinal scans revealed darkening of the ends of the onion bulb scales near the neck, and these dark regions increase in length along the scale outlines as the disease progresses. Some layer separation is evident, as the onion began to sprout during incubation, leading to the formation of voids between the actively growing shoots and the outer bulb scales.

The second bulb inoculated with Botrytis shows clear signs of damage in the final transverse cross sectional image (Figure 3.32). Several irregularly-shaped voids appear near the neck end of the bulb, and the tissue surrounding these voids appears deformed. The final

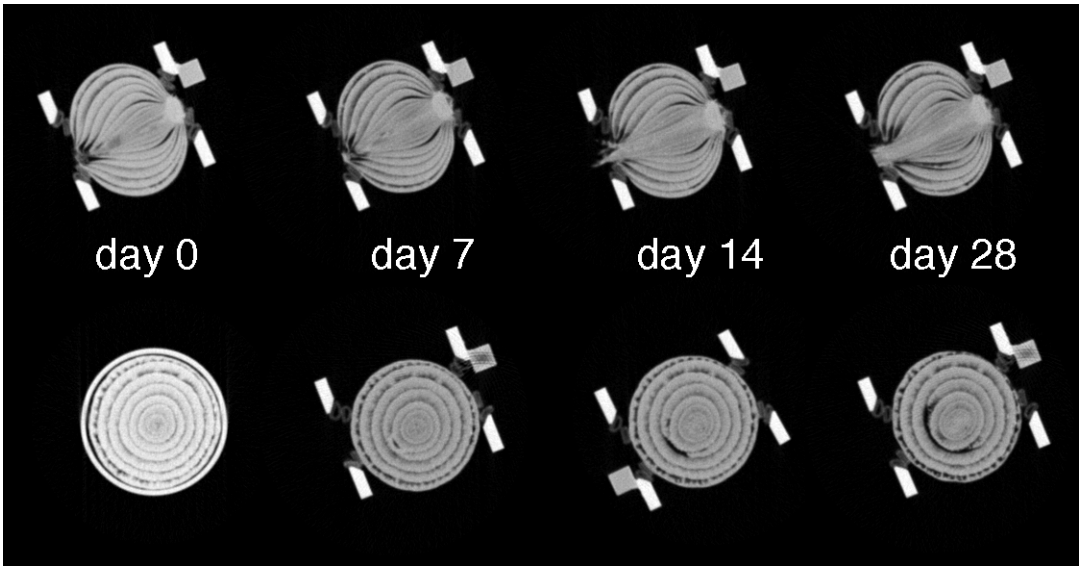

Figure 3.31: *The first Botrytis-inoculated Vidalia onion. Damage is evident by day 14 in the transverse image, where the fungal rot has been traveled down a single layer. In longitudinal cross section, the ends of the layers near the neck of the onion have begun to darken by day 28.*

transverse cross section image could also show evidence of damage; there are definite dark regions and voids, though this onion bulb began sprouting during incubation, so some of these dark regions could be attributed to morphological changes that occur as the shoots begin to emerge.

The third bulb inoculated with Botrytis shows clear, unambiguous evidence of internal rot in both transverse and longitudinal cross section (Figure 3.33). Early images show evidence of internal shoot formation and the accompanying dark voids that occur as the shoots grow. By day 14, the transverse image shows some light gray regions forming along the ends of the scales. The final transverse image shows the tissue deformation and dark voids that result as the infection is allowed to progress. The final transverse cross section image shows a thoroughly irregular and disordered inner core.

The fourth bulb inoculated with Botrytis had decayed so thoroughly by day 28 that it

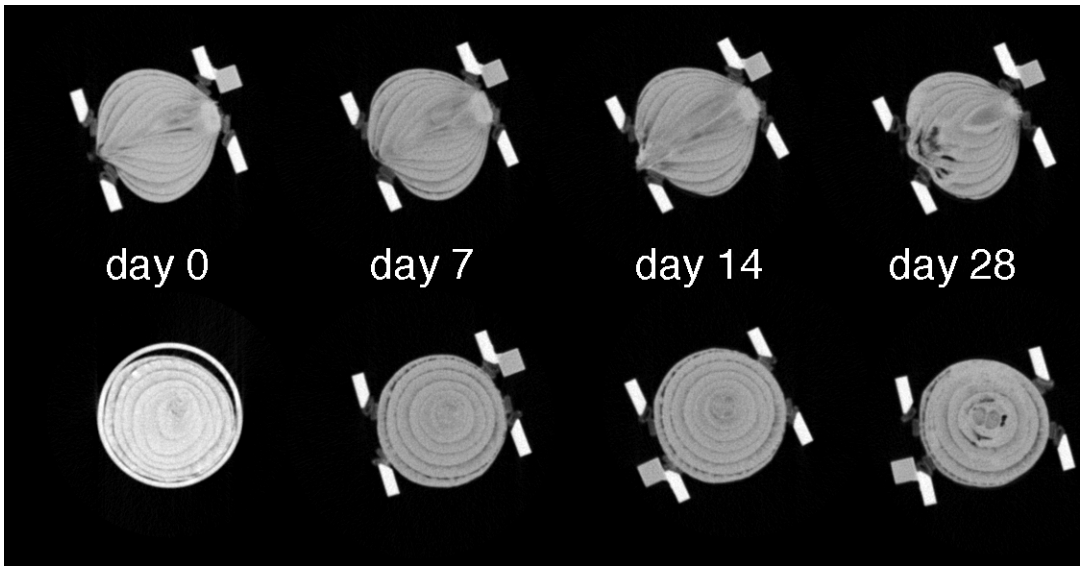

Figure 3.32: *The second Botrytis-inoculated Vidalia onion.*

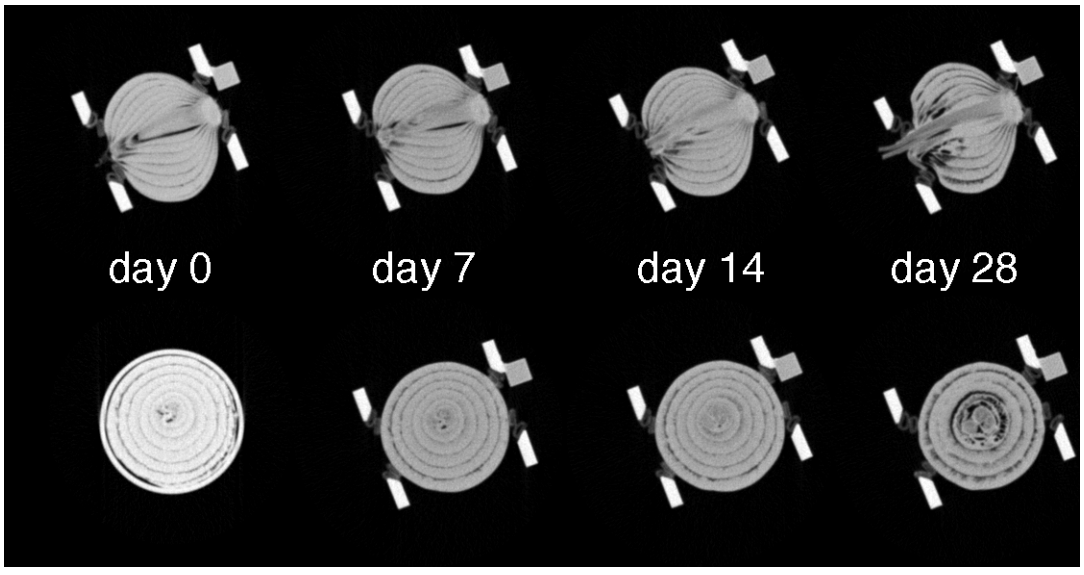

Figure 3.33: *The third Botrytis-inoculated Vidalia onion.*

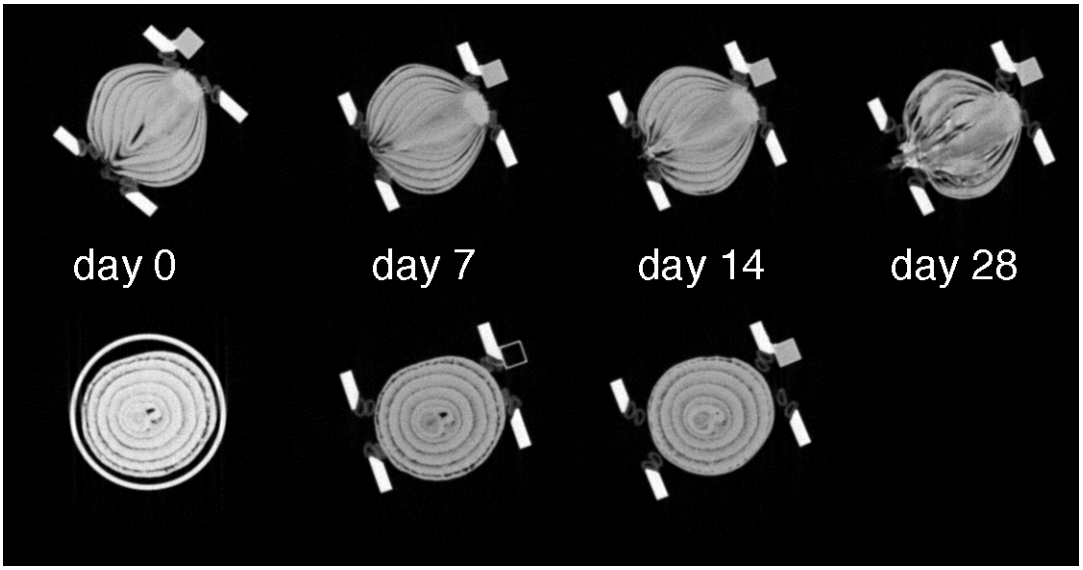

Figure 3.34: *The fourth Botrytis-inoculated Vidalia onion. Some minor darkening of the scale ends near the neck can be observed in the day 14 longitudinal image. By day 28, the damage was so extensive that the onion could no longer be reliably secured to the specimen holder for a transverse scan.*

could no longer be reliably held in the specimen holder for imaging, hence the lack of a day 28 transverse image (Figure 3.34). The bulb rot progressed rapidly between day 14 and 28; there is slight evidence of decay at the ends of the bulb scales in the day 14 longitudinal image, but the bulb has clearly completely rotted by day 28. Secondary infections could account for the more rapid decomposition of this particular specimen.

The fifth bulb inoculated with Botrytis began to exhibit signs of sour skin infection as well as neck rot after two weeks of incubation (Figure 3.35). Slight decay of the outer skin can be observed in the transverse image from day 14. By the following week, the bulb decay was so advanced that it could not be placed in a holder for imaging. Again, the longitudinal cross section images show a darkening of the neck-end scales of the bulb, indicating that the Botrytis infection is spreading downwards toward the center of the onion, leaving decayed tissues behind.

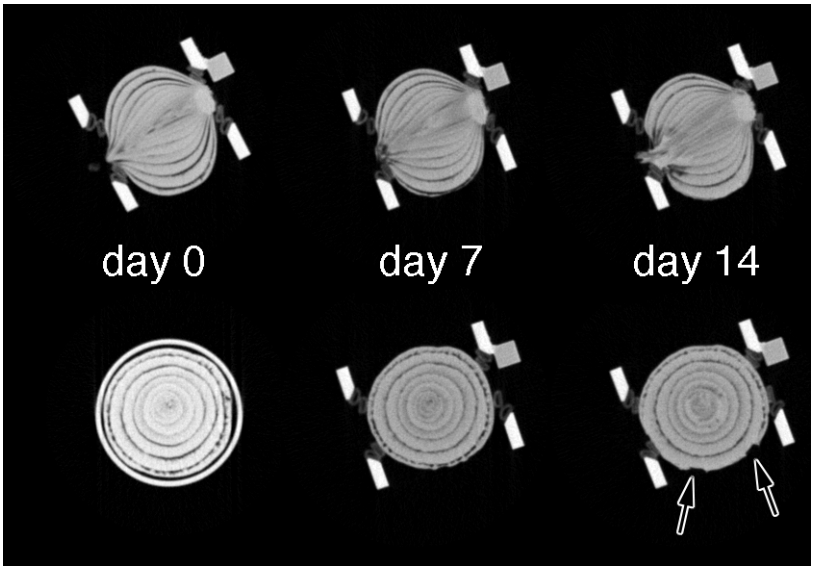

Figure 3.35: *The fifth Botrytis-inoculated Vidalia onion. Again, the telltale signs of Botrytis neck rot can be observed as darkening of the scale ends near the onion's neck in longitudinal cross section by day 14. Signs of a secondary infection on the surface of the bulb, possibly sour skin, can be seen in the day 14 transverse image, as indicated by arrows.*

Figures 3.36-3.40 show the results of segmentation of the transverse cross sectional images of inoculated and incubated onions after binary image value segmentation. Cluster analysis was conducted on the resultant isolated image features, and the characteristics of these features found in the first, second, and third Botrytis-inoculated onions are listed in Tables 3.4-3.6, sorted by feature size. The third and fourth onions inoculated with Botrytis exhibited only small dark regions that, while possibly caused by infection, could not be reliably distinguished from natural variation within onion tissues or image noise.

After segmentation, the first three specimens exhibited numerous small features in addition to a few larger features. In the interest of brevity, only the largest ten features are listed in the tables. While an abundance of small dark regions could be indicative of bacterial or fungal infection, the larger features were regarded as more reliable indicators of infection.

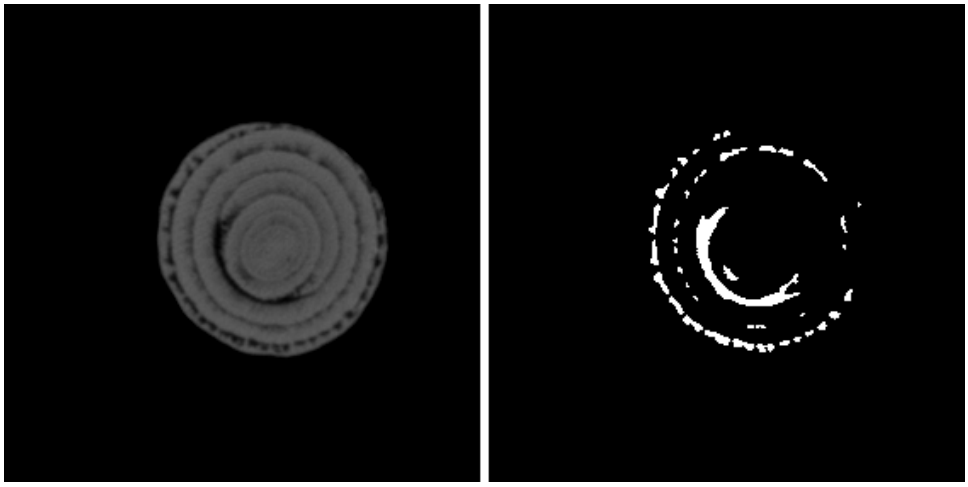

Figure 3.36: *Segmented features in the first Botrytis-inoculated onion*

These larger features tended to exhibit high compactness values compared to the other features. Such values are indicative of large and branching areas that are highly unlikely to occur naturally in onion tissues, making them good indicators of damage to the bulbs. Small features, on the other hand, are more difficult to characterize in terms of compactness and regularity, as the resolution of the images becomes a limiting factor in the calculation of these characteristics.

Table 3.4: Botrytis Onion #1 Feature Characteristics

Feature	Size (Pixels^2)	Size (mm^2)	Compactness	Aspect Ratio	Irregularity
1	600	150.00	83.49	4.36	0.35
2	61	15.25	17.56	7.81	0.46
3	47	11.75	27	9	0.55
4	47	11.75	15.19	8.6	0.52
5	47	11.75	16.33	7.28	0.49
6	45	11.25	25.13	10.44	0.58
7	45	11.25	13.59	7.21	0.5
8	44	11.00	21.36	8.06	0.49
9	39	9.75	24.02	9.9	0.58
10	36	9.00	13.08	6.4	0.46

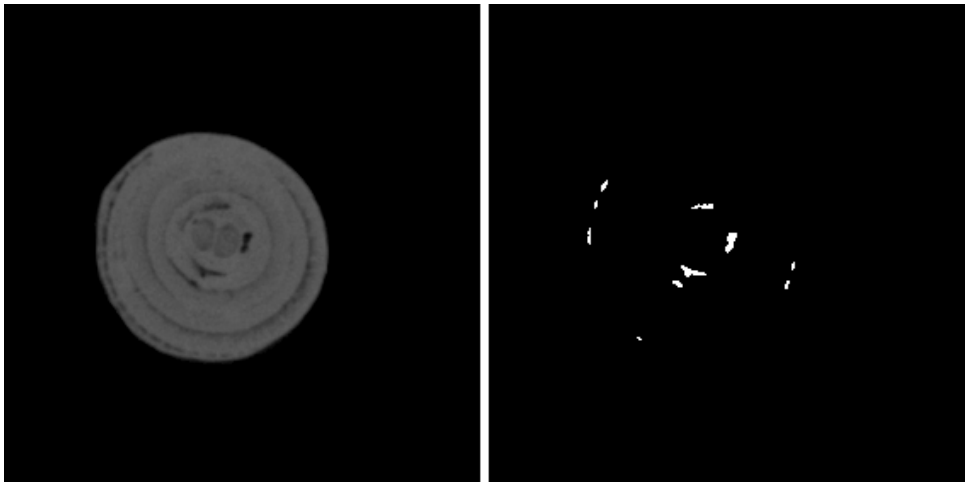

Figure 3.37: *Segmented features in the second Botrytis-inoculated onion*

The first Botrytis-inoculated bulb's most prominent feature is the crescent shaped region near the center. Such crescent shapes appear as fungal infection spreads through and decays a single layer of the onion without affecting the surrounding layers. The overall curvature of the shape leads to a relatively low aspect ratio, even though the damage occurs in a narrow channel within the onion. The compactness value, however indicates a feature that has a long outer perimeter compared to its surface area. The low irregularity value arises as the edges of the damage feature are bordered mostly by healthy onion layers which exhibit smooth edges.

The features isolated in the second Botrytis-inoculated onion are relatively small compared the ones in the first onion. The features near the outer edge of the bulb were likely natural dark spots that appear in the more dried outer layers of the bulbs, and the features closer to the center could be caused either by shoot formation or fungal decay. Discrimination between healthy tissues and damage is difficult in this particular specimen, as none of the features exhibits notably high or low compactness, aspect ratio, or irregularity values.

Table 3.5: Botrytis Onion #2 Feature Characteristics

Feature	Size (Pixels^2)	Size (mm^2)	Compactness	Aspect Ratio	Irregularity
1	48	12.00	13.8	7.07	0.42
2	44	11.00	21.36	9.22	0.51
3	27	6.75	20.57	7.07	0.52
4	15	3.75	16	5.1	0.51
5	15	3.75	9	3.61	0.44
6	14	3.50	9.6	3.61	0.44
7	9	2.25	10	2.83	0.51
8	7	1.75	8	2.24	0.55
9	7	1.75	8	2.24	0.55
10	3	0.75	4	1.41	0.7

This bulb displays extensive internal damage. The largest damage features, upon segmentation of the image, become connected, forming an especially large cluster with a high compactness value. Nevertheless, the irregularity of this feature is low, as the fungal decay is still constrained to specific layers within the bulb.

The fourth and fifth bulbs inoculated with Botrytis show no visible signs of decay in transverse cross section. The isolated features that emerge after binary segmentation are naturally occurring dark spots that sometimes appear between the layers. These features are characterized by their small size, and an automated quality evaluation system should only evaluate features above a set size threshold.

3.3.2 Three-Dimensional Images

The pathogens did not grow as readily in the set of Peruvian-grown sweet onions as they did in the Georgia-grown Vidalia onions, likely owing to the greater disease resistance of the Peruvian onions. In several cases, the onions were incubated for such a long period that their newly exposed necks dried out, leading to dark, low density regions in the CT images

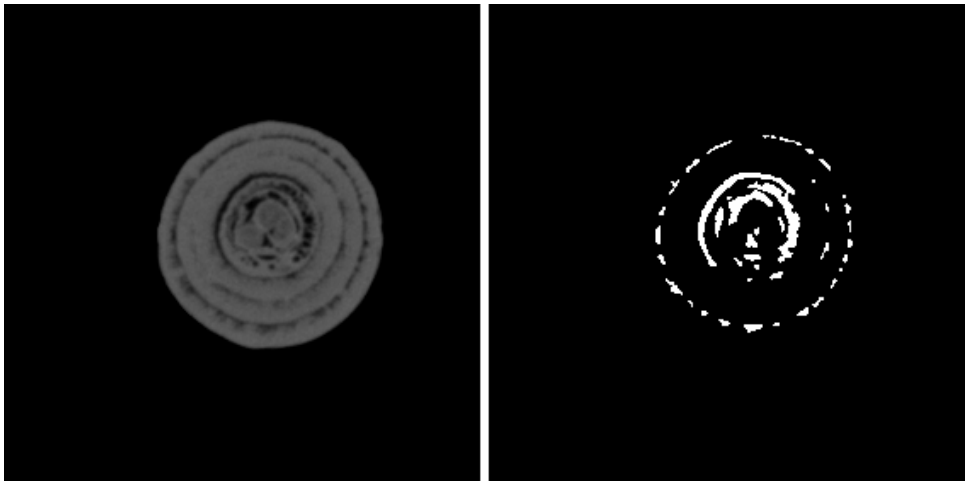

Figure 3.38: *Segmented features in the third Botrytis-inoculated onion*

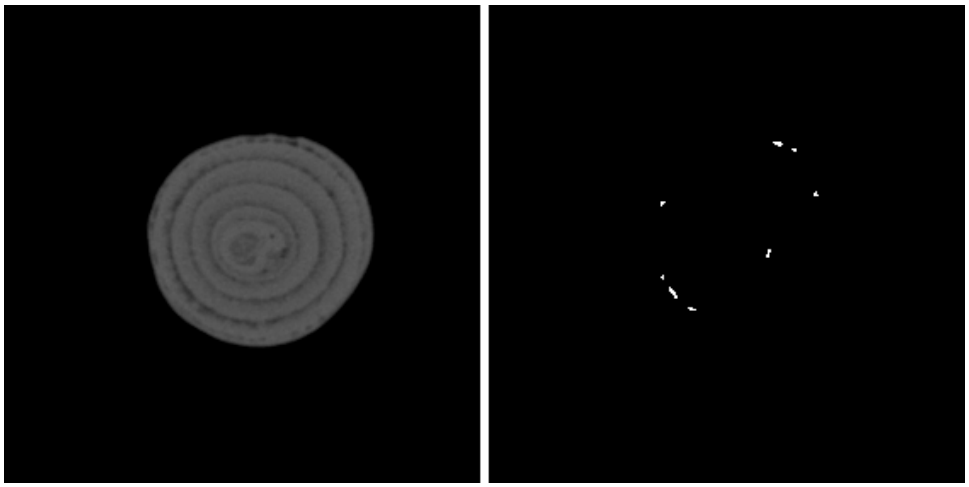

Figure 3.39: *Segmented features in the fourth Botrytis-inoculated onion*

Table 3.6: Botrytis Onion #3 Feature Characteristics

Feature	Size (Pixels^2)	Size (mm^2)	Compactness	Aspect Ratio	Irregularity
1	660	165.00	152.03	3.46	0.29
2	169	45.25	29.65	16.12	0.47
3	55	13.75	19.45	10	0.49
4	37	9.25	11.61	5	0.33
5	37	9.25	13.92	6.08	0.42
6	33	8.25	19.88	6.4	0.49
7	29	7.25	13.33	5.1	0.43
8	28	7.00	15.21	5.1	0.48
9	24	6.00	25	8.54	0.59
10	22	5.50	11.13	4.12	0.46

that are difficult to discern from damage caused by actual pathogen growth. One onion inoculated with *B. cepacia* exhibited signs of infection, one onion inoculated with *B. allii* exhibited signs of infection, and none of the onions inoculated with *P. viridiflava* displayed any signs of infection. The nine 3D-scanned onion bulbs are shown in Figures 3.41 – 3.49. Slices from initial, pre-inoculation scans are shown on the left-hand side of the figures, and slices from the final scans (when bulbs show signs of pathogen damage, or at the end of the study period) are shown on the right-hand side. The slices are presented in oblique view to show internal structure as well as spatial arrangement, though the interslice spacing has been enhanced to prevent slices from overlapping and occluding each other.

3.3.3 Multicenter Bulb Detection

Though the Peruvian sweet onions did not readily grow pathogens in the laboratory setting, they did exhibit other attributes that can be useful in the development of a CT-based onion quality control protocol, namely multiple centers. All but two of these nine specimens had at least two centers. In the transverse cross sectional images, regions in which multiple centers

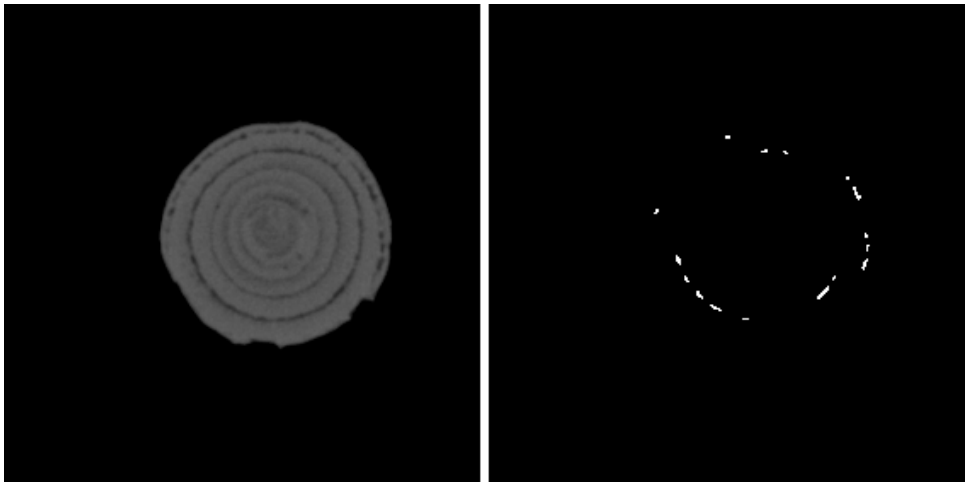

Figure 3.40: *Segmented features in the fifth Botrytis-inoculated onion*

collide tend to exhibit small, dark air gaps where the curvature of the onion scales will not fill the space. These air gaps were identified by computing a 3x3 pixel local variance of each slice. This operation effectively enhanced small image features in which there was great contrast between the feature and its surroundings, such as these air gaps between onion centers and the outline of the onion bulb against the black background. Figure 3.50 shows the results of running this 3x3 variance on each onion slice and recombining the slices via a mean value Z-projection. The single center bulbs display a relatively homogeneous internal texture, whereas the air gaps associated with multiple centers show up as bright regions near the center of bulbs with multiple centers.

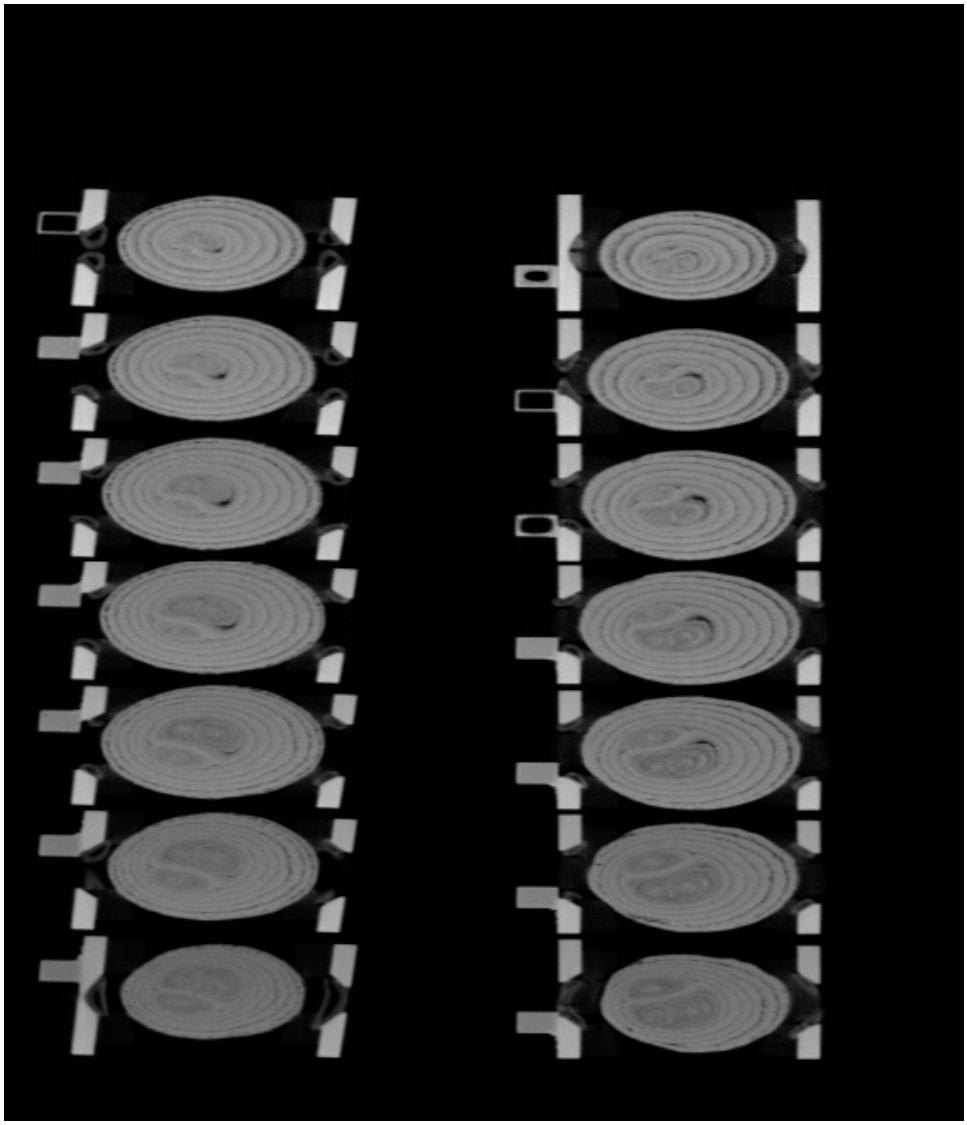

Figure 3.41: *The sixth* B. cepacia*-inoculated onion. No signs of damage were evident after the conclusion of the seven week study period.*

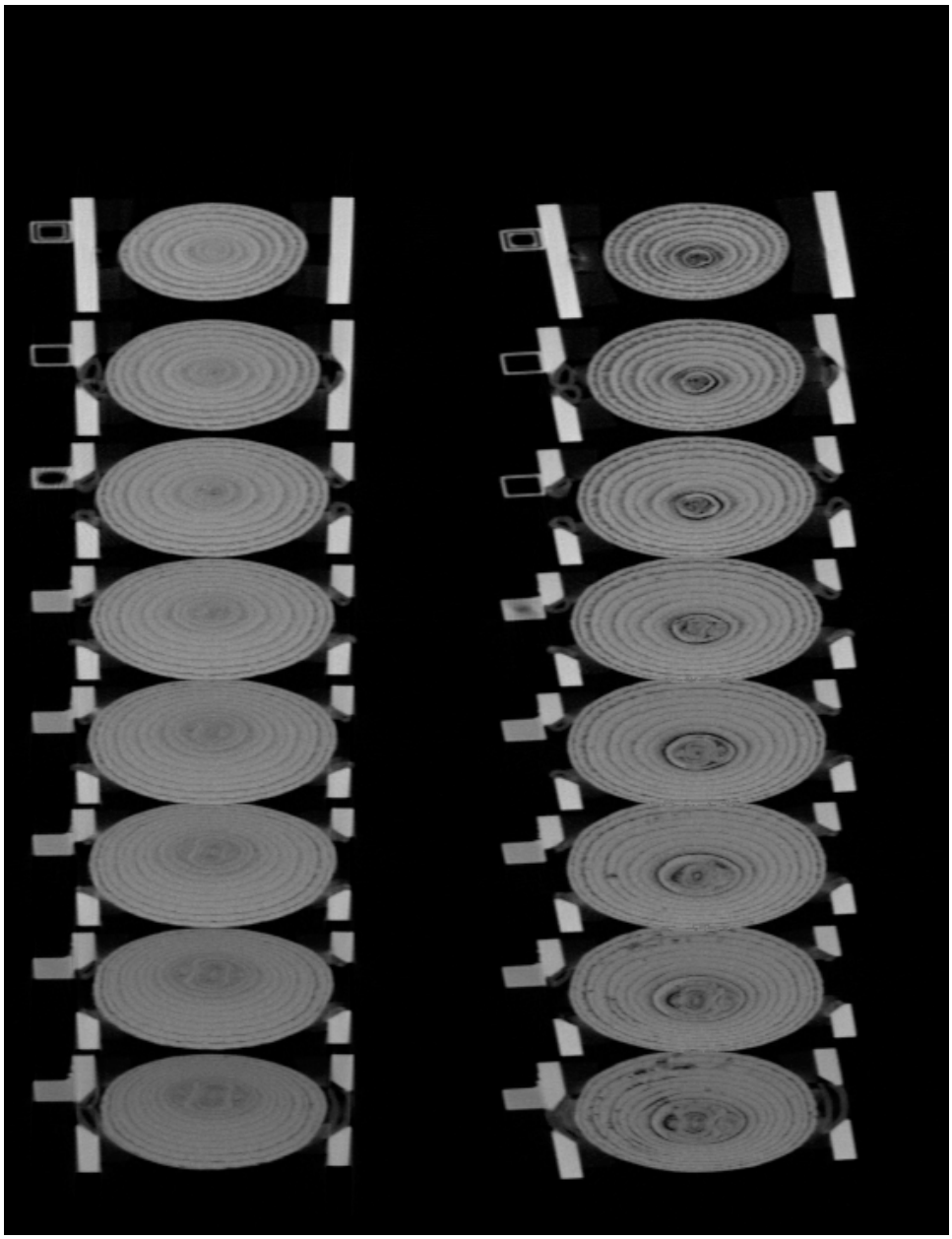

Figure 3.42: *The seventh* B. cepacia*-inoculated onion. Extensive damage is evident after five weeks of incubation, though the damage lesions appear near the root end of the bulb, rather than in the vicinity of the site of inoculation.*

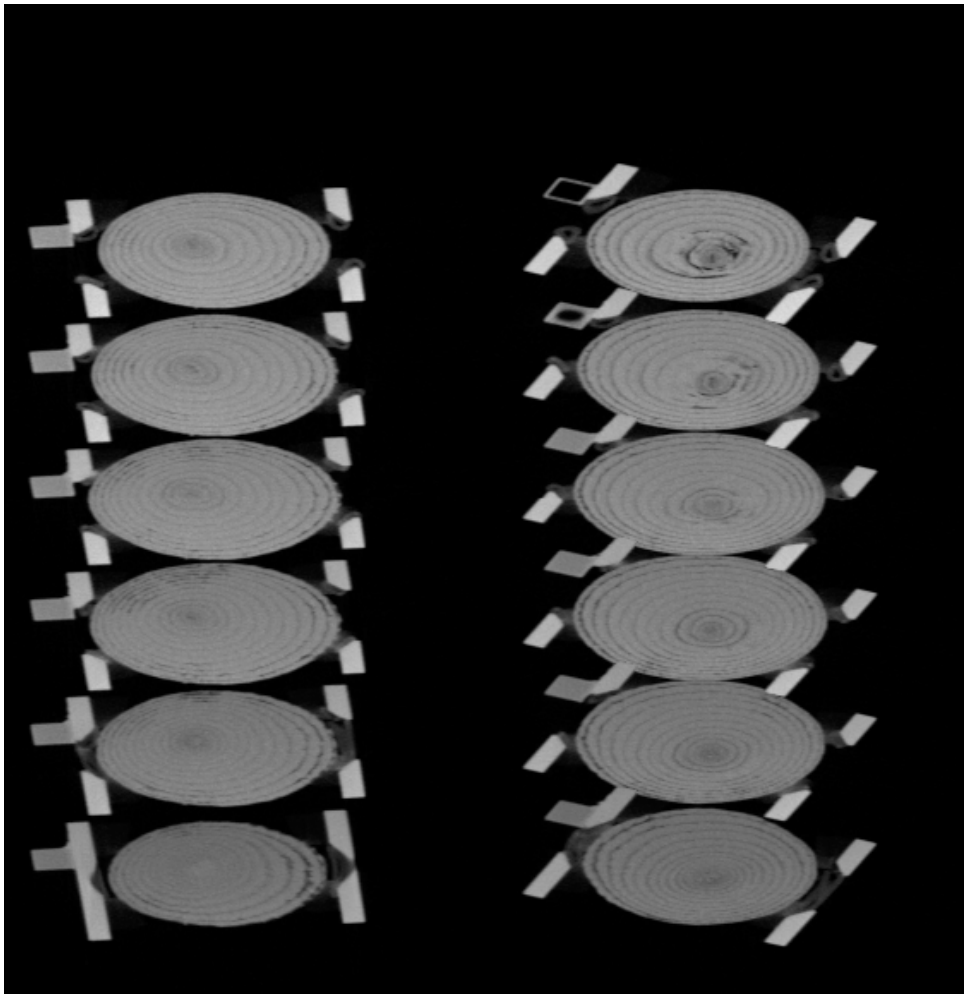

Figure 3.43: *The eighth* B. cepacia*-inoculated onion. Some slight darkening near the neck of the bulb is present after seven weeks of inoculation, though this was likely due to desiccation rather than infection.*

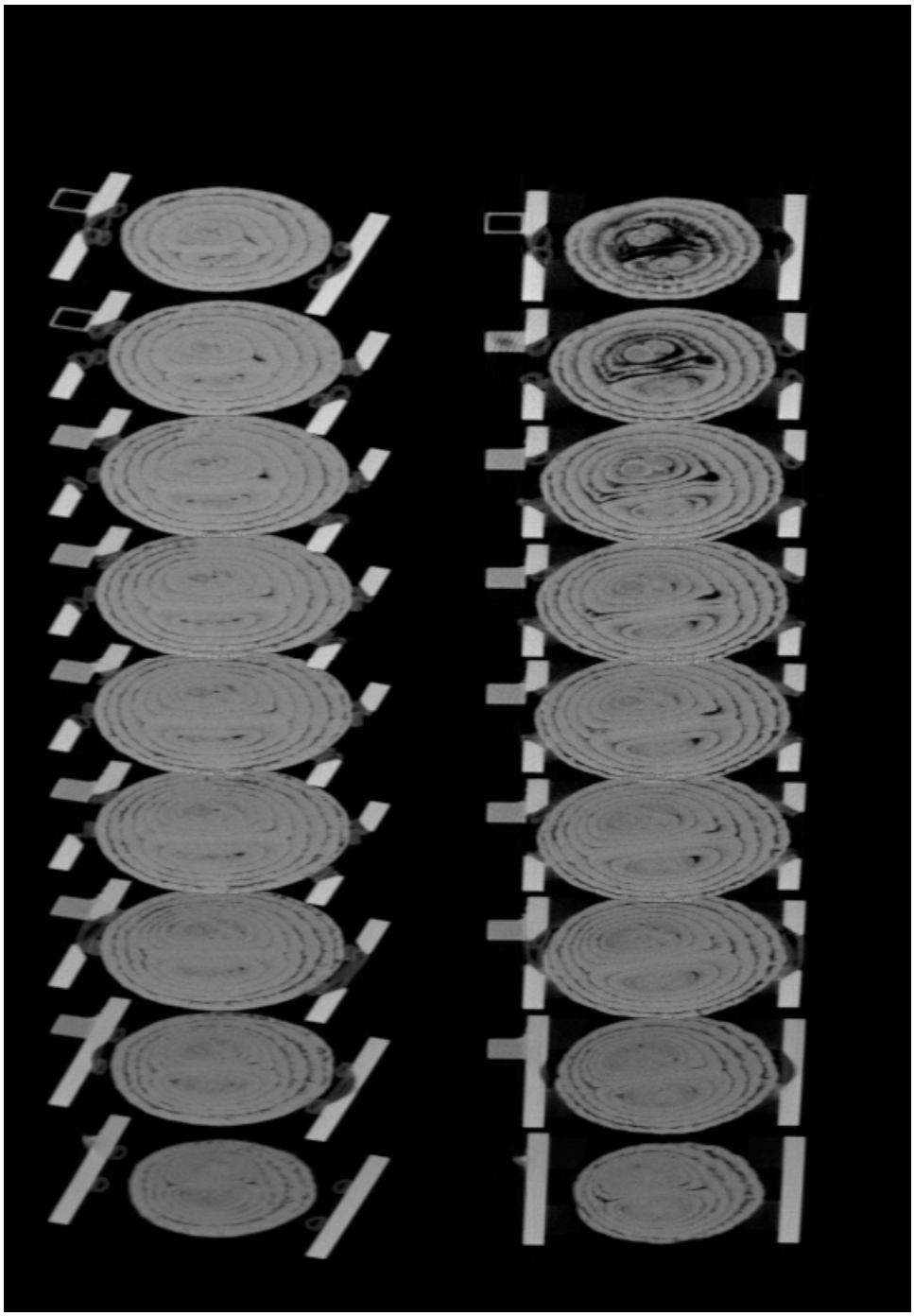

Figure 3.44: *The sixth* B. allii*-inoculated onion. Despite efforts to maintain a humid environment in the incubation vessel, the exposed tissues in the onion's neck dried over the course of the experiment, leading to the damage seen in this image.*

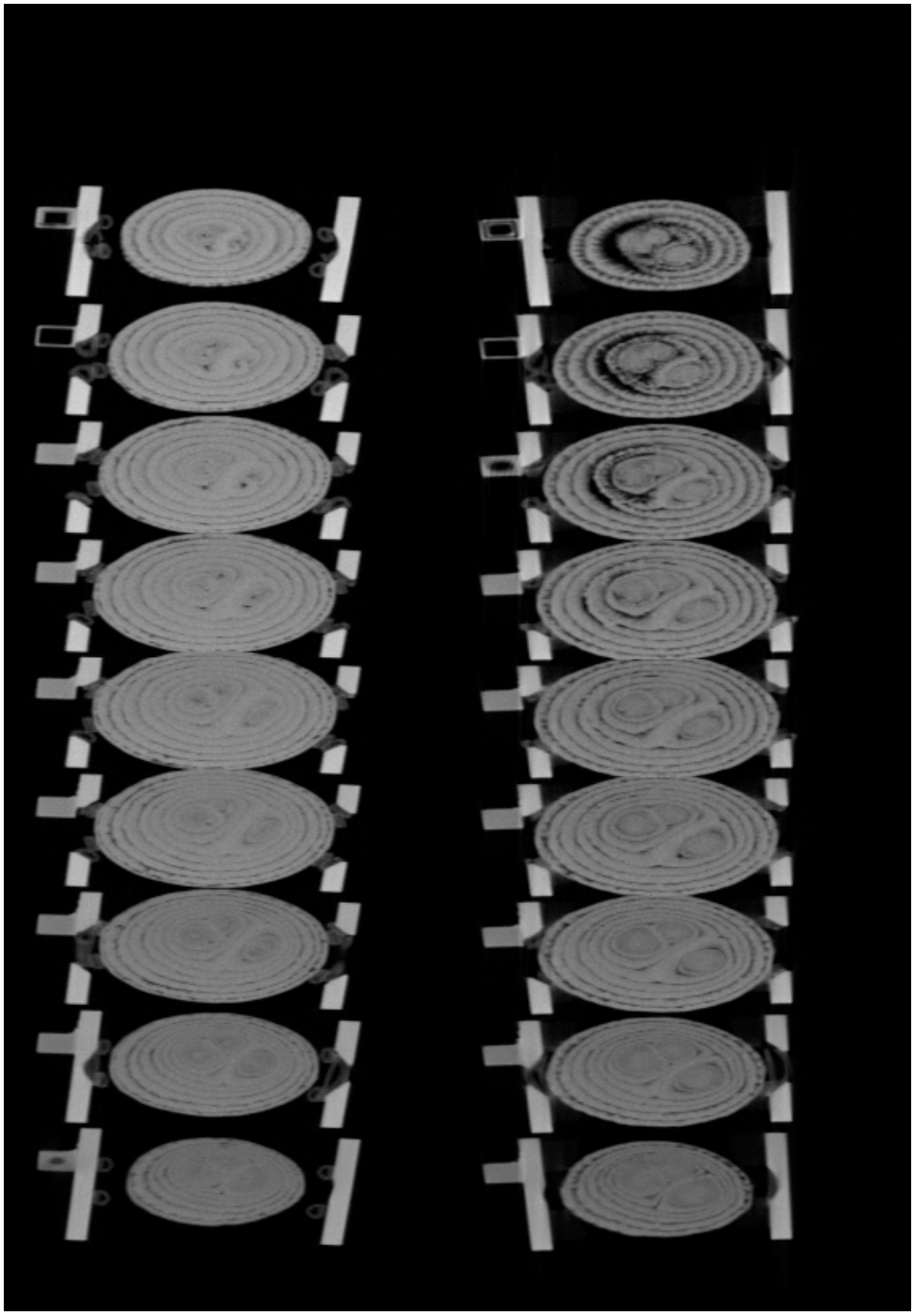

Figure 3.45: *The seventh* B. allii*-inoculated onion. Again, the apparent damage to the neck region of the onion was due to desiccation rather than fungal infection.*

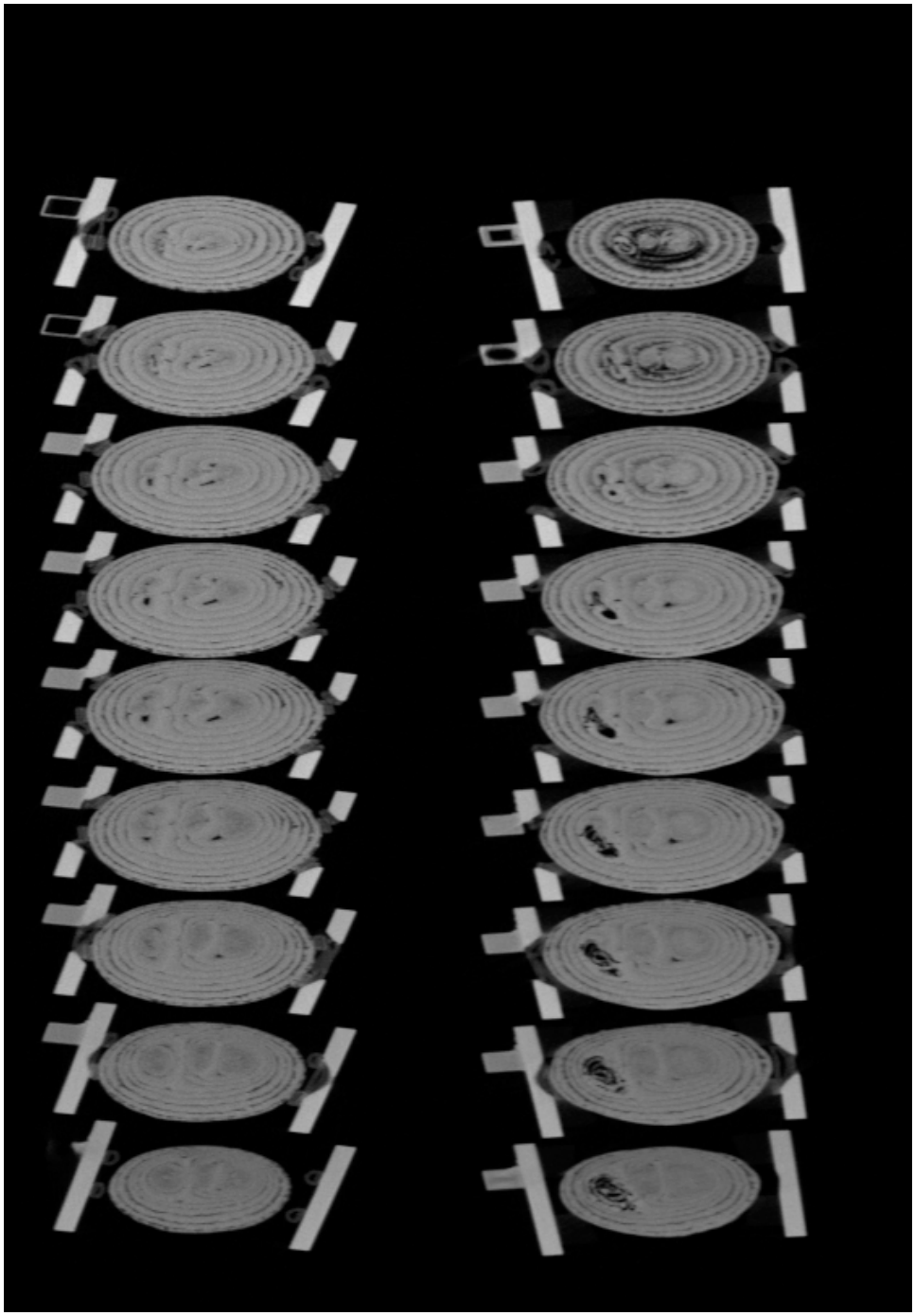

Figure 3.46: *The eighth* B. allii*-inoculated onion. This was the only Peruvian grown onion that was inoculated with* B. allii *to exhibit signs of infection.*

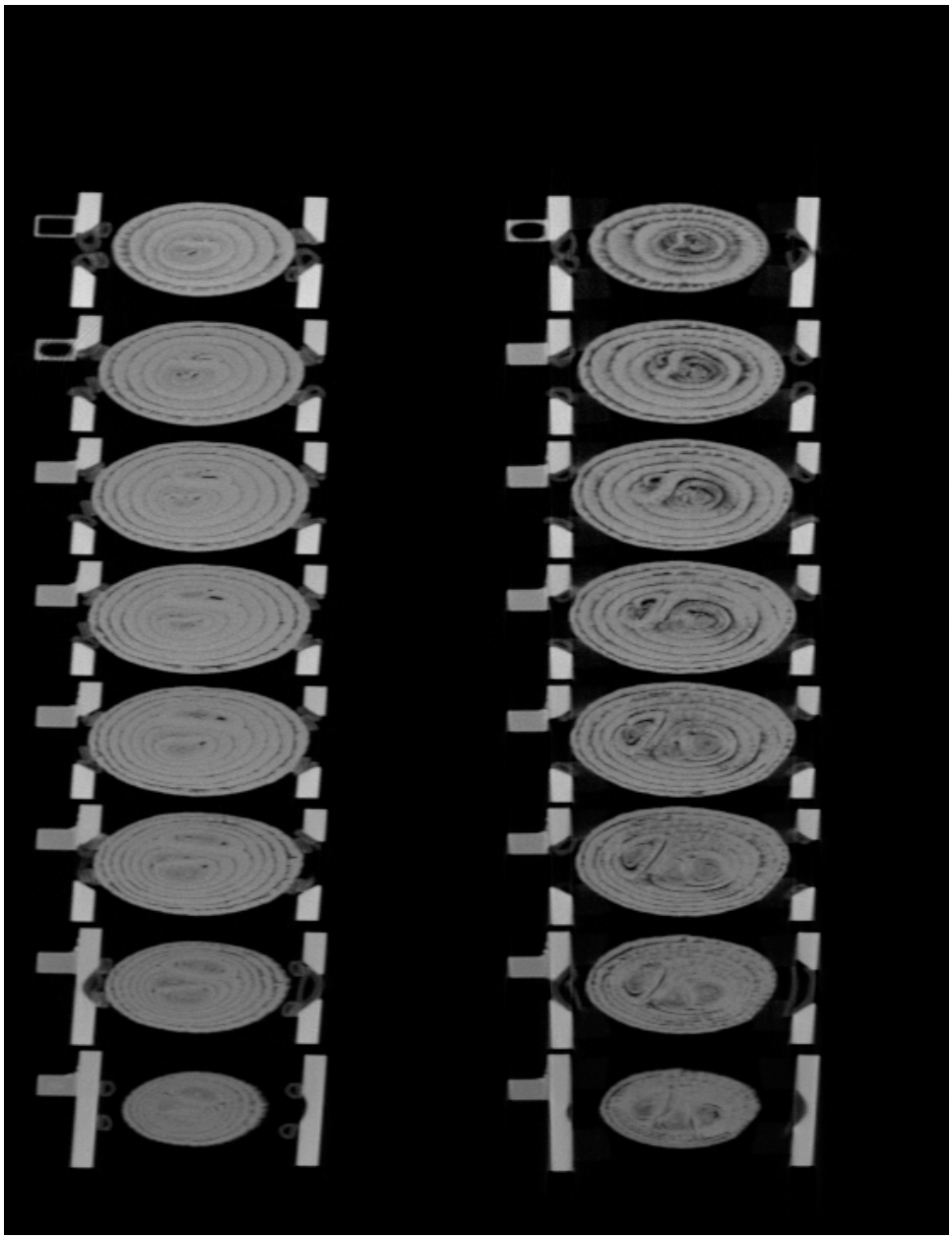

Figure 3.47: *The fifth onion bulb inoculated with* P. viridiflava. *Some slight darkening of the onion tissues can be observed, but this was most likely due to water losses in the incubation chamber over the course of the experiment.*

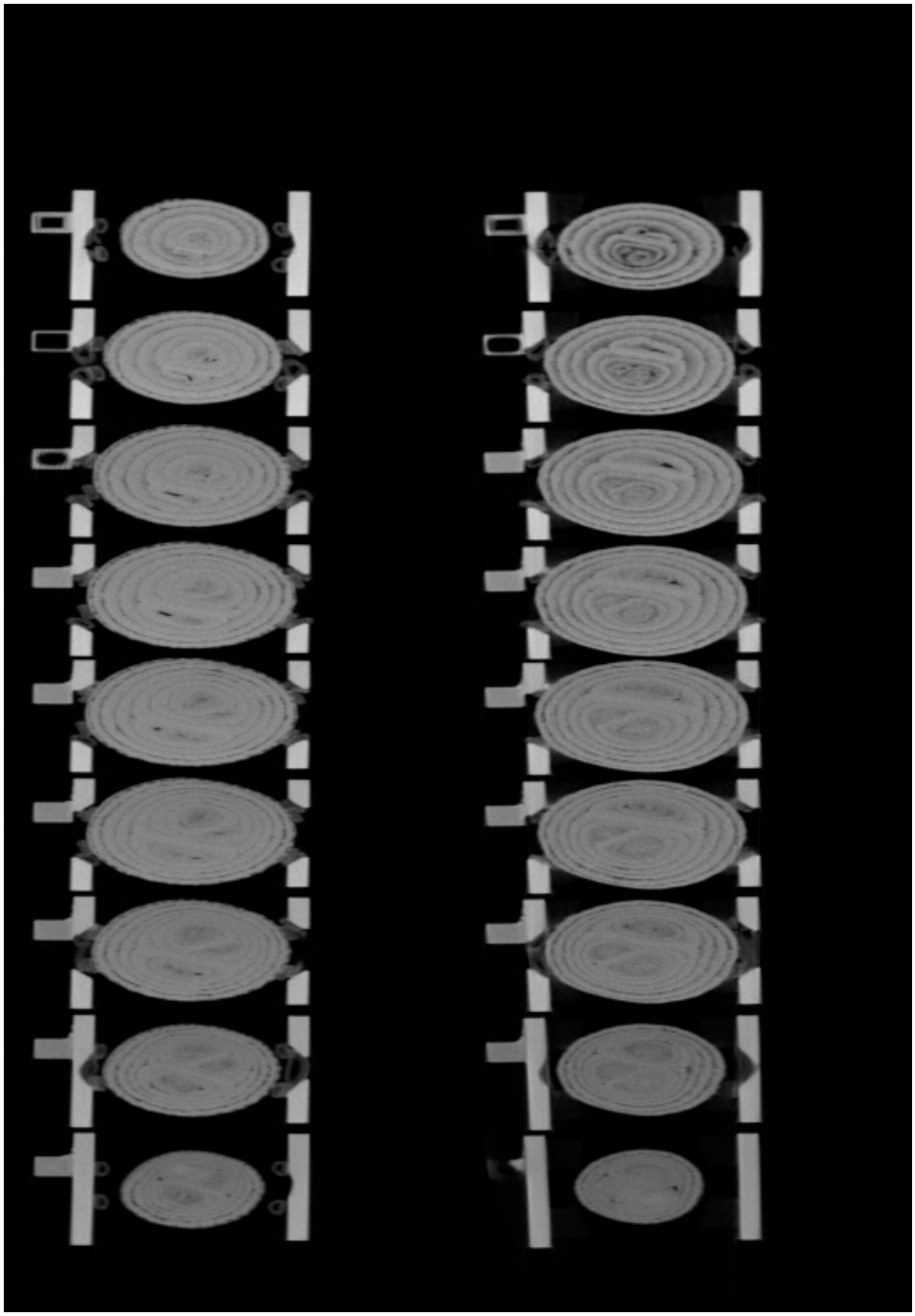

Figure 3.48: *The sixth* P. viridiflava*-inoculated onion. After seven weeks, the bulb is essentially unchanged.*

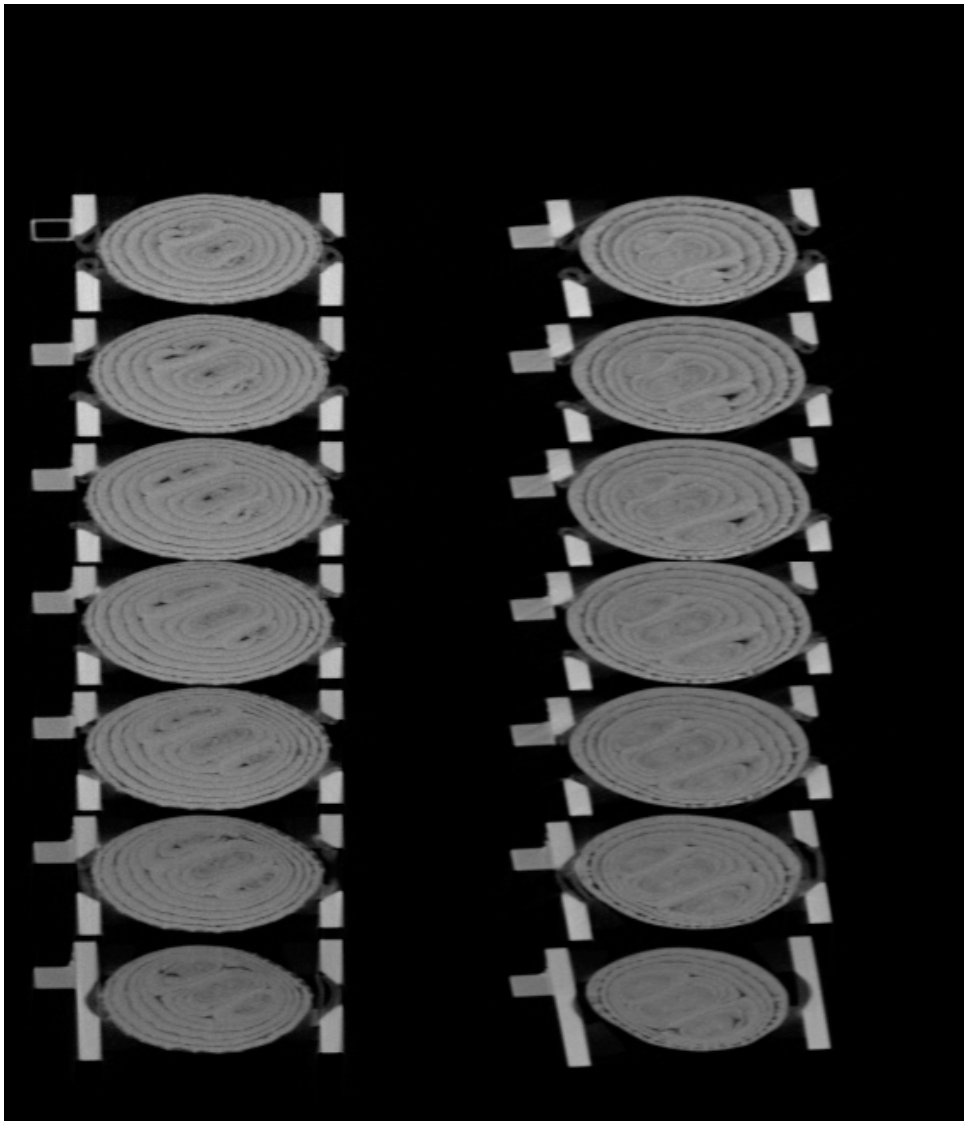

Figure 3.49: *The seventh* P. viridiflava*-inoculated onion. Again, no signs of pathogen-induced damage are evident.*

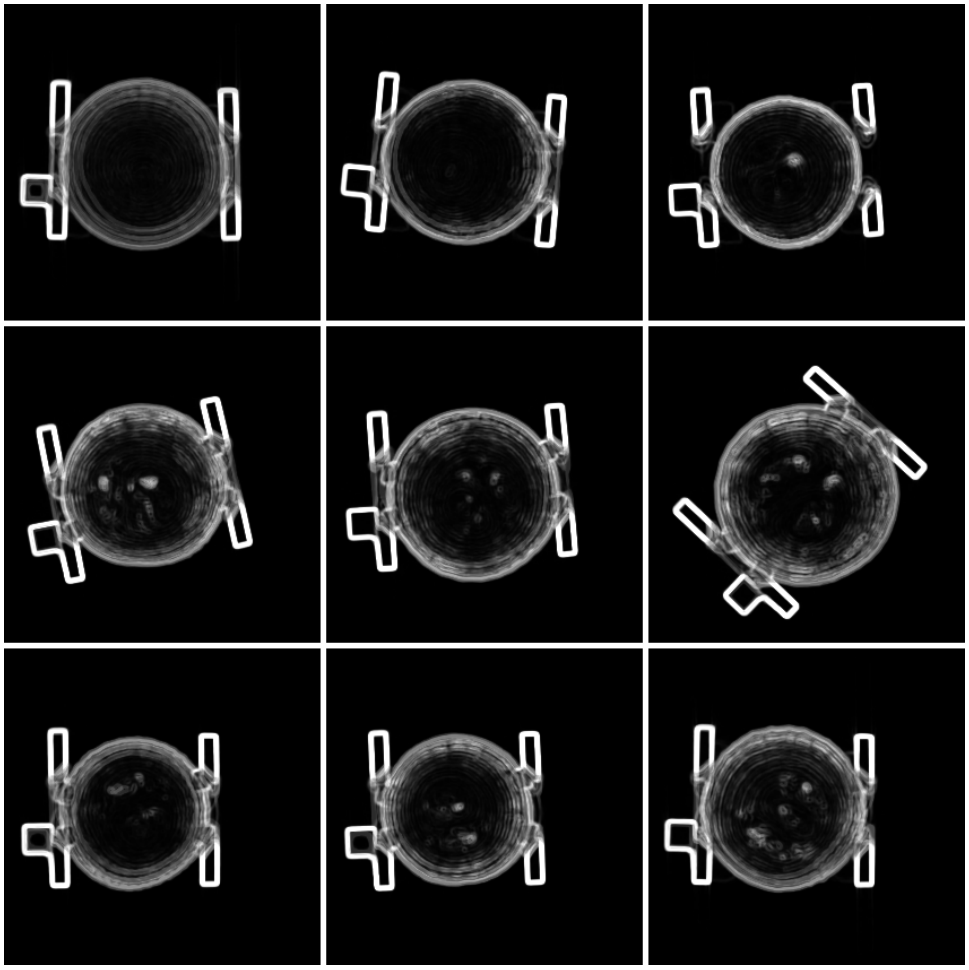

Figure 3.50: *Average intensity Z-projections of transverse cross section image stacks after a 1-pixel variance filter. The bulbs in the upper left and upper middle panels have single centers and the other bulbs have two or more centers. Small, localized regions near the center of the bulb exhibiting high variance are indicative of air gaps that occur between multiple onion centers.*

3.4 Experiment 4: Onion Bruising

The following image galleries show longitudinal and transverse cross sections of the bulbs dropped onto hard concrete. The first column shows cross sectional images of the onion bulb as received, prior to any laboratory-induced impact damage. The center column shows the onion bulb immediately after being dropped. Finally, the right-hand column shows the onion bulb three days after being dropped. Interestingly, evidence of damage becomes more prominent after the onions have been stored for a period of time; longitudinal images of the two bulbs dropped from 70 cm and 105 cm show slight signs of damage immediately after being dropped, though these signs are subtle, and it would be difficult to devise an automated system that would be able to discern such damage from natural variation inside the onion tissues without a priori knowledge that the bulb had been subjected to impact damage.

The bulb dropped repeatedly from 17.5 cm (Figure 3.51) exhibits characteristic damage patterns within its inner scales. Jagged, irregular dark regions appear inside the scales, but these features end where they coincide with the dark boundary regions between the scales. In other words, if one were to trace these dark scale boundaries, the interior edge (facing inward, towards the center of the onion) continues smoothly as in a healthy onion, whereas the outer edge exhibits jagged and irregular regions. This observation applies to the longitudinal images as well as the transverse images.

The bulb dropped from 35 cm (Figure 3.52) also exhibits these characteristic damage patterns. Additionally, in the transverse image, it appears that the impact has caused one of the inner scales to split completely in half.

The bulb dropped from 70 cm (Figure 3.53) exhibits some of the characteristic damage features observed in the bulbs dropped from shorter heights, though in its outer scales, the inter-scale dark regions have disappeared. Such high impact forces have apparently caused

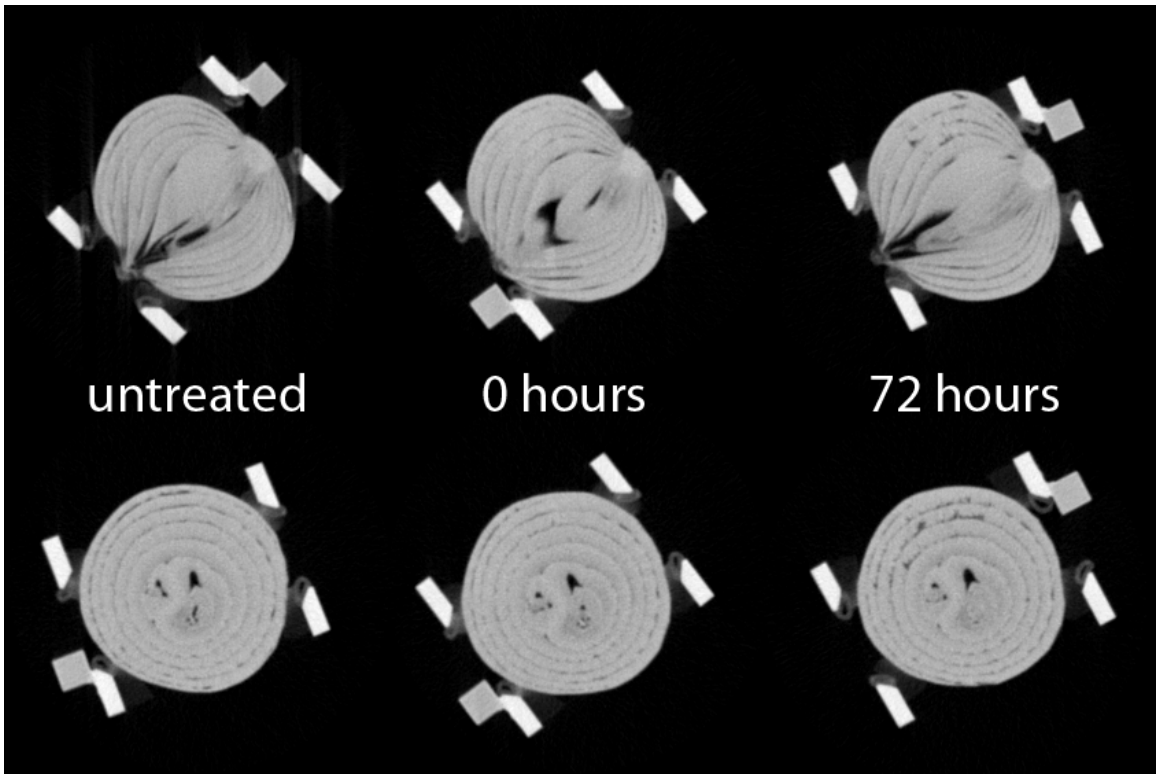

Figure 3.51: *Onion dropped six times from a height of 17.5 cm.*

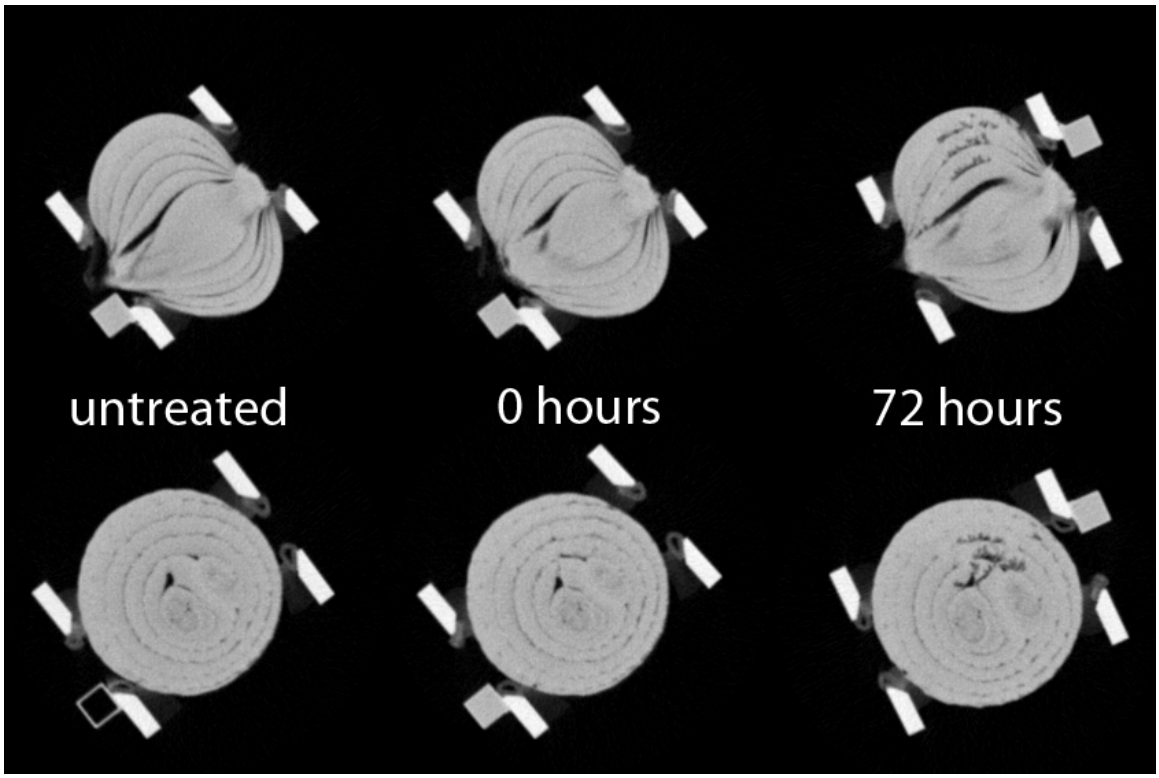

Figure 3.52: *Onion dropped six times from a height of 35 cm.*

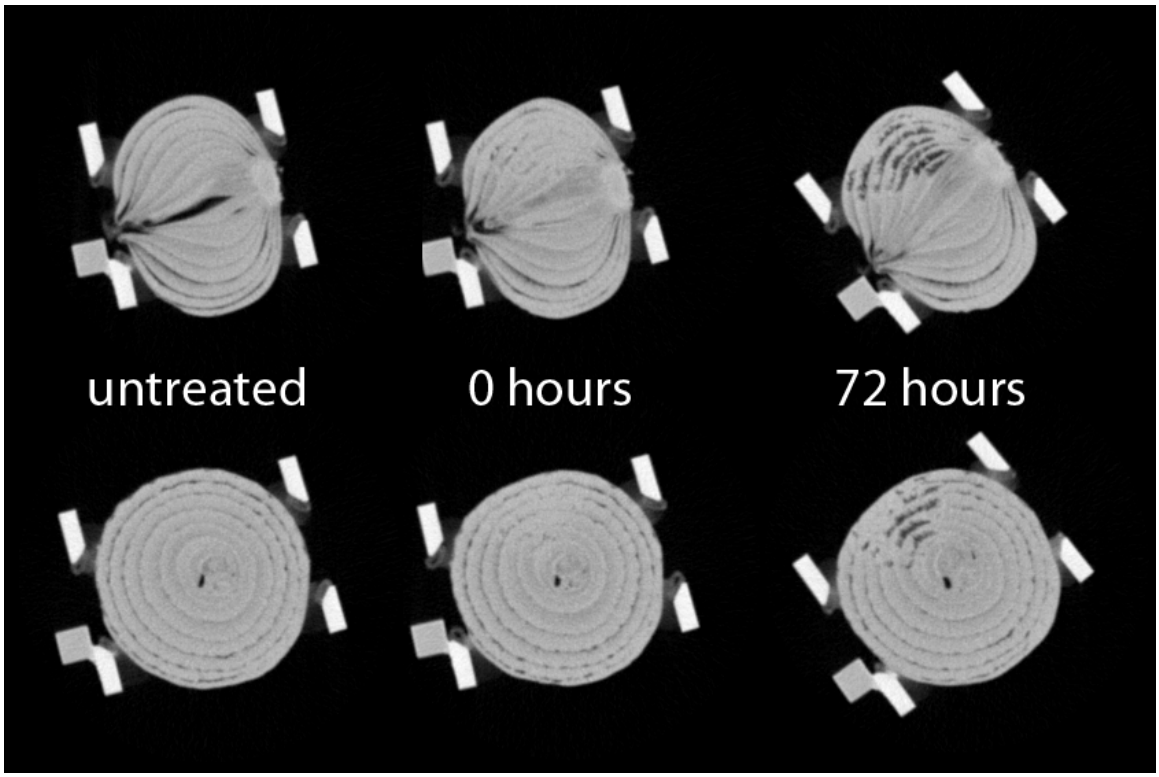

Figure 3.53: *Onion dropped twice from a height of 70 cm.*

such substantial damage to the scales that they can no longer be clearly discerned, perhaps due to fluid leakage filling these interlayer gaps. This effect can be observed in the images obtained immediately after the drop treatment, as the dark spaces between the scales merge together near the impact site, whereas one can easily follow them in the pre-treatment images.

The bulb dropped from 105 cm (Figure 3.54) also exhibited the damage patterns observed in the above specimens. However, the merging of the interlayer gaps is less prominent immediately after treatment than in the bulb dropped from 70 cm.

Damage features were easily isolated via a manual bilevel image value segmentation. Unfortunately, such a naive technique has drawbacks; hollow center shoots in the onions

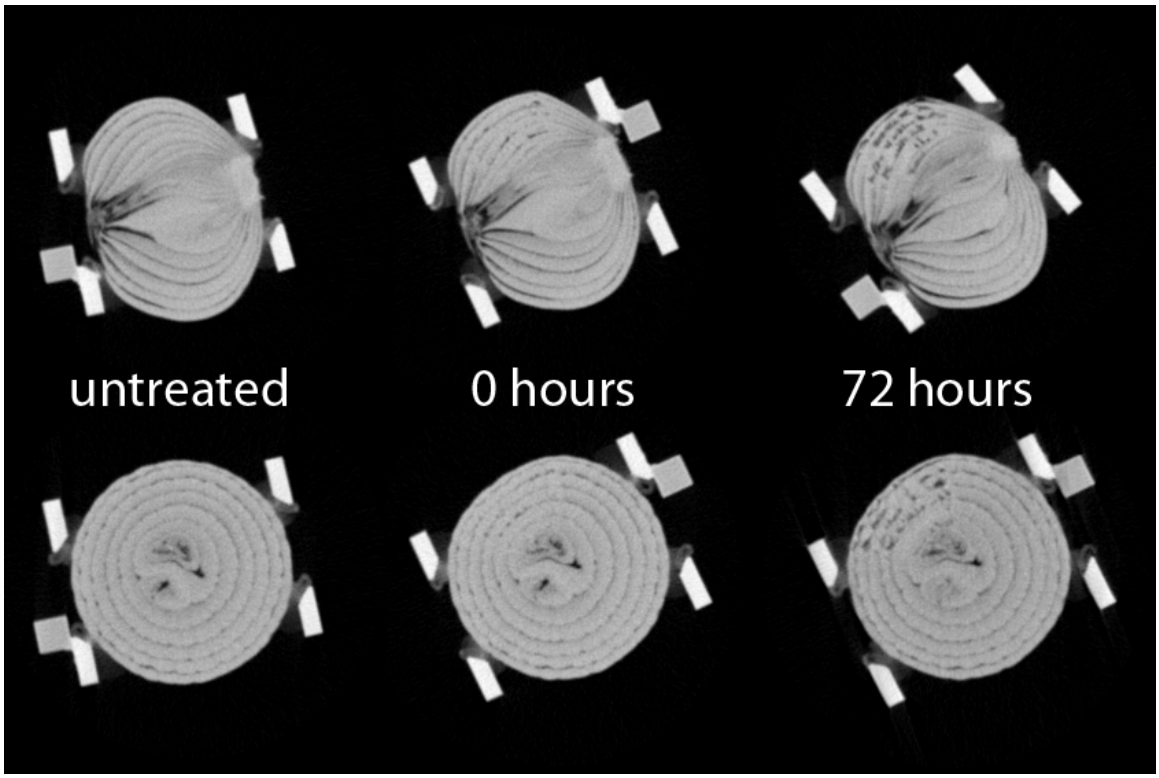

Figure 3.54: *Onion dropped once from a height of 105 cm.*

were often included in the segmented features, as were normal minor blemishes and some particularly dark inter-scale spaces. Figure 3.55 shows the transverse cross sectional images after manual removal of the specimen holder in the image and bilevel segmentation. In all specimens, with the exception of the one dropped from 35 cm, hollow bulb centers have been segmented along with bruise damage. The segmented image of the bulb dropped from 105 cm shows spurious dark regions in the bulb's tissue that were segmented along with the damage features.

Both proposed evaluation techniques show promise in discriminating bruise damage features from other low density regions inside onion tissues. The results of the scaled damaged area calculation that is based on a feature's distance from the onion centroid can be seen in Figure 3.56. Threshold values that determine whether a feature is considered part of a bruise were arbitrarily chosen. In Figure 3.56, gray-colored features have values between 5 and 10. Black-colored features have values of 10 and above. In practice, this weighted damaged area would likely have to be normalized, and threshold values would be between 0 and 1, thereby allowing for a wide range of different size onions to be evaluated. The higher the weighted damaged area value of a feature, the more likely this feature is to be part of a bruise.

Figure 3.57 shows the calculated center of bruise damage for each specimen and an associated neighborhood surrounding this center. If there exist several large pixel area regions that fall outside this central neighborhood, it could be an indication of widespread pathogen damage. Smaller features located outside this neighborhood, by contrast, could simply be vascular structures in the onion tissues that were included in the damage feature segmentation process.

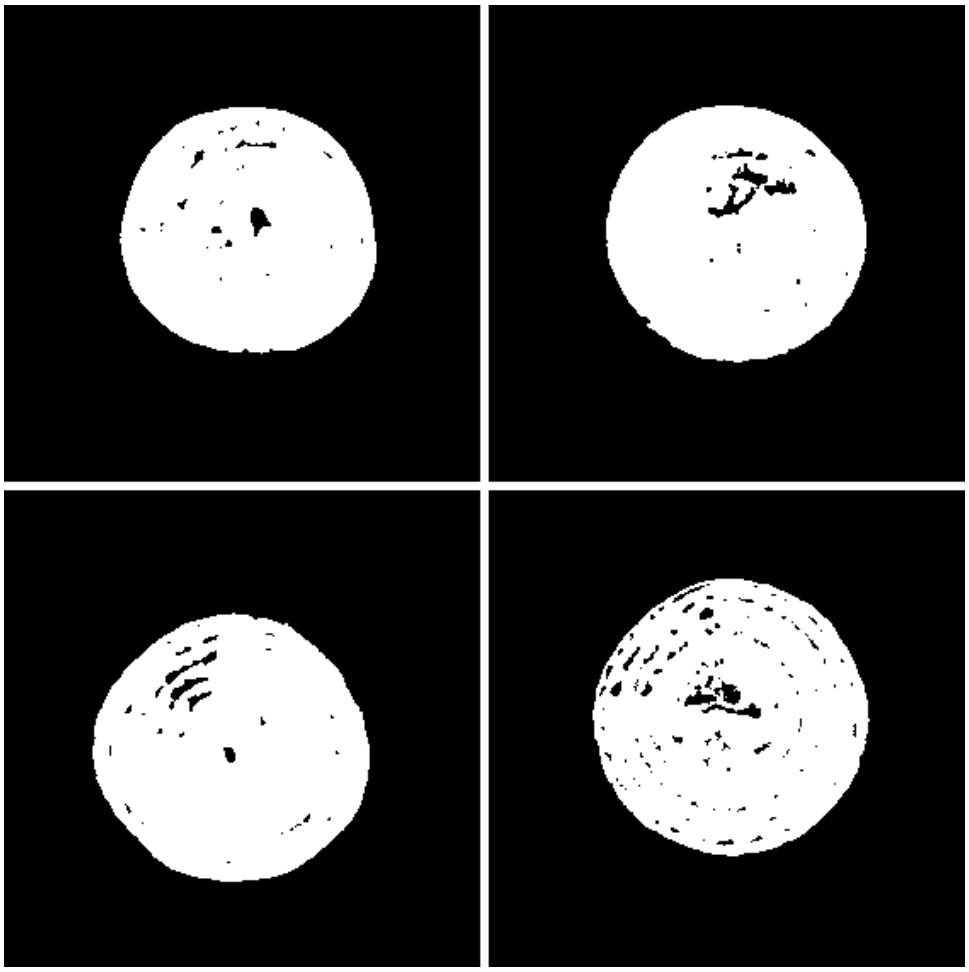

Figure 3.55: *Transverse cross sectional images of drop-tested onions after segmentation and removal of specimen holder.* ***Top Left****: Onion that was dropped six times from a height of 17.5 cm.* ***Top Right****: Onion that was dropped six times from a height of 35 cm.* ***Bottom Left****:Onion that was dropped twice from a height of 70 cm.* ***Bottom Right****: Onion that was dropped once from 105 cm.*

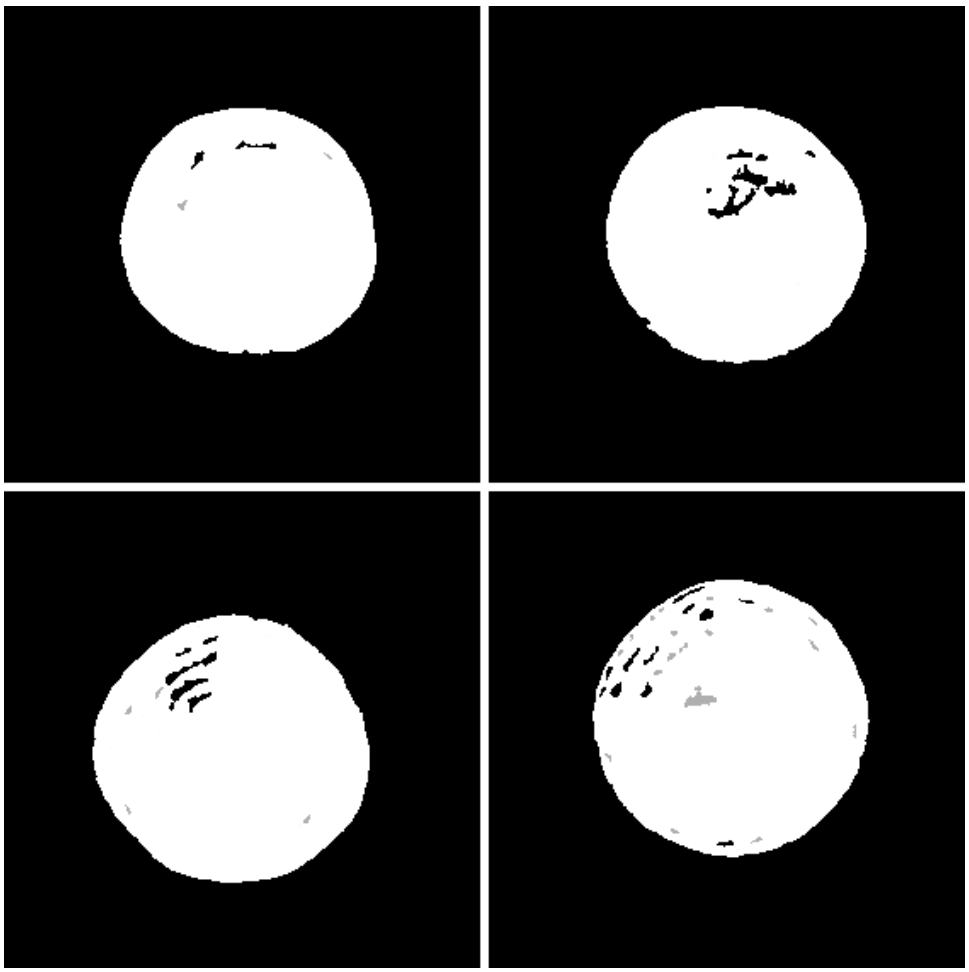

Figure 3.56: *Bruise damage features as determined by a weighted damaged area function. Black-colored features have a higher likelihood of being associated with bruise damage, whereas gray-colored areas are considered somewhat less likely to be part of a bruise.* ***Top Left****: Onion dropped six times from 17.5 cm. Two high likelihood bruise features and two intermediate likelihood features remain after analysis.* ***Top Right****: Onion that was dropped six times from 35 cm. Only high likelihood features remain.* ***Bottom Left****: Onion that was dropped twice from 70 cm. The largest, concentric features all rank as high likelihood bruise features.* ***Bottom Right****: Most spurious features have been excluded, though a few intermediate likelihood bruise features and one high likelihood feature remain around the periphery of the bulb.*

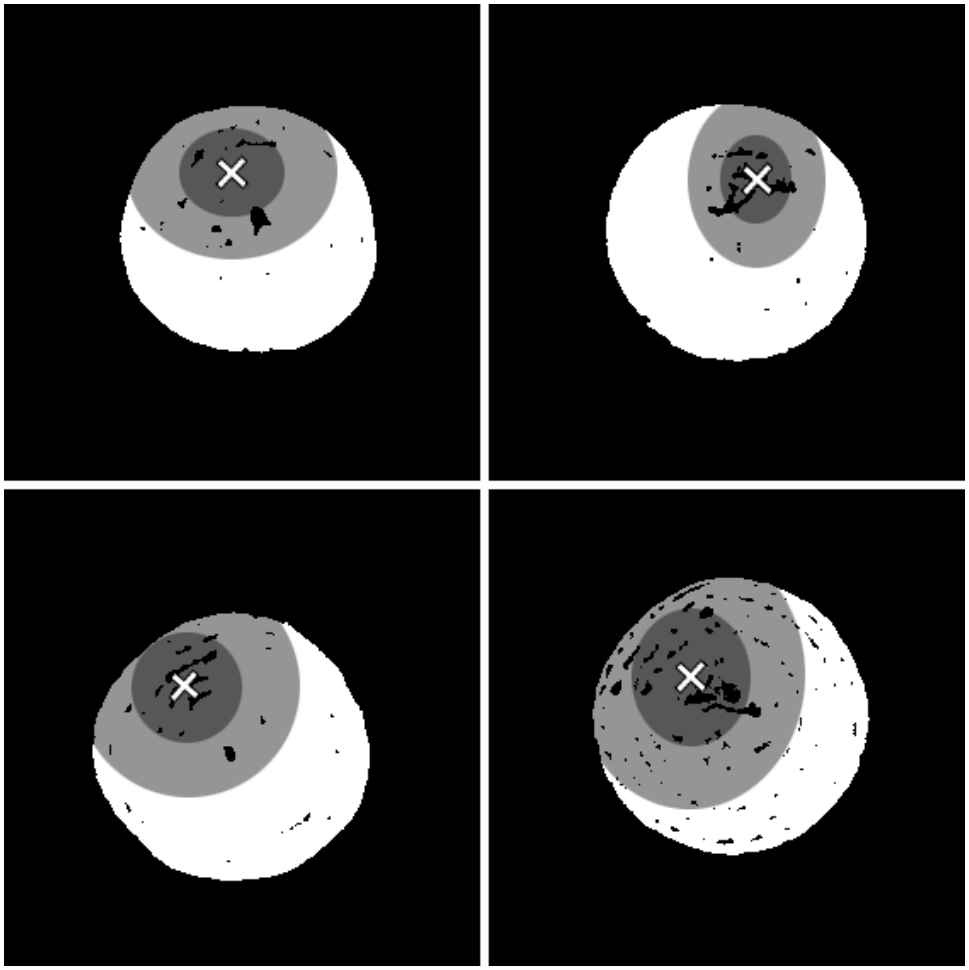

Figure 3.57: *Localization of damage features in the onion cross section images. White crosses indicate the predicted center of damage based on the arrangement of detected damage features. Dark gray shaded regions indicate a neighborhood within one standard deviation from the predicted center, and light gray regions indicate areas within two standard deviations of the center. Such statistical means are useful in screening features caused by mechanical damage to onion bulbs from other low density features in onion tissues that could be caused by natural morphological variation, uneven drying, or pathogen damage.*

Chapter 4

Conclusions

4.1 Experiment 1: Image Optimization

After some initial tuning, the low-cost CT scanner apparatus used in this project proved to be a reliable instrument for the imaging of agricultural specimens for quality control purposes. Mechanical stability was found to be of paramount importance, as even small vibrations or shifts of the object under study caused ghosting and blurring in reconstructed images. Collimation of the x-ray beam also proved to be an important factor affecting image contrast and sharpness. A round aperture with a 0.6 mm diameter at the x-ray beam and a 2.5 mm diameter aperture at the x-ray detector were found to offer the best compromise between contrast and sharpness. Finally, the anode voltage of the photomultiplier x-ray detector was adjusted to provide a wide range of pixel intensity values without saturating the detector. A setting of 800 V was found to be ideal for this particular apparatus.

4.2 Experiment 2: Hypodermic Inoculation

B. cepacia was found to grow readily in laboratory-inoculated Vidalia sweet onions, and lesions on onion bulb tissues were evident within 10-21 days after inoculation. Once damage was evident, the onion bulbs decayed rapidly over the course of 2-3 days. Surface damage to the onions caused irregularities in the bulbs' outlines in several cases, and these surface irregularities were detectable with binary image thresholding and Fourier shape analysis. Internal damage was characterizable by crescent-shaped regions of low density in the interior of the bulb in transverse cross section exhibiting large compactness values. Additionally, smaller dark regions tended to cluster around the point of infection near the periphery of the bulb, providing another possible cue for detection of this pathogen in harvested onions.

P. viridiflava did not grow as readily or as fast as *B. cepacia*, and only two of the four specimens exhibited any signs of infection by the end of the experiment. In both of the specimens that exhibited damage, transverse cross sectional images revealed small, round lesions near the outer edges of the bulbs.

In several instances, longitudinal cross section images of the bulbs provided a clearer view of pathogen damage as well as the progress of pathogens inside onion tissues. However, natural morphological variation between individual onion bulbs would make automated segmentation and characterization of damages difficult in images obtained at this projection orientation. Furthermore, each onion being imaged would have to be rotated about its root-shoot axis and re-imaged repeatedly to obtain sufficient coverage to locate localized damages. Multiple transverse images, by contrast, can be more easily obtained via a multi slice clinical CT scanner, and these slices have the advantage of more simplistic geometry (concentric circular rings), greatly simplifying the process of automatically and programatically identifying damages or other undesirable features.

4.3 Experiment 3: Neck Inoculation

The crescent shaped dark regions associated with *B. cepacia* were also found in transverse images of the Vidalia onion bulbs whose necks were inoculated with *B. allii*. These damaged regions, upon segmentation and shape analysis, tended to exhibit large compactness values and low irregularity values, as these elongated shapes tended to remain constrained within specific layers in the onion bulbs. Again, in some cases, longitudinal cross sections elucidated the path of the pathogen's damage throughout the onion bulb, but the high variability in onion tissue morphology in this projection made automated image processing extremely difficult.

The Peruvian-grown sweet onions did not decay as readily as the Vidalia-grown onions when inoculated with *B. allii*, *B. cepacia*, and *P. viridiflava*. However, these were found to be more likely to have multiple centers, and texture analysis was utilized to discriminate single center bulbs from those with multiple centers. By running a 3x3 pixel variance operator on multiple transverse cross sections obtained at differing depths over the onion, small dark voids that occur at the junctions of multiple centers were emphasized. These cross section images were then z-projected to form a single transverse image. Onion bulbs with multiple centers exhibited multiple "hot spots", near the center of the bulbs, where as single center bulbs did not.

4.4 Experiment 4: Onion Bruising

The onions subjected to drop damage did not display signs of damage in CT images until a couple days after being damaged. Bulbs subjected to repeated low impact forces displayed internal signs of damage, as did those subjected to single high impact events, though none of these bulbs exhibited external signs of damage.

As bruise damage tends to be localized to a specific section of the bulb near the outer

layers, methods were developed to pinpoint the point of impact and determine the likelihood that dark regions detected in transverse cross section images were due to bruise damage and not pathogen infection. The weighted damaged area function assigns weighting coefficients to segmented features based on their distance from the center of the onion bulb, and this metric was useful in eliminating features near the center of the bulb, leaving only those that were likely caused by mechanical impacts. Damage localization metrics also help to discriminate bruise damage from other types of damage or naturally occurring dark regions in transverse images by providing a center of impact and likelihood neighborhood surrounding this calculated impact center. Bulbs exhibiting large likelihood neighborhoods have more diffuse damage that is less likely due to impact forces, where as small neighborhoods are indicative of the localized damage associated with impact damage.

4.5 Suggestions for Future Research

Perhaps the greatest drawback associated with a CT-based onion inspection system is the cost of implementing, maintaining, and operating the system. This drawback could be mitigated in part by optimizing the speed at which a crop of onions could be scanned. High speed helical CT scanners used in clinical settings are already capable of axial scan speeds of forty centimeters per second, while obtaining 64 simultaneous slices. Additional research could be conducted to maximize the number of onions scanned per unit time, either by increasing the feed rate of individual bulbs through the machine, or by using parallel lanes through a single scanner that would image multiple onions simultaneously. With such high throughput, fewer devices would be necessary in the packinghouse, leading to lower operating costs. A mobile postharvest evaluation system, similar to the mobile CT and PET/CT imaging systems used in the medical field, could be developed and adapted for use at multiple packing houses.

The economic losses to onion growers due to discards, as mentioned by [35] could also

be partially mitigated. Because a full volumetric image of the onion bulbs is obtained by the CT scanner, lightly damaged bulbs, or bulbs that show localized latent infections could be partially salvaged. CT images could be used to pinpoint damaged regions in individual bulbs, and these damaged regions could be excised with computer-controlled shears, leaving a partially salable bulb. Such bulbs could then be frozen or dried onsite for use in processed foods, allowing the onion grower to recoup some value from what would have been a discarded bulb. Such techniques would lend themselves well to recovering value from bulbs infected with Botrytis, which in its early stages, affects only the upper neck region of the bulb, leaving an otherwise healthy lower bulb portion.

A truly robust postharvest evaluation system would most likely employ multiple sensory modalities. CT imaging has shown promise in the detection of actively growing pathogenic infections as well as bruise damage that can greatly increase an onion bulb's susceptibility to infection. However, an onion bulb infection must be sufficiently advanced so as to produce macroscopic damage to onion tissues before it can be detected in a CT image. Wang et al. [52] have demonstrated the capability of hyperspectral imaging in the detection of bacterial pathogens on the surfaces of onion bulbs. The fusion of surface imaging technologies such as hyperspectral imaging as well as CT would provide a more powerful system capable of detecting internal damage as well as the presence of pathogens on the surfaces of bulbs before the pathogens have caused extensive damage to onion tissues.

Bibliography

[1] E. G. Barcelon, S. Tojo, and K. Watanabe. X-ray computed tomography for internal quality evaluation of peaches. *Journal of Agricultural Engineering Research*, 73:323–330, 1999.

[2] E. G. Barcelon, S. Tojo, and K. Watanabe. Relating x-ray absorption and some quality characteristics of mango fruit (*Mangifera indica* L.). *Journal of Agriculture and Food Chemistry*, 47:3822–3825, 1999.

[3] P. Bertolini and S. P. Tian. Effect of temperature of production of *Botrytis allii* conidia on their pathogenicity to harvested white onion bulbs. *Plant Pathology*, 46(3):432–438, 1997.

[4] G. E. Boyhan and W. T. Kelley. 2007 Onion production guide, January 2007. URL `http://www.caes.uga.edu/applications/publications/files/pdf/B\%201198\-2\_2.PDF`. Accessed Oct 22, 2012.

[5] G. E. Boyhan and R. L. Torrance. Vidalia sweet onions - sweet onion production in southeastern Georgia. *Hort Technology*, 12(2):196–202, 2002.

[6] G. E. Boyhan, A. C. Purvis, W. M. Randle, R. L. Torrance, M. J. C. IV, G. Hardison, R. H. Blackley, H. Paradice, C. R. Hill, and J. T. Paulk. Harvest and postharvest

quality of short-day onions in variety trials in Georgia, 2000-03. *Hort Technology*, 15 (3):694–706, July-September 2005.

[7] J. K. Brecht, R. L. Shewfelt, J. C. Garner, and E. Tollner. Using x-ray computed tomography to nondestructively determine maturity of green tomatoes. *HortScience*, 26(1):45, 1991.

[8] J. Brewster. Biochemistry, health benefits, and food science of alliums. In J. Brewster, editor, *Onions and Other Vegetable Alliums, 2nd Edition*, Crop Production Science in Horticulture, chapter 8, pages 347–372. CABI Publishing, 2008.

[9] J. Brewster. The classification, origins, distribution and economic importance of the major vegetable crops. In J. Brewster, editor, *Onions and Other Vegetable Alliums*, Crop Production Science in Horticulture, chapter 1, pages 1–26. CABI Publishing, 2 edition, 2008.

[10] W. H. Burkholder. Sour skin, a bacterial rot of onion bulbs. *Phytopathology*, 40(1): 115–117, 1950.

[11] M. I. Chilvers and L. J. du Toit. Detection and identification of botrytis species associated with neck rot, scape blight, and umbel blight of onion. *Plant Health Progress*, November 2006. URL `http://onion.coop/wp-content/uploads/2011/11/Onion-Botrytis-Diagnostic-Guide-PHP-Nov-2006.pdf`. Accessed Oct 8, 2012.

[12] J. C. Diaz-Perez, A. C. Purvis, and J. T. Paulk. Bolting, yield, and bulb decay of sweet onion as affected by Nitrogen fertilizer. *Journal of the American Society of Horticultural Science*, 128(1):144–149, 2003.

[13] I. R. Donis-Gonzalez, D. E. Guyer, and A. Pease. Application of response surface methodology to systematically optimize image quality in computer tomography: A case

study using fresh chestnuts (*Castanea* spp.). *Computers and Electronics in Agriculture*, 87:94–107, 2012.

[14] L. J. du Toit and M. L. Deerie. Prevalence of *Botrytis* spp. in onion seed crops in the Columbia basin of Washington. *Plant Disease*, 88(10):1061–1068, October 2004.

[15] Food and Agriculture Organization of the United Nations. FAOSTAT crop production statistics, August 2012. URL `site/567/DesktopDefault.aspx?PageID=567`. Accessed Sep 23, 2012.

[16] J. H. Fromm, I. Sautter, D. Matthies, J. Kremer, P. Schumacher, and C. Ganter. Xylem water content and wood density in spruce and oak trees detected by high-resolution computed tomography. *Plant Physiology*, 127(2):416–425, October 2001.

[17] R. Gitaitis. Bacterial streak and bulb rot of sweet onion: II. Epiphytic survival of *Pseudomonas viridiflava* in association with multiple weed hosts. *Plant Disease*, 82(8), 1998.

[18] R. Gitaitis, R. Baird, R. Weaver, and D. Sumner. Bacterial blight of sweet onion caused by *Pseudomonas viridiflava* in Vidalia, Georgia. *Plant Disease*, 75(11):1180–1182, 1991.

[19] I. Gubb and H. MacTavish. Onion pre- and postharvest considerations. In H. Rabinowitch and L. Currah, editors, *Allium Crop Science: Recent Advances*, chapter 10, pages 233–266. CABI Publishing, 2002.

[20] M. A. Haidekker. Image analysis and visualization software. In *Advanced Biomdeical Image Analysis*, chapter 14, pages 441–474. John Wiley and Sons, Hoboken, 2011.

[21] M. A. Haidekker. Shape analysis. In *Advanced Biomdeical Image Analysis*, chapter 9, pages 276–309. John Wiley and Sons, Hoboken, 2011.

[22] M. A. Haidekker. Computed tomography. In *Medical Imaging Technology*, chapter 3, pages 37–54. Springer, New York, 2013.

[23] M. A. Haidekker. X-ray projection imaging. In *Medical Imaging Technology*, chapter 2, pages 13–36. Springer, New York, 2013.

[24] B. Herold, B. Oberbarnscheidt, and M. Geyer. Mechanical load and its effect on bulb onions due to harvest and post-harvest handling. *Journal of Agricultural Engineering Research*, 71:373–383, 1998.

[25] J. Lammertyn, T. Dresselaers, P. V. Hecke, P. Jancsok, M. Wevers, and B. Nicolai. MRI and CT study of spatial distribution of core breakdown in 'Conference' pears. *Magnetic Resonance Imaging*, 21:805–815, 2003.

[26] J. H. Leitão, S. A. Sousa, A. S. Ferreira, C. G. Ramos, I. N. Silva, and L. M. Moreira. Pathogenicity, virulence factors, and strategies to fight against *Burkholderia cepacia* complex pathogens and related species. *Applied Microbiology and Biotechnology*, 87(1): 31–40, 2010.

[27] C. Li, N. E. Schmidt, and R. D. Gitaitis. Detection of onion postharvest diseases by analyses of headspace volatiles using a gas sensor array and GC-MS. *LWT - Food Science and Technology*, 44:1019–1025, 2011.

[28] E. Mahenthiralingam, A. Baldwin, and C. Dowson. *Burkholderia cepacia* complex bacteria: opportunistic pathogens with important natural biology. *Journal of Applied Microbiology*, 104:1539–1551, 2008.

[29] G. Mark, R. Gitaitis, and J. Lorbeer. Bacterial diseases of onion. In H. Rabinowitch and L. Currah, editors, *Allium Crop Science: Recent Advances*, chapter 11, pages 267–292. CABI Publishing, 2002.

[30] B. W. Maw and B. G. Mullinix. Moisture loss of sweet onions during curing. *Postharvest biology and technology*, 35:223–227, 2005.

[31] B. W. Maw, Y. Hung, E. W. Tollner, D. A. Smittle, and B. G. Mullinix. Detecting impact damage of sweet onions using muriatic acid and x-rays. *Applied Engineering in Agriculture*, 11(6):823–826, 1995.

[32] B. W. Maw, D. A. Smittle, and B. G. Mullinix. The influence of harvest maturity, curing and storage conditions upon the storability of sweet onions. *Applied Engineering in Agriculture*, 13(4):511–515, 1997.

[33] B. W. Maw, D. A. Smittle, B. G. Mullinix, and J. S. Cundiff. Design and evaluation principles for mechanically harvesting sweet onions. *Transactions of the ASAE*, 41(3): 517–524, 1998.

[34] I. Meglinski, C. Buranachai, and L. Terry. Plant photonics: Application of optical coherence tomography to monitor defects and rots in onion. *Laser Physics Letters*, 7 (4):307–310, 2010.

[35] M. R. P. Mosqueda, E. W. Tollner, G. E. Boyhan, and R. W. McClendon. Predicting the economics of x-ray inspection technology in sweet onion packinghouses using simulation modelling. *Biosystems engineering*, 105(1):139–147, 2010.

[36] G. Q. Pelter, R. Mittelstadt, B. G. Leib, and C. A. Redulla. Effects of water stress at specific growth stages on onion bulb yield and quality. *Agricultural Water Management*, 68(2):107–115, 2004.

[37] B. Prithiviraj, A. Vikram, A. Kushalappa, and V. Yaylayan. Volatile metabolite profiling of onion inoculated with *Erwinia carotovora* spp. *carotovora*, *Fusarium oxysporum* and *Botrytis allii*. *European Journal of Plant Pathology*, 110:371–377, 2004.

[38] A. Purvis and J. Brock. Does *Botrytis allii* spread from infected onions to sound onions in controlled atmosphere storage? In J. Oosterhaven and H. Peppelenbos, editors, *Proceedings of the 8th International Controlled Atmosphere Research Conference*, number 600 in Acta Horticulturae, page 615. International Society for Horticultural Science, March 2003.

[39] A. Purvis and A. Hakim. Effect of bruising on weight loss and storage quality of two onion cultivars. In *1998 Georgia Onion Research-Extension Report*. University of Georgia College of Agricultural and Environmental Sciences, 1998. Cooperative Research-Extension Publication No. 3-99.

[40] H. F. Schwartz and S. K. Mohan. *Compendium of Onion and Garlic Diseases and Pests*. Disease compendium series of the American Phytopathological Association. APS Press, American Phytopathological Society, 2nd edition edition, 2008.

[41] M. A. Shahin, E. W. Tollner, R. D. Gitaitis, D. R. Sumner, and B. W. Maw. Classification of sweet onions based on internal defects using image processing and neural network techniques. *Transactions of the ASAE*, 45(5):1613–1618, 2002.

[42] L. Shepp and B. Logan. The fourier reconstruction of a head section. *IEEE Trans Nucl Sci*, 21(3):21–43, 1974.

[43] L. Sonego, R. Ben-Arie, J. Raynal, and J. Pech. Biochemical and physical evaluation of textural characteristics of nectarines exhibiting woolly breakdown: NMR imaging, X-ray computed tomography, and pectin composition. *Postharvest Biology and Technology*, 5: 187–198, 1995.

[44] N. Syed, M. Munir, A. A. Alizai, and A. Ghaffoor. Onion yield and yield components as function of the levels of Nitrogen and Potassium application. *Pakistan Journal of Biological Sciences*, 3(12):2069–2071, 2000.

[45] E. W. Tollner. Efficacy and economics of placing x-ray machines in an onion packing-house. *Recent Research Developments in Crop Science*, 1:55–69, 2004.

[46] E. W. Tollner, R. D. Gitaitis, K. W. Seebold, and B. W. Maw. Experiences with a food product x-ray inspection system for classifying onions. *Applied Engineering in Agriculture*, 21(5):907–912, 2005.

[47] E. W. Tollner, S. E. Prussia, and W. J. Florkowski. Modeling product flow through a generic postharvest distribution system. *Journal of Food Distribution Research*, 37(2): 23–34, 2006.

[48] United States Department of Agriculture. U.S. onion statistics (94013), 2010. URL `usda.mannlib.cornell.edu/MannUsda/viewDocumentInfo.do?documentID=1396`. Accessed Sep 23, 2012.

[49] University of Georgia College of Agricultural and Environmental Sciences Center for Agribusiness Economic Development. Georgia farm gate value report, 2002. URL `http://www.caes.uga.edu/center/caed/pubs/2003/documents/AR-03-01.pdf`. Accessed May 10, 2012.

[50] University of Georgia College of Agricultural and Environmental Sciences Center for Agribusiness Economic Development. Georgia farm gate value report, 2010. URL `http://www.caes.uga.edu/center/caed/pubs/2011/documents/AR-11-01.pdf`. Accessed May 10, 2012.

[51] A. Vikram, H. Hamzehzarghani, and A. Kushalappa. Volatile metabolites from the headspace of onion bulbs inoculated with postharvest pathogens as a tool for disease discrimination. *Canadian Journal of Plant Pathology*, 27:194–203, 2005.

[52] W. Wang, C. Li, E. W. Tollner, R. D. Gitaitis, and G. C. Rains. Shortwave infrared

hyperspectral imaging for detecting sour skin (*Burkholderia cepacia*)-infected onions. *Journal of Food Engineering*, 109(1):38 – 48, 2012.

[53] P. J. Wright and C. M. Triggs. Effects of curing, moisture, leaf removal, and artificial inoculation with soft-rotting bacteria on the incidence of bacterial soft rot of onion (*Allium cepa*) bulbs in storage. *Australian Plant Pathology*, 34(1):355–359, 2005.

[54] D. S. Yohalem, K. Nielsen, and M. Nicolaisen. Taxonomic and nomenclatural clarification of the onion neck rotting botrytis species. *Mycotaxon*, 85:175–182, 2003.